

1. Experimental Study of Gravity Tectonics by Means of Centrifuged Models

By

Hans Ramberg

“The method is unique, and may be expected ultimately to yield results of great importance, which are otherwise unobtainable.” M. KING HUBBERT, 1937.

ABSTRACT.—For experimental model studies of gravity tectonics the use of the centrifugal force in a strong, large-capacity centrifuge instead of the pull of gravity has great advantages. The choice of model materials increases and the models function and mature much faster than they would in corresponding systems at rest on the earth's surface.

Application of scale-model theory on a number of dome models has given the time of evolution of corresponding structures of geologic dimensions. Deformation- and flow patterns of several dome-type models are demonstrated experimentally and discussed in view of similar structures in nature. A number of classical types of plutonic bodies are reproduced in models of wax, bouncing putty, modelling clay etc. Examples are stocks, batholiths, lopoliths, laccoliths and sills.

Structures similar to submarine ridges and rift-valley systems are produced. Folding in connection with collapse of basins and spreading of “continents” is studied. The effect of convection current on crustal layers is shown experimentally.

In the Appendix certain aspects of the scale-model theory are discussed.

Contents

INTRODUCTION	2
EXPERIMENTAL TECHNIQUE.	4
Centrifuges employed	4
Materials used	5
SCALE-MODEL CONSIDERATIONS	7
Domes of stitching wax in putty overburden	8
Domes of bouncing putty in painter's putty	12
Domes in layered overburden of putty and modelling clay	14
A model with relatively strong overburden	20
Models of injection of magma as caused by buoyant forces	24
GENERAL FEATURES OF DOMES AND RELATED BODIES IN MODELS	28
Initiation of domes	28
Behavior of competent layers embedded in dome-forming material	31
Shape of domes and related structures	34
Structurs in overburden adjacent to domes	36
Marginal sinks	40
DISCUSSION OF INDIVIDUAL MODELS OF DOMES AND RELATED STRUCTURES	48
Introduction	48
Domes of stitching wax along discontinuities in overburden	49
Domes of bouncing putty along discontinuities in overburden	50
Low-density layers in and on overburden, and their effect on the behavior of domes	53
Model study of buoyancy of magma in solid surroundings	59

SOME GEOLOGICAL IMPLICATIONS OF MODEL STUDIES OF DOMES AND SIMILAR STRUCTURES	63
Island arcs and batholiths in orogenic zones.	63
Note on the so-called "bottom granites" in the Caledonides in Norway	69
Submarine ridges and rift valleys	71
Remarks on emplacement of basic and acidic rocks.	74
MODELS OF FOLDING OF SURFACE LAYERS CAUSED BY ADJUSTMENTS OF UNSTABLE DISTRIBUTION OF MASSES.	76
APPENDIX	84
Note on buoyancy in models	84
Buckling of a surface layer exposed simultaneously to lateral compression and the pull of gravity etc.	88

Introduction

One of the major objectives of endogene geology is to study the past and present motion of matter in the earth. For such motion the force of gravity plays a dominant role.

On a global scale the effect of gravity is strikingly manifested by the construction of the earth in the form of concentric shells with increasing density toward the center.

When it comes to geologic phenomena of somewhat smaller scale, however, such as folding of stratified rocks, the rise of batholiths and other plutonic bodies, volcanic activity, sinking of geosynclines, folding of strata and elevation of mountain chains, evolution of rift valleys, etc., the role played by gravity is less certain. Theories have been proposed which consider any one of the above-mentioned phenomena as direct results of the pull of gravity acting on unstable distributions of masses in and on the earth. The unstable distributions are either considered as primary conditions of an undifferentiated earth, or assumed formed periodically by expenditure of energy of nongravitational nature such as chemical or nuclear (energies).

The convection theory of geosynclines and fold mountains is a case in point: the internal thermal energy of the earth—as manifested by the geothermal gradient—creates unstable density distribution which in turn gives subcrustal convection currents that may result in buckling of the crust.

Periodic melting of deepseated rocks may conceivable decrease the density sufficient to make the magma rise by buoyancy as domes, batholiths and related intrusive bodies, or to surface as lava. Subsequent increase of density during cooling and crystallization may again cause the bodies to sink and create significant structural changes in the surrounding regions.

That salt domes rise due to buoyancy in the field of gravity is universally accepted by the students of such bodies, perhaps chiefly due to the striking experimental reproduction of this process by NETTLETON (1934), DOBRIN (1941), PARKER *et al.* (1955) and many others. The establishment of isostatic adjustments all over the globe (see discussion in HEISKANEN and VENING MEINESZ,

1958) is another striking manifestation of the significance of the force of gravity for crustal movements.

In order to study the effect of gravity on geologic processes, model experiments are necessary because the configuration and juxtaposition of rocks and magma masses in the earth is generally so complex as to defy reliable theoretical quantitative analysis. Even in the case of simple isostatic adjustment under a given surface load (HASKELL, 1935), or buckling of idealized stratified bodies (BIOT, 1961; RAMBERG, 1962) it appears that the mathematical theory becomes too complex to convey meaning to others than the specialists.

Granting that very significant model studies in the field of gravity tectonics have been reported from time to time (SMOLUCHOWSKI, 1909; NETTLETON, *op. cit.*; KING HUBBERT, 1937; DOBRIN, *op. cit.*, PARKER *et al.*, *op. cit.*; BUCHER, 1956; BELOUSSOV, 1960; and others) it seems that the activity in this important field lags far behind the activities in some other areas of experimental geology such as, for example, mineral chemistry and chemical petrology.

One of the reasons for this state of affairs may be the limited choice of materials suited for scale-model studies of the role of gravity in the evolution of geologic structures. (Incidentally, if gravity is not an important parameter in the model study, the choice of material is much wider as will become evident below.) For ordinary scale models which are at rest in the gravitational field of the earth, the relation between *density* and *mechanical* or *rheological* properties (viscosity, yield strength, ultimate strength) of suitable imitation materials must not vary beyond rather narrow limits for the very good reason that the experimenter has limited time and limited laboratory space to his disposal. If the yield strength is greater than a certain limit as determined by the density and the geometric dimensions the model will not be capable to perform at all.

At mechanically unstable mass distribution in such models the primary driving agency is the body force which per cubic centimeter of the material equals the density times the acceleration due to gravity, and the secondary buoyant force which is a function of the density differences times the acceleration due to gravity. The motive force in models at rest at the earth's surface is consequently limited by the densities of available liquids and solids which lie between about 1 g/cm³ and 22 g/cm³.

On the other hand the resistance against motion in gravity-driven models is a function of viscosity and strength of the materials. To keep operating time and dimensions of models within practical limits one is therefore restricted to the use of liquids such as oil, syrup; soft waxes, resins, some synthetic plastics; unconsolidated powder, or wet clay as rock-imitation materials. Materials of this kind were employed in the model experiments performed by the authors cited above.

In experimental studies of gravity-driven scale models one is thus faced with difficulties of the following nature:

- (1) It may not be possible at all to find materials which imitate rock in their

various mechanical properties closely enough to give realistic scaled-down models of many of the geologic structures we wish to study.

(2) Even if materials with adequate scale-model properties are available, such materials are often weak and soft to a degree prohibitive for the construction of the initial unstable model and for the study of structures in the final stage of the model. This difficulty was, for example, encountered during the salt-dome work by Parker *et al.*, *op. cit.* Cooling of the materials while constructing the desired model may help, but during subsequent heating to the proper temperature, the temperature distribution will be uneven and premature flow in the hotter regions of the model is apt to take place.

(3) In order to utilize some of the more viscous resins, waxes or asphalts in gravity-driven models the time is often undesirably long (days, weeks or even months), or the volume of material needed wastefully large. (The lapse of time for a given flow process in geometrically similar models of given materials decreases with increasing size of the model.)

Some of these difficulties may be eliminated if the motive body force is not restricted to the practically unchangeable pull of gravity at the earth's surface, but methods are devised by which models are exposed to body forces that are controlled by the experimenter. One could, for example, mix fine iron filings in the materials and expose the models to strong magnetic fields. If the embedded filings is fine-grained, motion of the filings through the embedding material under the effect of the magnetic field may be insignificant relative to bodily motion of the filings-carrying embedding material. However, a much simpler and probably more powerful technique is to expose models to centrifugal acceleration. The centrifuge technique was applied in tests of rock fracturing in mining operation by BUCKY in 1931, but this promising experimental method seems to have been shelved until the author, inspired by the recent activity in satellite research, started to apply a centrifuge in model studies some time ago.

Experimental technique

Centrifuges employed

In ordinary commercially available centrifuges, models measuring about 10 cm in diameter and weighing more than 1000 g can be exposed to acceleration up to about 2000 g (g = acceleration due to gravity). Smaller models may be run at much higher acceleration, but for structures of some complexity it is inconvenient, but by no means impossible, to work with models smaller than, say, 5 cm across. (If the availability of materials justifies the use of body forces much higher than those resulting from an acceleration of a few thousand g —e.g., if, for example, only certain crystalline solids are found to mimic the rheological properties of rock satisfactorily—it should not be difficult to develop a microtechnique for the use of ultracentrifuges giving 50,000 g or more.)

Some tests were performed in an "International Equipment Co. *SBV*" centrifuge of moderate power and capacity. Most of the tests, however, were run in a "Large Capacity International Serum Centrifuge" model 13 *L*, which was kindly placed at the author's disposal by the Enrico Fermi Institute, University of Chicago.

The diameter of the models was limited to 9.4 cm by the standard trunnion cups of this centrifuge, and the weight limited to about 1300 g. The maximum speed of the machine is 2300 rpm which corresponds to an acceleration of 2280 *g* at the bottom of the cups. With the materials used it was not found necessary to utilize the full power of the machine because the desired evolution of all models studied was reached between about 1 and 41 minutes at an acceleration not exceeding 1700 *g*.

(As commercially available centrifuges are constructed for the use of liquids, the heads and cups are not well suited for model work with solids and very viscous fluids. The capacity and performance of ordinary centrifuges may be more effectively utilized for this particular purpose by making certain changes in the head and cup constructions. Firstly the shape of the cups should be wider and lower for a given volume capacity because the horizontal dimension of most geologic structures one wishes to study is larger than the vertical dimension. Moreover, since most of the scale-model materials consist of solids or very viscous liquids one needs not consider spill over the edges or disturbing flow in the model while inserting or removing the cups. This means that one can take advantage of the great strength of rigid heads without having the disadvantage of the inclined positions of the cups in the ordinary models of such heads. Special rigid heads which now are under construction by the Wifug Company, Stockholm, are expected to combine large capacity with high centrifugal acceleration.)

Materials used

Stitching wax is a viscoelastic resin mixture which is brittle at impact but flows as a very viscous liquid at stress below its ill-defined ultimate strength (BUCHER, 1956). Its yield strength is very low, but probably not zero. There were no need to measure the ultimate strength and the yield strength of the wax because the stresses acting on the wax in the models were always somewhere between the two strengths as shown by the fact that the wax yielded but never fractured in the models. The density of the sample employed in the models is 1.01 g/cm³, and the viscosity coefficient at 20°C is approximately 3.2×10^7 poises as determined under an uniaxial stress of 6.1×10^4 dynes/cm². BUCHER, op.cit. gives a viscosity of 10^6 poises for a similar type of stitching wax at 25°C. As usual for viscous fluid of this kind the viscosity of the wax decreases rather rapidly with increasing temperature, but is not much effected by varying stress according to BUCHER, op. cit. That is, the wax approaches a Newtonian-type liquid. The stitching wax was mostly used to imitate dome-making geologic

bodies (salt domes, batholiths, etc.). It was also used as basement for folding strata in "geosynclines".

The batch of *modelling clay* used has a density equal to 1.71 g/cm³. It shows a yield strength and a sort of anisotropic hardening effect, i.e. under uniaxial compression its strength increases in the compressed direction but decreases for subsequent compression in perpendicular directions. Thus, strain-hardening in one direction is associated with softening in perpendicular directions.

As a measure of the yield strength it was found that an uniaxial compressive stress greater than some 4×10^5 dynes/cm² is necessary to start plastic flow. At stresses slightly above the yield strength a viscosity coefficient varying between 1.3×10^8 and 3.4×10^8 poises was determined at room temperature. The variation of viscosity with temperature is much less than for the stitching wax. At a few degrees below room temperature the latter is, for example, more viscous than the modelling clay, but at higher temperatures the opposite is true.

The viscosity value given above must be taken with reservations because it is impossible to control the hardening and softening which inevitably occur under preparation of the models.

The modelling clay was used to imitate competent strata in models. It would for example buckle and fracture (form boudinage) when enclosed in stitching wax and putty.

A type of slow drying, plastic base *painter's putty* has a density of 1.90 g/cm³. It shows erratic rheological behavior depending upon the history of the sample. When stress is first applied on a batch of relaxed putty it is very soft during an initial strain of considerable magnitude, but then exhibits a yield strength which in uniaxial compression corresponds to about 3×10^4 dynes/cm². At stresses a little above the yield strength a viscosity coefficient of about 7×10^5 poises was found in uniaxial compression tests.

Hardening in direction of the applied stress caused the effective viscosity to increase with increasing strain. This effect could not be measured unambiguously, particularly because a gentle shaking of the putty sample would cause some relaxation and recovery of the lesser strength. Hence the effective viscosity measured under gentle shaking is less than that measured under steady compression.

Measurements of rate of sinking of a small steel ball through putty in the centrifuge gave a viscosity of 8.4×10^5 poises after steady rate of fall had developed.

The putty was used to imitate dense rocks through which domes rose.

This special kind of putty is manufactured by Allen Putty Co., Chicago.

Bouncing putty is a silicone-base viscoelastic material manufactured by Dow Chemical Company.¹ The material is almost perfectly elastic at rapid impacts, fractures under fast extensive strain but is soft and flows as a liquid under low

¹ The author wishes to express his gratitude for the samples supplied by the Dow Chemical Company.

and moderate stresses. The bouncing putty flattens under its own weight even in very small pieces. Its density is 1.12 g/cm^3 and viscosity about 3×10^5 poises at room temperature.

The bouncing putty was used to imitate domes and related structures.

A mixture of powdered high-melting *hard wax* and *mineral oil* has a low density, viz. 0.85 g/cm^3 , and was found well suited to imitate light sediments.

Thin sheets of rather stiff *packing wax* were used in a few models to imitate competent strata.

An *aqueous solution of KMnO_4* with density 1.05 g/cm^3 has a viscosity about 10^{-2} poises at room temperature. This stands in relation to the viscosity of putty and modelling clay almost like the viscosity of a very viscous magma to the viscosity of crystalline rocks. Such an aqueous solution is therefore a suitable magma imitation in models with putty and modelling clay as rock imitations.

Scale-model considerations

In the present paper the writer wishes to demonstrate the great significance of the use of centrifugal force in model studies of gravity tectonics, and to discuss some of the more interesting flow pattern developed in models accelerated by this technique. Treated with caution many of the results are illuminating for gravity tectonics even though the models are only partly in proper scale with corresponding geologic structures.

To show quantitatively the extent to which some of the experiments approach scaled-down models of geologic structures some dome models will be considered. In so doing we shall proceed as follows: Firstly all known pertinent conditions of an experimental model are given. The model is then scaled up to a *geometrically similar* structure of reasonable geologic dimensions. By means of known or assumed densities, viscosities and/or strengths of *some* of the rocks involved and of *all* the materials in the models, model ratios of densities, viscosities and strength are determined. As these model ratios must be constant point for point and rock for rock throughout the experimental model and the corresponding geologic structure, as required by kinematic similarity, the densities, viscosities, and strength of all rocks in the geologic structure are determined by corresponding properties of the materials in the experimental model. The properties so determined may or may not be realistic for natural rocks; we shall therefore refer to the geologic structure which is scaled up in this manner as the *hypothetic geologic structure*. A comparison of such hypothetic geologic structures with geometrical analogous¹ known realistic geologic structures in terms of rock properties and time of evolution should then show in which respect and to what extent our experimental model departs from natural conditions.

¹ Unless we are considering very simple structures it will be practically impossible to find a truly geometrically similar natural counterpart to the models.

Domes of stitching wax in putty overburden

A 3 mm thick layer of stitching wax was placed under a 20 mm thick layer of painter's putty in a centrifuge cup with 94 mm diameter. After 15 minutes' run at an acceleration corresponding to 1100 g (i.e. 1600 rpm in the 13 L model centrifuge) several domes penetrated the surface. The diameter of the trunk portion of the mushroom-shaped domes varied somewhat, but 4 mm would be close to an average. Figs. 25 and 26 show the result of a similar experiment.

For convenience let these domes represent salt domes with diameter 400 m. This is a small diameter for domes but it gives a convenient model ratio of length, viz. 10^{-5} . The density of the wax is 1.01 g/cm^3 which will be rounded off to 1.00 g/cm^3 . The density of salt is taken as 2.2 g/cm^3 . The model ratio of density is thus 0.455.

The viscosity of the wax, which shows no or negligible yield strength, is about 3×10^7 poises at room temperature at which the run was performed. A viscosity of 10^{18} poises may be assigned to the salt, although values varying from 2.5×10^{17} to 2×10^{18} are quoted in literature (Parker *et al.*, op. cit., p. 205). This gives a model ratio of viscosity equal to 3×10^{-11} .

Under the slow motion of a salt dome salt seems to exhibit very low or no yield strength. We shall therefore disregard the strength of salt. (The yield strength of salt measured in some laboratory experiments is not applicable to flow of salt in nature because slow creep caused by annealing or recrystallization is not considered in most tests.)

The properties of wax and salt thus fixes the model ratio of density and that of viscosity, as shown in Table 1.

The overburden in the experimental model has a density 1.90 g/cm^3 , and a somewhat ill-defined viscosity of about 7×10^5 poises (see p. 6). The corresponding density of the overburden in the hypothetic geologic structure is 4.18 g/cm^3 , and its viscosity 2.3×10^{16} poises. The scaled-up density of the overburden is definitely too high, and the viscosity probably several order of magnitude too low. The effect of these deviations (from true rock properties) upon the rate of rise of the domes will be discussed below.

The overburden in the experimental model has a certain yield strength, and it is probable that the sedimentary cover above salt layers also shows strength. As discussed on p. 6 the strength of the putty overburden is not a well defined property. When stress is first applied on a putty sample, it shows practically no yield strength, but it hardens after some initial strain and exhibits a yield strength equal to about $3 \times 10^4 \text{ dynes/cm}^2$.

When the yield strength of the model overburden is given, similarity between a model exposed to a centrifugal acceleration, a , and rocks exposed to the acceleration due to gravity, g , requires that the strength, s_0 , of the rock overburden be given by

$$\frac{s_m}{s_0} = \sigma = \delta \lambda \frac{a}{g} = 5.005 \times 10^{-3}, \quad (1)$$

Table I.

	Experimental model	Hypothetic geologic structure	Model ratios	Realistic geologic structure	Modified ratios
Dome diameter	4 mm	400 m	$\lambda = 10^{-5}$	400 m	
Dome height	20 mm	2000 m	$\lambda = 10^{-5}$	2000 m	
Source-layer thickness	3 mm	300 m	$\lambda = 10^{-5}$	300 m	
Overburden thickness	20 mm	2000 m	$\lambda = 10^{-5}$	2000 m	
Density of source layer	1.00 g/cm ³	2.2 g/cm ³	$\delta = 0.455$	2.2 g/cm ³	
Density of overburden	1.90 g/cm ³	4.18 g/cm ³	$\delta = 0.455$	2.4 g/cm ³	
Density contrast	0.90 g/cm ³	1.98 g/cm ³		0.2 g/cm ³	
Viscosity of source layer	3.0×10^7 poises	10^{18} poises	$\psi = 3.0 \times 10^{-11}$	10^{18} poises	$\Delta\delta = 4.5$
Viscosity of overburden	7.0×10^5 poises	2.33×10^{16} poises	$\psi = 3.0 \times 10^{-11}$	2.33×10^{16} poises	
Strength of overburden	3.0×10^4 dynes/cm ²	6×10^6 dynes/cm ³	$\sigma = \delta\lambda \frac{a}{g} = 5.0 \times 10^{-3}$	6.06×10^5 dynes/cm ²	$\Delta\sigma = \Delta\delta\lambda \frac{a}{g} = 4.95 \times 10^{-2}$
Acceleration or body force per unit mass	10.79×10^5 cm/sec ²	981 cm/sec ²	$\gamma = 1.1 \times 10^8$	981 cm/sec ²	$\tau' = \psi\Delta\sigma^{-1} = 6.06 \times 10^{-10}$
Time	9.0×10^2 sec	1.5×10^{11} sec	$\tau = \psi\sigma^{-1} = 6 \times 10^{-9}$	1.5×10^{12} sec	

where s_m is the strength of the model overburden, δ is the model ratio of density and λ that of length. The numerical value refers to our particular case. Eq. (1) and most of the other scale-model equations in the following are from KING HUBBERT's classic treatment, *op. cit.* Eq. (1) in particular is a combination of eq. (44) and the equation on bottom of p. 1491 in KING HUBBERT's paper.

The corresponding strength of the sedimentary overburden in the hypothetical geologic structure, *viz.* 6×10^6 dynes/cm², seems low but perhaps not unreasonable, see PARKER *et al.*, *op. cit.*

The model ratio of time may be determined by the relation

$$\tau = \psi\sigma^{-1}, \quad (2)$$

where σ is the model ratio of stress and ψ the model ratio of viscosity.¹ The time needed for the domes in the hypothetical geologic structure to ascend from the source layer to the surface is accordingly 1.50×10^{11} seconds or about 5000 years. (One year = 3.15×10^7 seconds.)

This is obviously much too short time of evolution for a realistic geologic structure which is geometrically similar to the experimental model. Salt domes require several millions of years to reach levels some thousands of meters above their source layers.

The large time discrepancy between the experimental model and a realistic salt-dome evolution must chiefly be sought in the unrealistically high density and low viscosity of the overburden in the hypothetical geologic structure. If the density of the real sedimentary overburden be 4.18 g/cm³, its strength 6×10^6 dynes/cm² and its viscosity but 2.3×10^{16} poises, which is much less than that of the salt itself, there is little reason to doubt that salt domes geometrically identical to the hypothetical geologic structure would have ascended in the course of a time close to the estimated few thousands of years.

In relatively simple structure such as that above it is possible to make corrections for the lack of kinematic similarity due to density discrepancy between the hypothetical geologic structure and a corresponding realistic one. (It is unfortunately much more difficult and uncertain to correct for the obviously much too low viscosity of the overburden in the model. Such corrections requires complex fluid dynamic theory which is outside the scope of the present paper.)

If we assign a density of for example 2.4 g/cm³ to the sedimentary overburden rather than 4.18 g/cm³ the buoyant force acting on the salt as long as it is enclosed in the overburden, changes by a factor of about 0.1. This means that the velocity decreases approximately by the same factor provided that the viscosities of the overburden and the salt do not change with magnitude of stress, and that a certain adjustment of the yield strength of the overburden is accomplished at the same time, see Appendix, p. 84.

In order that the velocity shall change proportional to the change in the

¹ Note that the model ratio of stress equals the model ratio of strength.

buoyant force, the strength of the sedimentary overburden in the real structure is no longer given by

$$s_0 = s_m \frac{g}{a} \lambda^{-1} \delta^{-1}, \quad (3)$$

but assumes a smaller value. When 4.18 g/cm^3 is used as the density of the overburden the "punching" stress across the top surface of a dome of height h is

$$\sigma_p = (4.18 - 2.2)hg \text{ dynes/cm}^2 \quad (4)$$

when hydrostatic equilibrium exists through the column of salt. For this density contrast between overburden and salt, which is in proper scale relation to the experimental model, the scale-determined strength of the overburden is given by $s_m g a^{-1} \lambda^{-1} \delta^{-1}$. However, if the density contrast between overburden and salt is reduced to $(2.4-2.2) \text{ g/cm}^3$, which is out of scale with the model, the "punching" stress across the top surface of the dome is correspondingly reduced to

$$\sigma'_p = (2.4 - 2.2)hg \text{ dynes/cm}^2, \quad (5)$$

provided hydrostatic equilibrium prevails in the salt column. Therefore an overburden of sediments with a density 2.4 g/cm^3 must have a smaller strength in order to correspond to the given strength of the model overburden. The new model ratio of strength is

$$\frac{s_m}{s_0} = \Delta\sigma = \lambda\Delta\delta \frac{a}{g}, \quad (6)$$

where $\Delta\delta$ is the model ratio of *density contrast* between overburden and doming material, i.e.

$$\Delta\delta = \frac{(1.9 - 1.0) \text{ gm/cm}^3}{(2.4 - 2.2) \text{ gm/cm}^3} = 4.5. \quad (7)$$

The corresponding strength of the sedimentary overburden with density 2.4 is consequently only about $6 \times 10^5 \text{ dynes/cm}^2$. See also Appendix, p. 86.

Provided this be the strength and 2.4 g/cm^3 the density of the overburden the model ratio of time, τ , between the experimental model and the new structure, which no longer are strictly similar, is given by the relation

$$\frac{t_m}{t_0} = \tau = \psi \Delta\sigma^{-1} = \psi \lambda^{-1} \Delta\delta^{-1} \frac{g}{a}, \quad (8)$$

which gives $t_0 \cong 50,000$ years for the modified geologic structure.

Although the use of a more reasonable density of the overburden increases the time of evolution by one order of magnitude, the time is definitely still much too short. The chief reason for this is provided by the unrealistically low viscosity (and strength) assigned to the overburden by the viscosity ratio between salt and stitching wax.

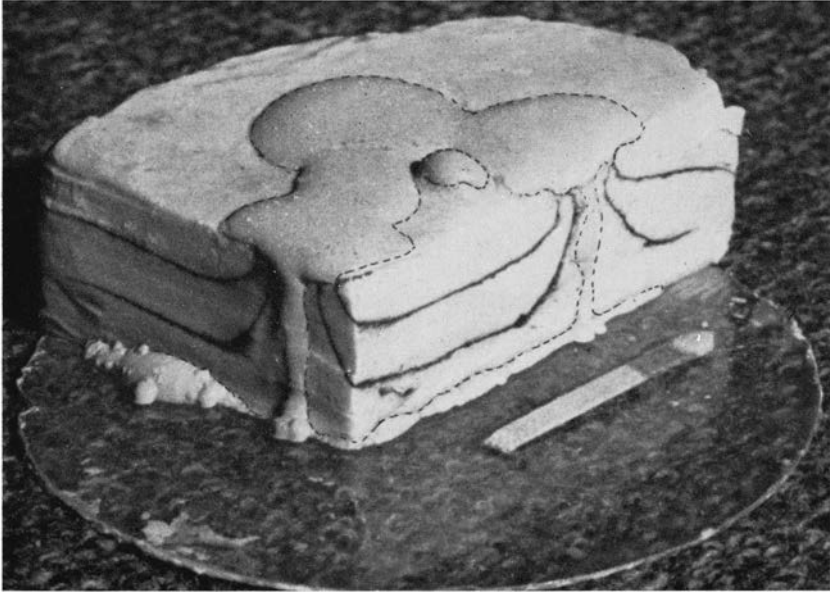


Fig. 1. Part of model of surfaced domes of bouncing putty in overburden of painter's putty. Before cutting, the cylindrical outer boundary of the model coincided with the circumference of the sheet of plexiglass at the bottom. Stipled lines outline the domes and the bottom source layer; see text.

Variation of strength and viscosity of overburden have been shown to affect rate of rise of dome very significantly, more so than variation in these properties of the salt itself. (DOBRIN, *op. cit.*; PARKER *et al.*, *op. cit.*). This effect is shown in the following experimental models whose dome and overburden materials have viscosity ratios closer to what one may expect to find in nature. One obvious requirement is that the overburden material have a greater effective viscosity than the dome material. We shall see that models of such materials give better rate agreement with corresponding natural structures.

Domes of bouncing putty in painter's putty

In the same centrifuge cup as described above a 2.7 mm thick layer of bouncing putty (see p. 6) was placed under a 24 mm thick layer of the same kind of painter's putty as used in the previous experiment. After between 3 and 4¹ minutes' run at 1000 g the bouncing putty had penetrated the surface.

Bouncing putty has a density 1.12 g/cm³ which, for the purpose of scale calculations, will be rounded off to 1.10 g/cm³. Its viscosity is about 3×10^5 poises. The properties of the painter's putty are given above.

¹ As the centrifuge had to be stopped and opened for inspection in lack of stroboscopic light arrangement, the time could not be determined more accurately.

	Experimental model	Hypothetic geologic structure	Model ratios	Realistic geologic structure	Modified ratios
Dome diameter	3 mm	300 m	$\lambda = 10^{-5}$	300 m	
Dome height	24 mm	2400 m	$\lambda = 10^{-5}$	2400 m	
Source-layer thickness	2.7 mm	270 m	$\lambda = 10^{-5}$	270 m	
Overburden thickness	24 mm	2400 m	$\lambda = 10^{-5}$	2400 m	
Density of source layer	1.10 g/cm ³	2.2 g/cm ³	$\delta = 0.5$	2.2 g/cm ³	
Density of overburden	1.90 g/cm ³	3.8 g/cm ³	$\delta = 0.5$	2.4 g/cm ³	
Density contrast	0.80 g/cm ³	1.6 g/cm ³		0.2 g/cm ³	
Viscosity of source layer	3.0×10^5 poises	10^{18} poises	$\psi = 3.0 \times 10^{-13}$	10^{18} poises	$\Delta\delta = 4.0$
Viscosity of overburden	7.0×10^5 poises	2.33×10^{18} poises	$\psi = 3.0 \times 10^{-13}$	2.33×10^{18} poises	
Strength of overburden	3.0×10^4 dynes/cm ²	6.0×10^6 dynes/cm ²	$\sigma = \delta\lambda \frac{a}{g} = 5.0 \times 10^{-8}$	7.5×10^5 dynes/cm ²	$\Delta\sigma = \Delta\delta\lambda \frac{a}{g} = 4.0 \times 10^{-2}$
Acceleration or body force per unit mass	9.81×10^5 cm/sec ²	9.81×10^8 cm/sec ²	$\gamma = 10^3$	9.81×10^2 cm/sec ²	$\tau' = \psi\Delta\sigma^{-1} = 7.5 \times 10^{-12}$
Time	2.10×10^2 sec	3.5×10^{12} sec	$\tau = \psi\sigma^{-1} = 6.0 \times 10^{-11}$	2.8×10^{13} sec	

The average value of the diameter of the trunk portion of the several mushroom-shaped domes (Fig. 1) was taken as 3 mm.

The model may be scaled up to a geometrically and kinematically similar hypothetical geologic structure by the same method as employed above, using $\lambda = 10^{-5}$ as the model ratio of length, and assuming that the salt's density is 2.2 g/cm^3 and its viscosity 10^{18} poises. The pertinent properties of the experimental model and its similar hypothetical geologic structure are given in Table 2. It may be noted that the density of the overburden in the hypothetical structure has decreased a little, and its viscosity increased somewhat relative to the case reported in Table 1. This is a trend in the right direction toward natural conditions. The model ratio of time has decreased, and in spite of the fact that the actual running time of the present model is considerably shorter than for the wax model, the time of evolution for the corresponding hypothetical geologic structure is longer. The lapse of time is still unrealistically short, however, but adjustment for the overburden density from 3.8 g/cm^3 in the hypothetical structure to 2.4 g/cm^3 in a geometric identical real geologic structure makes the model ratio of time change from 6×10^{-11} to 7.5×10^{-12} , and the time of evolution from 3.5×10^{12} seconds to 2.8×10^{13} seconds = 8.9×10^5 years provided that the strength of the sedimentary overburden be adjusted to that required by the new scale, viz. to 7.5×10^5 dynes/cm² from 6×10^6 dynes/cm².

The recalculation procedure is analogous to that discussed in connection with model I, and the values are given in Table 2. See also Appendix.

The time for the density-adjusted geologic structure is still short. A discrepancy of this kind is to be expected in view of the yet too great weakness of the sedimentary overburden whose viscosity and strength are scaled to the painter's putty in the model. We shall therefore attempt to increase the strength and viscosity of the overburden in the model by selecting another material.

Domes in layered overburden of putty and modelling clay

The sedimentary overburden of salt domes and salt layers is generally a heterogeneous column of stratified rocks with unlike mechanical properties and unlike thickness. Even for most homogeneous rocks it is difficult to know how to assign such properties as yield strength and viscosity in spite of the fact that properties of this nature have been measured in laboratories. During the length of geologic time little understood recrystallization flow or creep may make laboratory-measured strength and viscosity of little use for studies of the behavior of rocks in their natural conditions. When it comes to the response to stress of heterogeneous layered rocks very little is known indeed. It seems reasonable, though, that provided the thickness of layers in a sedimentary column is small relative to the dimension of a penetrating dome, then the overburden will behave mechanically somewhat like a uniform body with properties intermediate between the individual layers. When considered in detail, however, one should expect that a layered structure behaves different from an

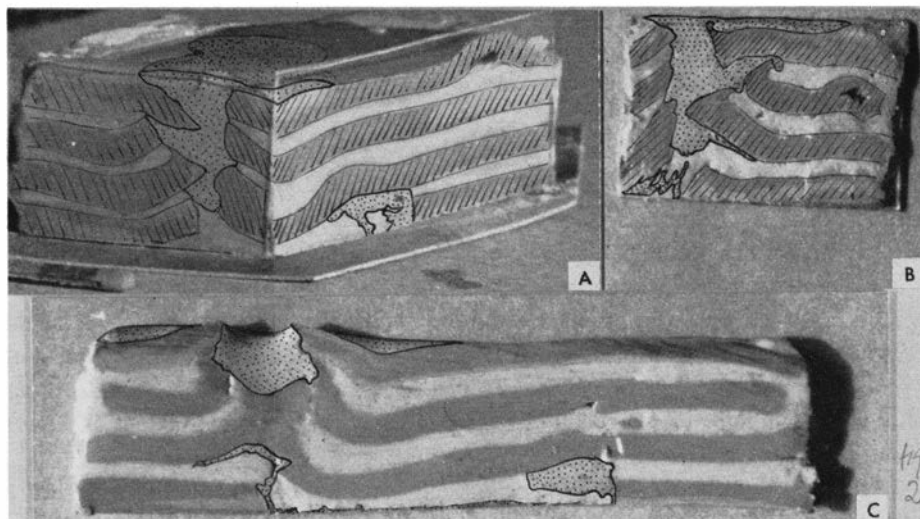


Fig. 2. Cuts of model of irregular domes of bouncing putty (dotted) in layered overburden of modelling clay (hatched and dark grey) and painter's putty (uniform light grey).

A Segment of the model with thin sheets of plexiglass cemented on the fresh vertical cuts. A dome has penetrated the layered overburden and spread on the surface, another has only been able to cause gentle doming of the deepest layer of modelling clay.

B Detail of dome which has pierced the surface of the overburden.

C Diagonal cut through the model. Note the marginal sink close to the penetrating dome (which is connected with the remains of the bottom source layer either behind or in front of the cut shown).

uniform rock. In the former important local concentrations of stresses will occur in the competent layers. Such stress concentrations may well be necessary in order that certain dome structures shall penetrate the overburden if the average "punching" stress created by the dome is too weak to overcome the strength of the rocks.

In order to make the models more realistic than those described above the writer used multilayered overburden in several tests. Two of these will be described as examples on scale models with overburden considerably stronger and more viscous than the dome material.

Model A:—In the center at the bottom of the centrifuge cup a 4 mm thick circular layer of bouncing putty with 44 mm diameter was placed. A 4 mm thick ring of modelling clay of the type described on p. 6 covered the rest of the bottom of the cup whose diameter is 94 mm. Six alternating layers of painter's putty and modelling clay all about 4 mm thick were placed above the bottom layer. Painter's putty covered the bouncing putty and a sheet of modelling clay finished the column at the top, see Fig. 2. This gave a rather strong and tough overburden on account of the properties of the modelling clay.

The model was run for 33 minutes at an acceleration of 1300 g in the centrifuge. (The time does not include the periods during which the centrifuge was

stopped for inspection.) After about 31 minutes the bouncing putty pierced the surface.

The densities of the modelling clay is 1.70 g/cm³, its strength about 4×10^5 dynes/cm² and its viscosity about 2×10^8 poises.

Neither the strength nor the viscosity are well defined properties but depend somewhat upon the history of the sample. The viscosity also depends upon the rate of strain. The values above must be considered as averages at stresses slightly above the yield strength.

As seen from the cross sections Fig. 2, the resulting "dome" is very irregular with a shape strongly influenced by the layered structure of the overburden. Several domes, for example, spread laterally in layers of painter's putty without penetrating the stronger layers, but at one spot on the edge of the source layer of bouncing putty an irregular dome-shaped body reached up through all layers and spread on the free surface.

Let us scale this structure up geometrically to a hypothetic geologic structure as before. The layers of modelling clay and painter's putty may for example be compared with alternating rather thick layers of sandstone and shale, and the bouncing putty with irregular injections of salt. Scaling up the densities and viscosities of the modelling clay and painter's putty layers on basis of the corresponding properties of bouncing putty and salt leads to the values given in Table 3.

The densities of the overburden layers in the hypothetic geologic structure are again much too high. The viscosity of the incompetent overburden layers is too low, but the viscosity of the competent set of layers seems rather reasonable, viz. more than 10^{20} poises.

The strength, s_0 , of the overburden layers in the hypothetic structure is determined by the relation $s_m/s_0 = \sigma = \delta\lambda(a/g)$, and the time by $t_m/t_0 = \tau = \psi\sigma^{-1}$.

In the previous two cases it was possible to make valid corrections for the lack of true scale relation between the density of the natural overburden and of the overburden in the models. Such ready adjustments for scale deviation of densities are unfortunately not always possible because nonscale relations in this property may make model and original become kinematically dissimilar in unpredictable ways as discussed in the Appendix. If the thickness of individual layers in overburden is not small relative to the diameter of the dome, for example, the rising dome is apt to behave very different as it passes through layers with unlike densities. If some layers are less dense and others more dense than the dome material, then the rising dome spreads in the light layers and becomes pinched in the dense layers. The dome may indeed not be able to pass through a low-density layer at all. This situation is encountered in several of the experimental models, see Figs. 32, 34 and 38.

For less extreme density differences between the various overburden layers the dome may pass through all layers but the exact rate is not only determined by the average density contrast between overburden and rising dome but also

Table 3.

	Experimental model	Hypothetic geologic structure	Model ratios	Realistic geologic structure	Modified ratios
Dome diameter	variable (irregular)	variable	$\lambda = 10^{-5}$	variable	
Dome height	24 mm	2400 m	$\lambda = 10^{-5}$	2400 m	
Source-layer thickness	4 mm	400 m	$\lambda = 10^{-5}$	400 m	
Competent layer thickness	4 mm	400 m	$\lambda = 10^{-5}$	400 m	
Incompetent layer thickness	4 mm	400 m	$\lambda = 10^{-5}$	400 m	
Density of source layer	1.10 g/cm ³	2.2 g/cm ³	$\delta = 0.5$	2.2 g/cm ³	
Density of competent layer	1.70 g/cm ³	3.40 g/cm ³	$\delta = 0.5$	2.371 g/cm ³	
Density of incompetent layer	1.90 g/cm ³	3.80 g/cm ³	$\delta = 0.5$	2.429 g/cm ³	
Density contrast between source and competent layer	0.6 g/cm ³	1.2 g/cm ³		0.171 g/cm ³	$\Delta\delta = 3.5$
Density contrast between source and incompetent layer	0.8 g/cm ³	1.6 g/cm ³		0.229 g/cm ³	$\Delta\delta = 3.5$
Mean density contrast	0.7 g/cm ³	1.4 g/cm ³		0.200 g/cm ³	$\Delta\delta = 3.5$
Viscosity of source layer	3.0×10^5 poises	10^{18} poises	$\psi = 3.0 \times 10^{-13}$	10^{18} poises	
Viscosity of competent layer	2.0×10^8 poises	6.67×10^{20} poises	$\psi = 3.0 \times 10^{-13}$	6.67×10^{20} poises	
Viscosity of incompetent layer	7.0×10^5 poises	2.33×10^{18} poises	$\psi = 3.0 \times 10^{-13}$	2.33×10^{18} poises	
Strength of competent layer	4.0×10^5 dynes/cm ²	6.15×10^7 dynes/cm ²	$\sigma = \delta\lambda \frac{a}{g} = 6.5 \times 10^{-3}$	8.79×10^6 dynes/cm ²	$\Delta\sigma = \Delta\delta\lambda \frac{a}{g} = 4.55 \times 10^{-2}$
Strength of incompetent layer	3.0×10^4 dynes/cm ²	4.62×10^6 dynes/cm ²	$\sigma = 6.5 \times 10^{-3}$	6.6×10^5 dynes/cm ²	$\Delta\sigma = 4.55 \times 10^{-2}$
Acceleration or body force per unit mass	$a = 12.75 \times 10^5$ cm/sec ²	$g = 9.81 \times 10^2$ cm/sec ²	$\gamma = 1.3 \times 10^3$	$g = 9.81 \times 10^2$ cm/sec ²	
Time	1.86×10^3 sec	4.02×10^{13} sec	$\tau = \psi\sigma^{-1} = 4.62 \times 10^{-11}$	2.82×10^{14} sec	$\tau' = \psi\Delta\sigma^{-1} = 6.6 \times 10^{-12}$

by the exact relation between the densities of the various overburden layers. This condition makes it unsafe to attempt adjustment of rate of motion and time ratio in cases where the original and the experimental model are not similar with respect to density distribution. With this prewarning we shall venture to make a rough recalculation of the ratio of time between the model and a natural situation which is similar to the experimental model in terms of geometry but not in terms of density distribution.

The buoyant force acting on the dome is related to the density contrast between the overburden and the dome. We want therefore to ascertain that the model ratio of density contrast between each of the two kinds of overburden rock and the salt is the same, and moreover that this same model ratio holds for the contrast between the mean density of the overburden and the density of the salt. By doing so we are approaching similarity as close as we can in lack of model materials with the correct-to-scale densities. If we arbitrarily chose 2.4 g/cm^3 as the mean density of the natural overburden the densities of the two sets of rock strata in the overburden are given by two simultaneous equations:

$$\frac{d_1 - 2.2}{1.7 - 1.1} - \frac{d_2 - 2.2}{1.9 - 1.1} = 0, \text{ and} \quad (9)$$

$$\frac{1}{2}d_1 + \frac{1}{2}d_2 = 2.4 \text{ g/cm}^3, \quad (10)$$

where d_1 is the density of the competent layers and d_2 of the incompetent layers.

The first equation requires that the model ratio of density contrast between overburden and dome be the same for the two types of materials in the overburden. The second equation states that the mean density of the sediments in the overburden be 2.4 g/cm^3 . We remember that the layers have equal thickness and the two sets occur in equal number. Solving for d_1 and d_2 gives values as shown in Table 3.

The model ratio of density contrast between overburden and salt is then $\Delta\delta = 3.5$ for both kinds of overburden layers as well as for the mean density of the overburden.

Because of the increased ratio of density contrast the model ratio of strength has increased to

$$\Delta\sigma = \Delta\delta\lambda\frac{a}{g} = 3.5 \times 10^{-5} \times 1300 = 4.55 \times 10^{-2}, \quad (11)$$

and the model ratio of time has correspondingly decreased to

$$\tau = \psi\Delta\sigma^{-1} = 3 \times 10^{-13} / 4.55 \times 10^{-2} = 6.6 \times 10^{-12}. \quad (12)$$

Hence the evolution of the model which occurred in the course of 1.8×10^3 seconds corresponds to a similar evolution of the geologic structure in the course of 2.82×10^{14} seconds or about 8.8 million years. It appears then that the increased viscosity and strength of the layered overburden has brought us closer to a true scale model of salt-dome evolution.

Model B:—In this model the overburden of modelling clay and painter's putty was made more thin-layered than in the model above. Such a construction probably represents a more realistic replica of many dome-type structures. The thin-layered overburden behaves more as a uniform body with viscosity and strength intermediate between those of the two sets of layers. Domes rising through a thin-layered overburden are apt to be more regular in shape than those formed in the model described above.

The overburden of the model consisted of alternating layers of modelling clay and painter's putty, 7 layers of each set. The layers of putty were about 3 mm thick and the layers of modelling clay 1.2 mm thick on an average.

The source layer of bouncing putty which were placed on the bottom of the centrifuge cup was 2 mm thick. Painter's putty was in direct contact with the source layer and a sheet of modelling clay finished the column at the top.

After 21 minutes' run in the centrifuge at an acceleration corresponding to 1000 times the acceleration due to gravity the bouncing putty had penetrated the overburden and started to spread out underneath the top sheet of modelling clay as shown in Fig. 3.

Under the assumption that the bouncing putty represents salt and that the model ratio of length is 10^{-5} the properties of a hypothetical geologic structure which is geometrically and kinematically similar to the model are reported in Table 4.

Adjustment of time ratio and ratio of strength to a natural structure with a mean overburden density of 2.4 is done in the manner described under Model A. The relation

$$\frac{d_1 - 2.2}{1.7 - 1.1} = \frac{d_2 - 2.2}{1.9 - 1.1} \quad (13)$$

leads to constant model ratio of density contrast between doming material and the two unlike materials respectively, of the overburden. d_1 is the density of the set of competent, and d_2 that of the set of incompetent rock strata. Since the ratio of thickness of competent and incompetent layers is 1.2/3, and both sets occur with the same number of layers, the relation

$$\frac{1.2d_1 + 3d_2}{4.2} = 2.4 \text{ g/cm}^3 \quad (14)$$

requires that the mean density of the overburden be 2.4 g/cm³.

Solving for d_1 and d_2 gives 2.361 g/cm³ and 2.416 g/cm³ respectively, for the two types of rocks in the overburden. The corresponding model ratio of density contrast is 3.70 as given in Table 4. The consequent model ratios of strength and of time are given in the table together with the adjusted strengths of the overburden rocks and the adjusted time of evolution of the geologic structure. The time is somewhat less than the time of the geologic structure

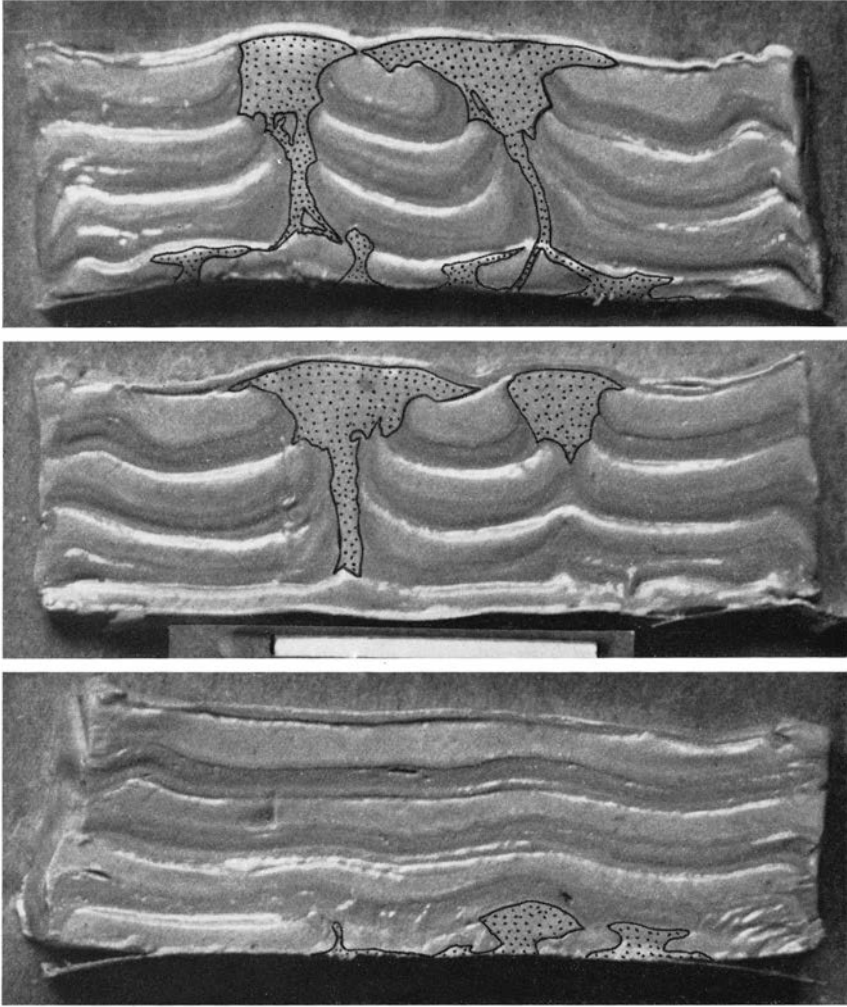


Fig. 3. Slices cut through model of bouncing-putty domes (dotted) in layered overburden of painter's putty (light grey layers and thick dark grey layers) and modelling clay (dark grey sheets on the top, and at the boundaries between the dark and light grey layers of putty).

based upon model *A*. This is to be expected because the average strength of the overburden is greater and its viscosity higher in model *A*.

A model with relatively strong overburden

In the models described above the rise of the domes was too fast to fit geologic structures of similar geometry. The chief reason for the lack of time conformity between models and reality is probably that the overburden is too weak and too fluid even in the models with the putty—modelling clay interlayered overburden.

Table 4.

	Experimental model	Hypothetic geologic structure	Model ratios	Realistic geologic structure	Modified ratios
Dome diameter	variable	variable	$\lambda = 10^{-5}$	variable	
Dome height	29.5 mm	2950 m	$\lambda = 10^{-5}$	2950 m	
Source-layer thickness	2.0 mm	200 m	$\lambda = 10^{-5}$	200 m	
Competent layer thickness	1.2 mm	120 m	$\lambda = 10^{-5}$	120 m	
Incompetent layer thickness	3.0 mm	300 m	$\lambda = 10^{-5}$	300 m	
Density of source layer	1.1 g/cm ³	2.2 g/cm ³	$\delta = 0.5$	2.2 g/cm ³	
Density of competent layer	1.70 g/cm ³	3.4 g/cm ³	$\delta = 0.5$	2.361 g/cm ³	
Density of incompetent layer	1.90 g/cm ³	3.8 g/cm ³	$\delta = 0.5$	2.416 g/cm ³	
Density contrast between source and competent layer	0.6 g/cm ³	1.2 g/cm ³		0.161 g/cm ³	$\Delta\delta = 3.7$
Density contrast between source and incompetent layer	0.8 g/cm ³	1.6 g/cm ³		0.216 g/cm ³	$\Delta\delta = 3.7$
Mean density contrast	0.74 g/cm ³	1.48 g/cm ³		0.2 g/cm ³	$\Delta\delta = 3.7$
Viscosity of source layer	3.0×10^5 poises	10^{18} poises	$\psi = 3.0 \times 10^{-13}$	10^{18} poises	
Viscosity of competent layer	2.0×10^5 poises	6.67×10^{20} poises	$\psi = 3.0 \times 10^{-13}$	6.67×10^{20} poises	
Viscosity of incompetent layer	7.0×10^5 poises	2.33×10^{18} poises	$\psi = 3.0 \times 10^{-13}$	2.33×10^{18} poises	
Strength of competent layer	4.0×10^5 dynes/cm ²	8.0×10^7 dynes/cm ²	$\sigma = \delta\lambda \frac{a}{g} = 5 \times 10^{-3}$	1.08×10^7 dynes/cm ²	$\Delta\sigma = \Delta\delta\lambda \frac{a}{g} = 3.7 \times 10^{-2}$
Strength of incompetent layer	3.0×10^4 dynes/cm ²	6.0×10^6 dynes/cm ²	$\sigma = 5 \times 10^{-3}$	8.11×10^5 dynes/cm ²	$\Delta\sigma = 3.7 \times 10^{-2}$
Acceleration of body force per unit mass	9.81×10^5 cm/sec ²	9.81×10^2 cm/sec ²	$\gamma = 10^3$	$g = 9.81 \times 10^2$ cm/sec ²	
Time	12.6×10^2 sec	2.1×10^{13} sec	$\tau = \psi\sigma^{-1} = 6 \times 10^{-11}$	1.55×10^{14} sec	$\tau' = \psi\Delta\sigma^{-1} = 8.11 \times 10^{-12}$

There is a limit to the yield strength which the overburden may have. If it is too strong domes are unable to rise from given irregularities because the buoyant punching force created by the irregularities may not be sufficient to build up stresses capable to overcome the yield strength of the overburden material.

The modelling clay has a viscosity which is related to that of the dome-imitating putty in a manner which give a reasonable viscosity of the overburden in corresponding geologic structures, viz. ca. 10^{20} poises. The strength of the modelling clay corresponds to a strength of natural overburden which also seems reasonable, viz. ca. 10^7 dynes/cm². This is exactly the order of magnitude assigned to the strength of sedimentary overburden by PARKER *et al.*, op. cit. p. 2400. However, a simple calculation indicates that the strength of this magnitude may be too high to fit conditions assumed to exist in salt-dome regions. The maximum punching stress across the top of a dome of height h is

$$\sigma_p = (2.4 - 2.2)hg \text{ dynes/cm}^2 \quad (15)$$

if 2.4 g/cm^3 is selected as the density of the overburden. The punching strength of a substance—i.e. the force per area needed to make an anelastic impression on the surface of a body which is large in relation to the diameter of the impression—is considerably greater than the strength under simple uniaxial compression. The modelling clay, for example, showed between 5 and 10 times as high punching strength as its strength under simple uniaxial compression. If we assume that the punching strength of the rock overburdens also is about 5 to 10 times their strength under uniaxial compression, the rock which corresponds to modelling clay has a punching strength in the order of 10^8 dynes/cm². The minimum height of an initial dome which is able to ascend through an overburden with this strength is determined by the relation below which follows from eq. (15)

$$h = \frac{10^8 \text{ dynes/cm}^2}{(2.4 - 2.2) \text{ g/cm}^3 \cdot 981 \text{ dynes/g}} \approx 5 \times 10^5 \text{ cm} = 5000 \text{ m.} \quad (16)$$

This seems quite an unreasonable minimum height for an initial irregularity capable to develop into a dome. It is probably two orders of magnitude too large. It appears then that the modelling clay is too strong to represent a realistic rock overburden. The test reported below shows that this conclusion is correct.

In the discussion above we have disregarded the thickness of the overburden which is an important factor in determining its punching strength. Now the punching strength increases with increasing thickness only until the thickness reaches a certain limit. At greater thickness its variation is consequently of no significance for the punching strength. This thickness limit depends upon the diameter of the punching dome and the mechanical properties of the overburden. For the materials used in the models described here the punching

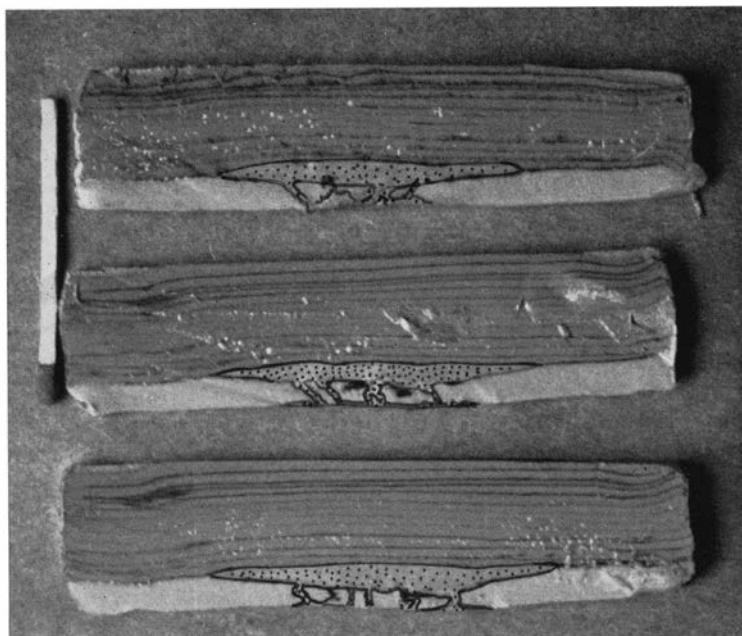


Fig. 4. Slices cut through model of subsurface "dome" or "sill" of bouncing putty (dotted) under overburden of layered modelling clay (dark grey). Light grey bottom layer consists of painter's putty through which the doming material has ascended, see text.

strength of the overburden is not significantly effected by the thickness if the latter is more than about 5 times the diameter of the dome.

Description of the model:—A 2 mm layer of bouncing putty was placed in the center of the bottom of the centrifuge cup with a ring of painter's putty occupying the rest of the area. This base layer was covered with a 4 mm thick layer of painter's putty on the top of which a stack of sheets of modelling clay was placed. This stack consisted of 12 individual sheets with markers of wet paint between, the whole column being about 14 mm thick.

The bottom layer of painter's putty was put on in order to facilitate initiation of domes because the smallest irregularity on the surface of bouncing putty seems to be able to initiate doming in an overburden of painter's putty. Indeed it has not been possible to prevent doming in putty overburden by making the subjacent source layer as even as our somewhat crude technique permits. The reason for the ease at which domes initiate in putty overburden is found in the almost vanishing strength of painter's putty under the initial period of strain as mentioned on p. 6.

The initial domes formed in the layer of painter's putty immediately above the source layer would be 4 mm high before reaching the modelling clay overburden. With a model ratio of length of 10^{-5} the 4 mm initial domes correspond

to 400 m high domes in nature. Initial domes of this size would probably encounter no great difficulty in continuing to force their way up through most sedimentary overburdens.

This model was run in the centrifuge at 1700 *g* for 41 minutes without dome structures visible on the surface. As there were no visible motion of the surface at all through the last part of the run—i.e. no variation of level—it was believed that the model had reached a certain state of equilibrium. The run was discontinued and the model cut and photographed, see Fig. 4.

It appeared that the source layer of imitation salt had moved up through the bottom layer of putty and assembled itself as a lenticular body underneath the column of sheets of modelling clay. A very gentle anticlinal bending of the modelling clay overburden was caused by the lenticular shape of the bouncing putty, but there was no tendency for the latter to penetrate the overburden in the form of domes.

Hence it seems that the strength of modelling clay is too high for domes to form under conditions described above.

The structure in the painter's putty underneath the lense of bouncing putty is quite interesting. It consists of an irregular network of thin veins of bouncing putty, the thickness of the veins being only a fraction of one mm. These are the remnants of the bouncing putty which passed through the painter's putty when the layers exchanged places.

Models of injection of magma as caused by buoyant forces

The viscosity of the solid earth has been estimated to about 10^{22} poises by HASKELL (1935) and others. If we accept this value for an average crystalline rock in the earth's crust, and want to use the modelling clay described above (p. 6) as rock-imitation material the model ratio of viscosity is

$$\psi = \frac{2 \times 10^8}{10^{22}} = 2 \times 10^{-14}. \quad (17)$$

If we wish to include magmas in our models we find that even water is much too viscous to represent most silicate melts. Viscosities of some magmas and glasses are shown in Table 5. A fluid which in the model would correspond to Hawaii flow, for example, must have a viscosity coefficient determined by

$$\mu_m = \mu_0 \psi = 4.3 \times 10^4 \text{ poises } 2 \times 10^{-14} = 8.6 \times 10^{-10} \text{ poises}, \quad (18)$$

which is less than the viscosity of gasses at standard conditions.

A model material suited to represent obsidian at 800°C, which is the most viscous among silicate glasses or melts, must have a viscosity given by

$$\mu_m = 10^{12} \text{ poises } 2 \times 10^{-14} = 2 \times 10^{-2} \text{ poises}. \quad (19)$$

This is only twice the viscosity of water at 20°C.

Table 5. Viscosities of silicate melts from WAHLSTRÖM, 1950, p. 224.

Magma	Temperature in degree centigrades	μ in poises
Diabases	1400	15-400
Olivine basalt	1150	37,900
	1200	3,180
	1300	296
	1400	127
Obsidian	800	10^{11} - 10^{12}
	1000	10^9 - 10^{10}
	1200	10^7 - 10^8
Hornblende granite	1400	2×10^6
Hawaii flows		$4.3 - 4.77 \times 10^4$

It would be rather difficult to work with materials more fluid than water in the models, hence the experiments were limited to a study of the behavior of an aqueous solution (representing a very viscous silicate melt or glass) in modelling clay and putty (representing solid rocks).

Description of a model:—A 3.2 mm thick ring of painter's putty was placed on the bottom of the centrifuge cup, the central hole being 40 mm in diameter and the outer diameter of the ring 94 mm which coincides with the diameter of the cup. The hole was filled with a concentrated solution of KMnO_4 . Such a solution gives a brown stain when it comes in contact with putty or modelling clay and thus leaves a mark where it passes the overburden even if the liquid itself is completely squeezed out.

The overburden consisted of 6 sheets of modelling clay about 1.2 mm thick interlayered with 7 sheets of painter's putty 3 mm thick, the complete column being 30 mm high.

The model was run at 700 rpm corresponding to an acceleration of 210 *g* for 4.5 minutes in the centrifuge. The KMnO_4 "magma" penetrated the surface sometime between 3 and 4.5 minutes after the run was started. The fact that much fluid remained in lenticular pockets (secondary "magma" chambers) below several of the modelling clay layers when the run was discontinued after 4.5 minutes (Fig. 5) indicates that the liquid pierced the surface only a few seconds before the run was discontinued. (Experience from several other runs with fluids enclosed in putty and modelling clay shows that all the enclosed fluid will be squeezed out in the course of a few seconds after piercing the surface.) After 3 minutes' run there were no penetration of the surface although a dome-shaped elevation had developed showing that the "magma" was on the way up through the layered overburden and probably was temporarily trapped below some of the relatively strong sheets of modelling clay. The time needed

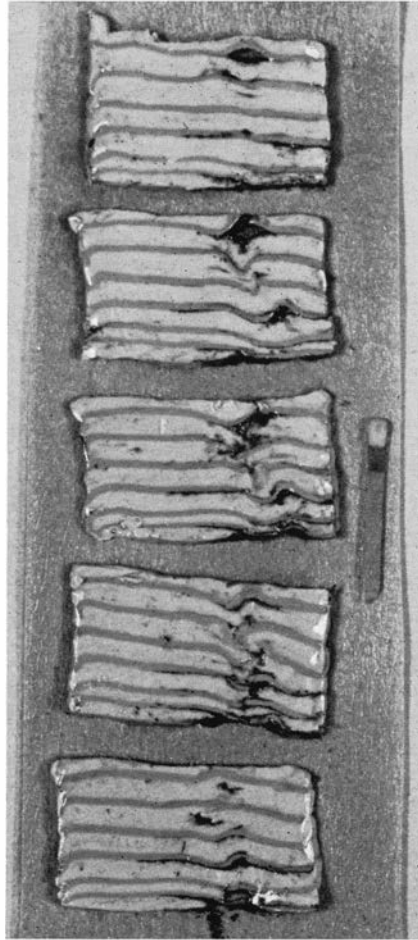


Fig. 5. Slices about 2 mm thick cut through model of painter's putty (light grey) and modelling clay (dark grey) through which a solution of KMnO_4 have ascended; see explanation in text above. The black lenticular and irregular areas are chambers and openings in the overburden lined with a stain of manganese oxide from the ascending solution. Sections Nos. 3 and 4 from top contain the main vent for the solution, note strong deformation and fracturing of the competent modelling clay layers. Length of cuts covers only half the diameter of the model.

for the "magma" to rise through the 30 mm thick overburden is then 3.75 ± 0.75 minutes.

Let us scale the model up to geologic dimensions by assuming that the initial magma chamber was located at the bottom of the continental crust at 30 km below the surface. This fixes the model ratio of length to 10^{-6} which gives the dimensions of the layers in the crust and the magma chambers etc. as shown in Table 6.

The density of the KMnO_4 -solution is 1.05 g/cm^3 , and the density of an obsidian melt may be taken as 2.4 g/cm^3 . The average density of the model overburden is approximately

Table 6.

	Experimental model	Hypothetic geologic structure	Model ratios	Realistic geologic structure	Modified ratios
Thickness of overburden or earth's crust	29.6 mm	29,600 m	$\lambda = 10^{-6}$	29,600 m	
Thickness of competent layers	1.2 mm	1,200 m	$\lambda = 10^{-6}$	1,200 m	
Thickness of incompetent layers	3.2 mm	3,200 m	$\lambda = 10^{-6}$	3,200 m	
Thickness of initial magma chamber	3.2 mm	3,200 m	$\lambda = 10^{-6}$	3,200 m	
Length of initial magma chamber	40 mm	40,000 m	$\lambda = 10^{-6}$	40,000 m	
Max. diameter of present chambers	10 mm	10,000 m	$\lambda = 10^{-6}$	10,000 m	
Average density of crust	1.85 g/cm ³	2.8 g/cm ³	$\delta = 0.66$	2.8 g/cm ³	
Density of magma	1.05 g/cm ³	1.59 g/cm ³	$\delta = 0.66$	2.4 g/cm ³	
Viscosity of competent layers	2×10^8 poises	10^{22} poises	$\psi = 2 \times 10^{-14}$	10^{22} poises	
Viscosity of incomp. layers	7×10^8 poises	3.5×10^{19} poises	$\psi = 2 \times 10^{-14}$	3.5×10^{19} poises	
Viscosity of magma	10^{-2} poises	5×10^{11} poises	$\psi = 2 \times 10^{-14}$		
Strength of competent layers	4×10^5 dynes/cm ²	2.9×10^9 dynes/cm ²	$\sigma = \delta\lambda \frac{a}{g} = 1.39 \times 10^{-4}$	9.5×10^8 dynes/cm ²	$\Delta\delta\lambda \frac{a}{g} = 4.2 \times 10^{-4}$
Strength of incompetent layers	3×10^4 dynes/cm ²	2.16×10^8 dynes/cm ²	$\sigma = \delta\lambda \frac{a}{g} = 1.39 \times 10^{-4}$	7.15×10^7 dynes/cm ²	
Body force per unit mass, or acceleration	$a = 2.06 \times 10^5$ cm/sec ²	$g = 9.81 \times 10^8$ cm/sec ²	$\gamma = 210$	9.81×10^8 cm/sec ²	$\tau' = 4.8 \times 10^{-11}$
Time	2.25×10^2 sec	1.56×10^{12} sec	$\tau = \psi\sigma^{-1} = 2.44 \times 10^{-10}$	4.7×10^{12} sec	
Density contrast between magma and average crust	0.80 g/cm ³	1.21 g/cm ³		0.4 g/cm ³	$\Delta\delta = 2.0$

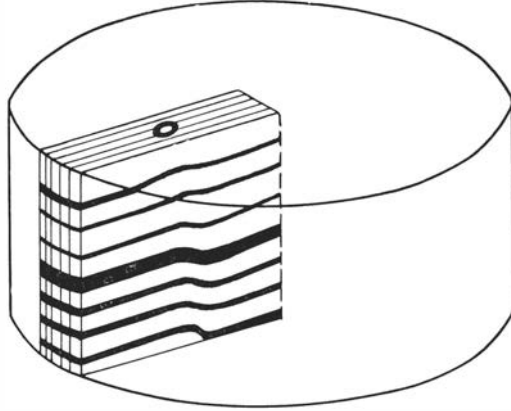


Fig. 6. Sketch showing how the cuts in Fig. 5 are situated in the model.

$$d_{\text{ave}} = \frac{1.70 \text{ g/cm}^3 \cdot 0.12 \text{ cm} + 1.90 \text{ g/cm}^3 \cdot 0.3 \text{ cm}}{0.42 \text{ cm}} = 1.85 \text{ g/cm}^3. \quad (20)$$

The average density of the earth's continental crust down to 30 km may be taken as 2.8 g/cm^3 .

Hence the model ratio of density contrast is

$$\Delta\delta = \frac{1.85 - 1.05}{2.8 - 2.4} = 2.0, \quad (21)$$

which gives a model ratio of buoyant stress

$$\Delta\sigma = \Delta\delta \lambda \frac{a}{g} = 2 \times 10^{-6} \cdot 2.1 \times 10^2 = 4.2 \times 10^{-4}. \quad (22)$$

The model ratio of time is consequently

$$\tau = \psi \Delta\sigma^{-1} = 2 \times 10^{-14} / 4.2 \times 10^{-4} = 4.8 \times 10^{-11}. \quad (23)$$

The time required for the obsidian magma or glass to rise to the surface from the magma chamber at 30 km depth is accordingly

$$t_0 = \frac{t_m}{\tau} = (225 \pm 45) \text{ seconds} \frac{1}{4.8} 10^{11} = (4.7 \pm 1) 10^{12} \text{ seconds} \quad (24)$$

$$\approx 150,000 \text{ years.}$$

This, perhaps, seems not an unreasonable figure.

General features of domes and related bodies in models

Initiations of domes

Domes and similar structures as formed by buoyancy of a light substance in heavy surroundings develop readily in models accelerated in centrifuges. If

a layer of stitching wax or bouncing putty, whose densities are 1.01 g/cm^3 and 1.12 g/cm^3 respectively, is placed under an overburden of painter's putty with density 1.90 g/cm^3 , domes or stocks rise through the overburden and pierce the surface after a few minutes' run at about $1000 g$ in a centrifuge.

When painter's putty is used as overburden, or a layer of stratified column containing both painter's putty and modelling clay, then domes will form even if all layers were made as smooth and even as possible. This haphazard initiation of domes is apparently determined by minute unpredictable irregularities in the initial models. This is understandable in view of the fact that stitching wax and bouncing putty, both used as source material, have zero or at least vanishingly small yield strength, and that the strength of the painter's putty also is negligible during the initial periode of deformation (see discussion of this point on p. 23). Thus the punching stress across the top of a small bump needed to make it start growing and develop into a dome is vanishingly small.

Not until protuberances from the source layer have penetrated a moderate distance into the putty overburden, does the local strain make the putty strain-harden and develop a certain yield strength. But at this moment the initial domes have reached a height, h , which appears to be sufficient to give a punching stress, σ_p , across the top of the domes somewhat greater than the punching strength of the hardened putty. The punching strength of hardened putty measured on slabs thicker than the critical thickness (p. 22) is about $1.4 \times 10^5 \text{ dynes/cm}^2$. The punching stress executed by an initial dome of stitching wax h cm high is

$$\sigma_p = (1.9-1.0) \text{ g/cm}^3 \cdot h \text{ cm} \cdot 9.81 \times 10^5 \text{ dynes/g}, \quad (25)$$

where 1.90 g/cm^3 and 1.0 g/cm^3 are the densities of putty and stitching wax respectively, and $9.81 \times 10^5 \text{ dynes/g}$ is the acceleration in the centrifuge run at $1000 g$. In order that a dome h cm high shall grow, the punching stress must exceed $1.4 \times 10^5 \text{ dynes/cm}^2$. Hence the minimum value of h is given by

$$h > \frac{1.4 \times 10^5 \text{ dynes/cm}^2}{0.9 \times 9.81 \times 10^5 \text{ dynes/cm}^3} = 0.16 \text{ cm}. \quad (26)$$

That is the initial minute irregularities along the boundary between source layer and overburden must be able to grow to a height of some 1.6 mm before the putty adjacent to the embryonal domes becomes hardened enough to acquire its maximum punching strength of $1.4 \times 10^5 \text{ dynes/cm}^2$. If the putty hardens before the domes reach 1.6 mm further growth is theoretically not possible under the conditions described above.

(Incidentally, if the model was at rest in the field of gravity of the earth rather than run in a centrifuge at $1000 g$, the minimum height of a dome capable of growing would be $h > (1.4 \times 10^5 \text{ dynes/cm}^2)/(0.9 \times 981 \text{ dynes/cm}^3) = 159 \text{ cm}$.

This simple calculation demonstrates one of the many advantages of the centrifuge technique: for given materials models run in centrifuges may be

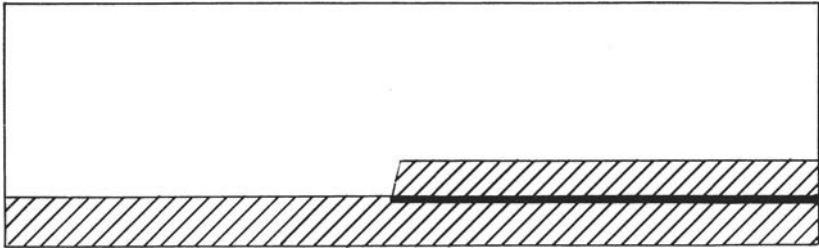


Fig. 7. Initial arrangements in model with layer of stitching wax (hatched) below painters putty. Black layer in wax is modelling clay. Doming starts at step in source layer.

made much smaller than geometrically similar models at rest in the gravitational field of the earth.)

The above-described haphazard initiation of domes may be suppressed by making arrangements in the initial models which cause domes to grow at predetermined sites.

Local thickening of the source layer or thinning of the overburden represent obvious sites of dome initiation and growth.

Abrupt variations of thickness of either overburden or source layer generally initiate domes along the discontinuity, Fig. 7. An abrupt change in density has the same effect. If an extra layer of some material is placed on top of the overburden domes tend to form directly below the edge of the extra layer, as shown in Figs. 25 and 29.

In many models the source layer of bouncing putty or stitching wax covered only a part of the bottom of the centrifuge cup. In such cases domes would almost without exceptions develop at the edge of the source layer, such as shown in Figs. 27 and 28. This happened invariably when the doming material was very fluid relative to the overburden; for example, when an aqueous solution was placed in a flat circular chamber underneath an overburden of putty and/or modelling clay. The fluid would burst out from a point somewhere along the edge of the chamber, see Figs. 5 and 40.

That domes tend to form along discontinuities in overburden load or in thickness of source layer is related to the rather abrupt increase of the horizontal pressure gradient across such discontinuities. The steep horizontal component of the pressure gradient at the discontinuities gives maximum rate of flow in the source layer at these localities, the flow being directed out from underneath the extra load. As a consequence a local bulge develops in the source layer just outside the edge of the load provided the overburden is not rigid. In a non-rigid overburden some flow extends out from the region above the marginal bulge in the source layer. The local thinning of the overburden makes it possible for domes to protrude from the bulge as demonstrated in many models, Fig. 29.

The material in the marginal bulge and domes is chiefly taken from the source

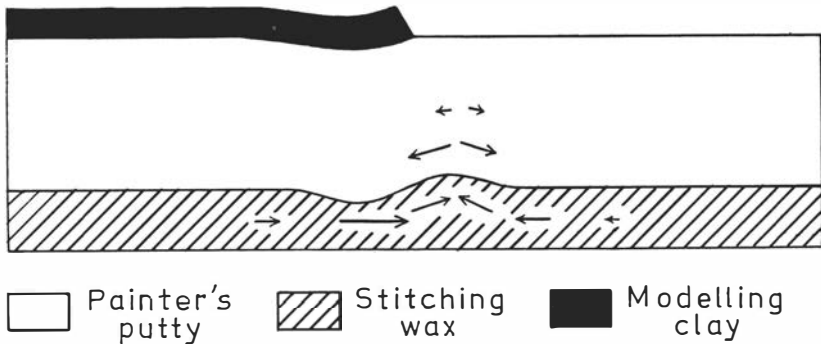


Fig. 8. Initiation of bulge underneath the edge of excess overburden. Flow lines indicated by arrows.

layer underneath the loaded overburden where pressure is highest. The most pronounced marginal sink therefore develops inside the edge of the extra load on the overburden. A smaller marginal sink forms on the opposite side of the bulge and domes, showing that material is supplied to the domes also from the part of the source layer which exists outside the loaded overburden. This is understandable because at the moment a bulge have formed for some reason or other the pressure in the bulge becomes less than the pressure at the same level in the source layer also outside the loaded part of the overburden. Fig. 8 indicates the flow pattern in the model.

Behavior of competent layers embedded in dome-forming material

When domes rise from a horizontal sheet-shaped layer the magnitude of extensive and compressive strains may easily reach several hundred percent. Centripetal convergent flow predominates in the source layer around the dome and extension flow generally occurs along the axis of the dome. If competent sheets are embedded in the source layer they will buckle or rupture depending upon the character of the flow in the adjacent part of the doming material.

The centripetal convergent flow in the source layer around an active dome represents a shortening parallel to the circumference and a lengthening in direction of the radius. Embedded competent sheets consequently are exposed to stresses which tend to make the sheets buckle about a fold axis which coincides with the radius in the region just outside the root of the dome. Within the dome itself the geometry of strain is essentially a quasi-uniform compression in the plane normal to the axis and a uniaxial extension parallel to the axis of the dome. This geometry of strain creates buckling of embedded competent sheets with fold axis oriented along the axis of the dome.

BALK (1949) has made an excellent study of such folds of embedded strata in the Grand Saline dome in Texas. ESCHER *et al.* (1929) have reproduced similar structures by extruding multilayered bodies through a circular hole in a stiff

plate. In these experiments the flow of the dome-imitating material was not generated by buoyant forces in the field of gravity or in a field of acceleration (e.g. in a centrifuge) but simply by putting pressure on the stiff plate. Models formed under such conditions are of course not at all kinematically similar to domes formed by buoyancy, and it is unsafe to consider experimental flow pattern of this kind representative of the flow pattern of natural domes formed by buoyant forces.

Some details of the flow pattern in domes were also indicated by deformed air bubbles in the experimental domes studied by NETTLETON *op. cit.*

Observations pertaining to the flow pattern in domes were also recorded during the study of the writer. Although the observations were less systematic than what seems desirable in hindsight some points of interest will be noted.

A layer of stitching wax about 7 mm thick and containing two 0.5 mm thick sheets of modelling clay was layed down in a centrifuge cup with 44 mm diameter. A 10 mm thick layer of painter's putty was placed as an overburden. To initiate doming at a predetermined site a small bump about 1 mm high was made on the wax surface in the middle of the cup.

After 8 minutes' run at 1300 *g* the dome had pierced the surface and reached stage *E* in Fig. 9.

The two sheets of modelling clay embedded in the stitching wax reflect the flow pattern in the wax in a rather informative manner. In the root portion of the dome, and in its trunk portion (the dome is mushroom-shaped with a distinct hat formed by lateral spreading of the upper part of the dome) the sheets of modelling clay are strongly folded about axes which gradually rotate from almost horizontal position in the outer root regions to vertical in the trunk, Fig. 9 *F*.

In the hat region of the dome the sheets of modelling clay have been stretched beyond their ultimate strength by the spreading of the wax. Numerous inclusions of the fractured sheets of modelling clay occur in this portion of the dome, Fig. 9 *E*.

In the marginal sink just outside the root of the dome the sheets of modelling clay have developed fractures oriented normal to the radius. These are tension fractures formed in response to the extension flow in the wax parallel to the radius, Fig. 9 *F*.

Boudinage-like structures in the region of the marginal sink or in the hat region of model domes were common features. Particularly well developed tension fractures and boudins were seen in a rather large stitching-wax dome made in the 94 mm diameter centrifuge cup, see Fig. 10

Figs. 11 and 12 shows several domes of stitching wax, with embedded sheets of modelling clay, which have spread on the overburden surface after penetration. The centers of penetration are indicated by the numbers I, II, III, IV and V. IV and V are late domes which have barely pierced the surface but not yet started to spread on the surface at the time the run was stopped. The ink-

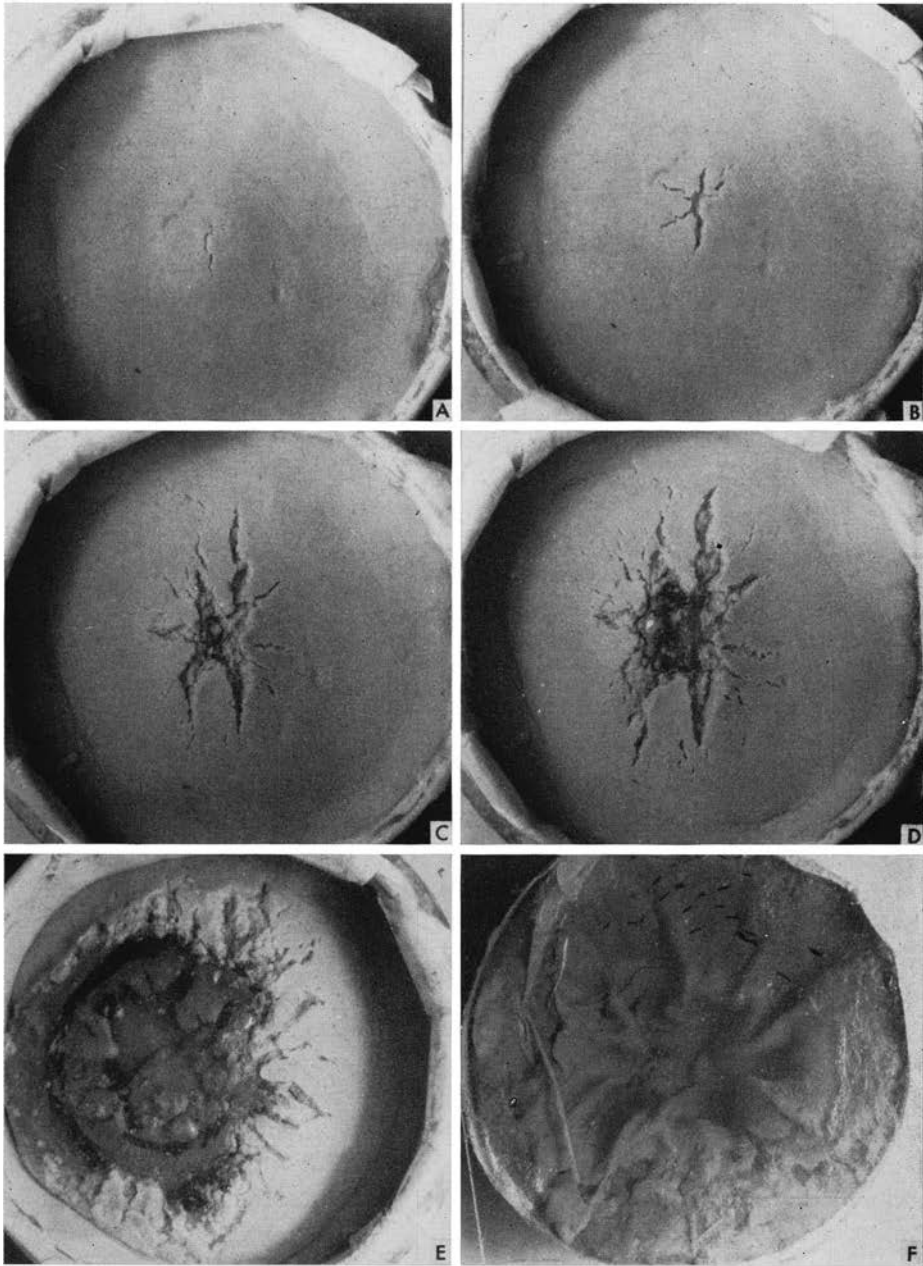


Fig. 9. Stages of evolution of a stitching-wax dome in overburden of painter's putty. Note the two embedded sheets of modelling clay in the transparent wax dome in stage *E*. *F*: Folded pattern of the embedded sheets of modelling clay seen through the transparent wax dome from below. Small tension fractures marked by ink.

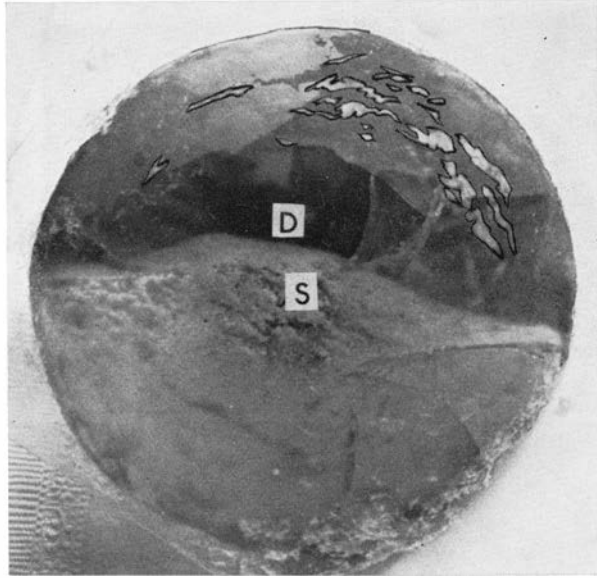


Fig. 10. Same model as shown in Figs. 7 and 23 photographed from below to show tension fractures (outlined with ink) in the embedded sheet of modelling clay in the region of the marginal sink. Dark grey: sheet of modelling clay with tension fractures (white) shown through the bottom layer of transparent wax. Light grey: cover of painter's putty shown through the bottom sheet of stitching wax. *D*: center of dome. *S*: center of marginal sink.

marked curves around points II and III represent the borders which separate the flows from the two centers from the flow extruded from center I.

The light grey structure at center IV is the dome-shaped upper sheet of modelling clay embedded in the transparent stitching wax. In the strongly spread flows around centers I, II and III the same sheets of modelling clay have been torn to widely separated small fragments (light grey bodies of variable size).

The rupturing of the embedded competent sheets and the separation of the fragments, result in structures very similar to some often seen in deep-seated gneissic and granitic rocks. In such rocks the extension flow is of course not due to spreading on a free surface but rather to extension in direction of least resistance in the surroundings. Subsurface spreading of this kind occurred in a number of the models run by the writer. Some examples are described on pp. 55 and 59, and shown in Figs. 32 and 34.

Shape of domes and related structures

Domes of stitching wax and bouncing putty grown from a basement layer into a uniform overburden were rod-shaped or shaped like elongate drops with the thickest part pointing upward. The cross section of most domes formed was circular although oblong shape generally developed in the lower portions

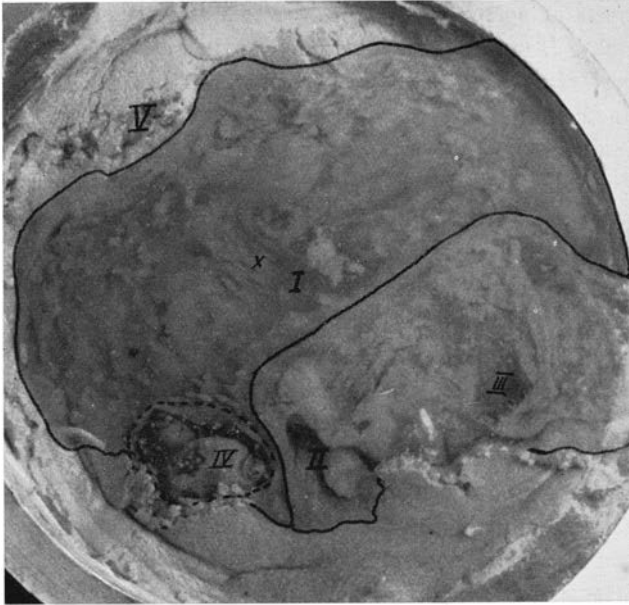


Fig. 11. Domes of transparent stitching wax spread on the surface of painter's putty. I, II and III indicate vents of extrusion. IV marks dome just surfaced (note embedded layer of modelling clay in the transparent wax dome). V marks spot where a small dome has just broken the surface. Grey irregular fragments in flows are remnants of the ruptured sheets of modelling clay embedded in the original source layer of stitching wax, see also text p. 32. Diameter of model 45 mm.

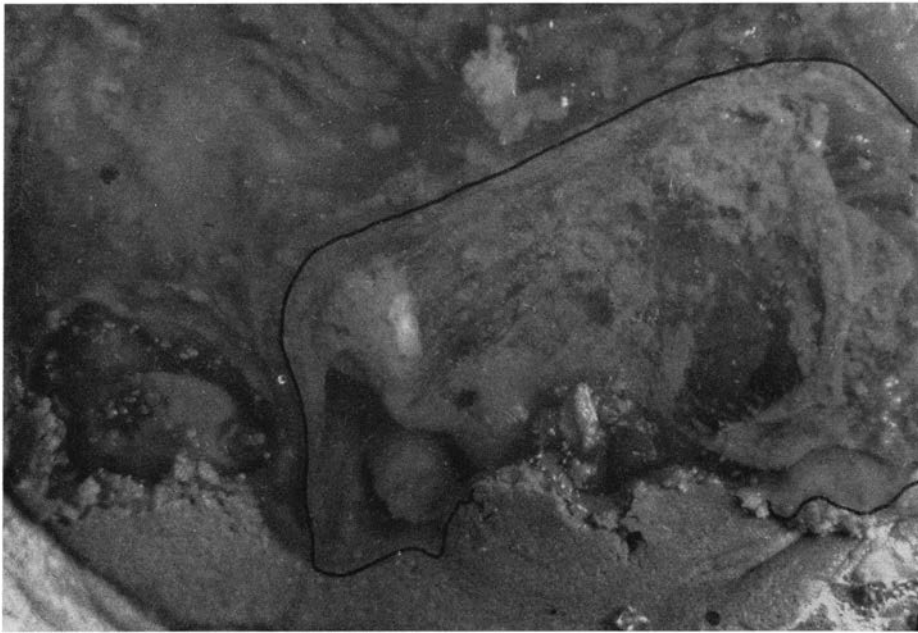


Fig. 12. Details of the fractured sheet of embedded competent modelling clay in the flow around vent III in Fig. 11.

of domes formed along line discontinuities in overburden or source layer, i.e. domes protruding from the marginal bulge in the source layer.

The diameter of the domes was approximately equal to the thickness of the source layer, a condition also noted by PARKER *et al.*, *op. cit.*

The marginal bulge which developed in the source layer along line discontinuities in overburden was, however, considerably thicker than the thickness of the source layer. This observation is of interest in connection with theories of emplacement of batholiths inasmuch as many of these huge plutonic massifs, some of which, at least, rose in response to buoyant forces (see GROUT, 1945), are elongate bodies often situated along line discontinuities in the earth's crust (for example along the continental edge around the Pacific Ocean). The width of elongate batholiths, if such bodies may be compared with the marginal bulge formed in the models, should therefore be considerably greater than the thickness of a possible source layer.

In this connection it is important to realize that the source layer in the model studied was resting on a rigid substratum that could not participate in the flow toward the root region of the domes. In the earth it is more natural to assume that the substratum below potential quartzo-feldspathic source layers is more or less plastic or fluid (that does not mean liquid!). Such substrata will participate in the lateral, centripetal flow toward the root of the ascending domes, although of course not being able to rise with the doming material. This means that the source layer behaves as if it was thicker than it actually is. Thus the rising batholiths, domes, or stocks should display horizontal dimensions that may be much larger than the thickness of the source layer itself. Since batholithic bodies may measure more than 50 km across it would be rather difficult to understand that they rose from a source layer that was roughly equally thick. It is therefore comforting to a defender of the proposed theory to find that the diameter of domes or batholiths may well be greater than the thickness of possible source layers, even if the exposed level is below the near-surface portion of the body that generally tends to spread laterally as demonstrated by a number of experiments described in this paper.

Domes grown in layered overburden showed structures similar to laccoliths, lopoliths, funnels and sills. Examples of such bodies are illustrated in Figs. 3, 32, 34 and 38. Structural patterns exhibited by these bodies were all developed due to lateral spreading either underneath strong sheets in the overburden, underneath or within layers with lower density than the doming material or within the region of low pressure close to the surface of the overburden.

Structures in overburden adjacent to domes

Beside the marginal sinks the most striking deformation structure in overburden adjacent to domes is the bending of horizontal layers caused by drag along the boundary between dome and surroundings. Such drag effects show

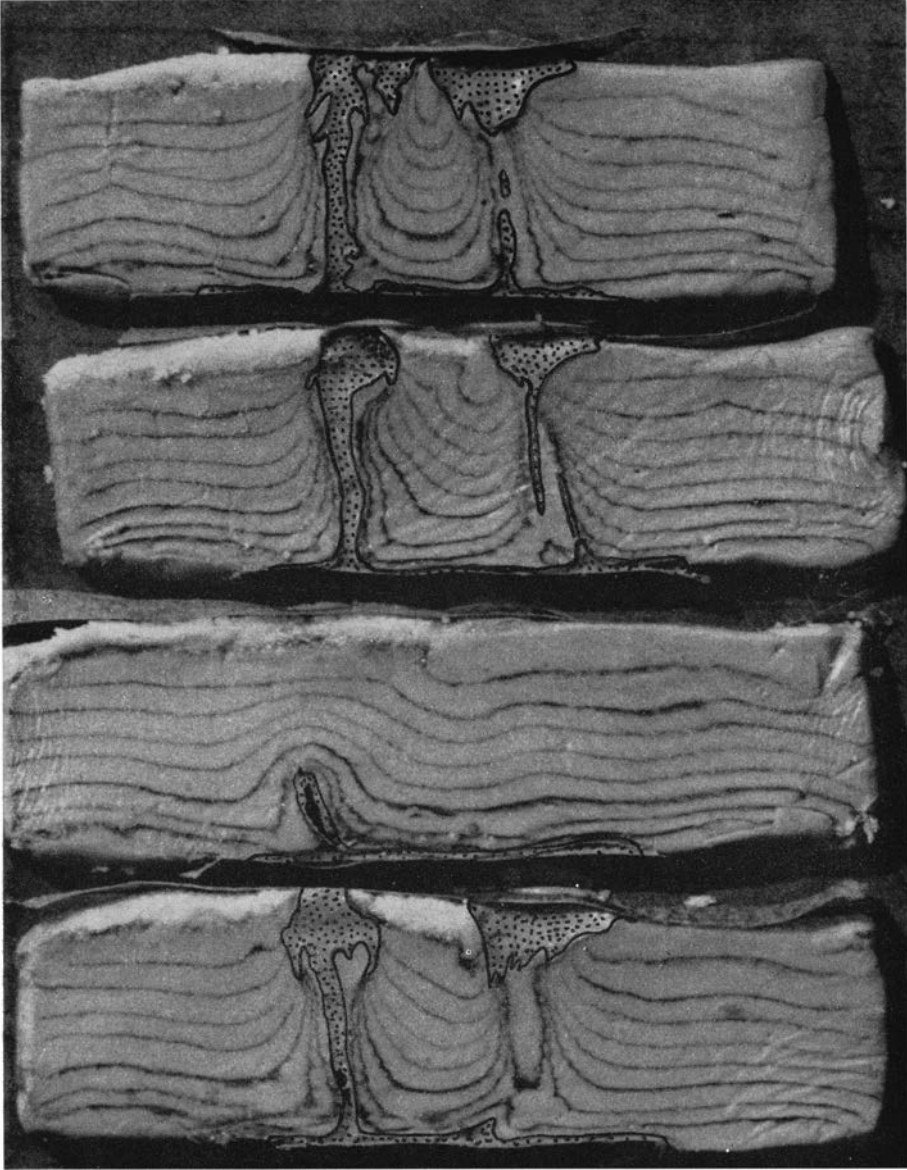


Fig. 13. Cuts through model of domes (dotted) which have risen through multilayered overburden of painter's putty and a surface layer of powdered wax (white granular stuff on upper left side). Dark curved lines are originally plane markers of paint in the putty.

up excellently in models with horizontal markers placed in the initial stage, Figs. 13, 14 and 34.

The less strong and the less viscous the overburden relative to the material of the dome the more intensive the deformation in the contact region. For example, an overburden of painter's putty alone is more intensively deformed

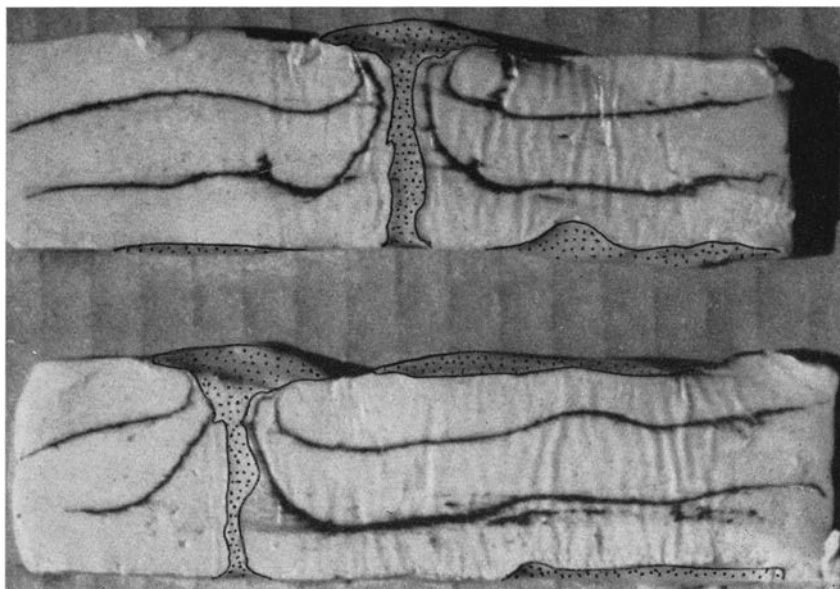


Fig. 14. Model similar to 13, but without surface layer of wax. Diameter of model 94 mm.

adjacent to domes of bouncing putty than overburdens strengthened by embedded layers of modelling clay, compare Figs. 13 and 2.

An overburden of painter's putty is so weak relative to domes of bouncing putty that layers from the bottom of the overburden are pulled up and dragged along the surface by the spreading top portion of the dome. This movement is shown by marker planes in the overburden, Fig. 13.

Domes which pierce the surface of layered overburden often invert the surrounding strata and make the layers dip toward the center of the funnelshaped intrusions. An example of this structure, as shown in Fig. 3, is strikingly similar to the Vredefort granite dome in South Africa (DuToit, 1954, p. 68), Fig. 15.

According to model tests of flow of magmas in solid surroundings (see p. 59) it seems not possible that inverted structures of this kind can develop if the viscosity contrast between overburden and intruded material approaches the strong contrast between crystalline rocks (10^{20} – 10^{22} poises) and silicate melts of even the most viscous type, viz. an obsidian at low temperature (10^{12} poises). Since the Witwatersrand and Ventersdorp rocks adjacent to the Vredefort massif unquestionably were crystalline when the dome rose we are led to the conclusion that the intruded material either was completely crystalline or that it consisted of a mush with so little liquid material that the strength and viscosity of the body approached that of the surrounding solid rocks.

On the map of the area reproduced in DuToit's book the region around the dome is marked "Extremely Deep Syncline". This supports the conclusion that the Vredefort dome rose due to buoyant forces acting on a more or less

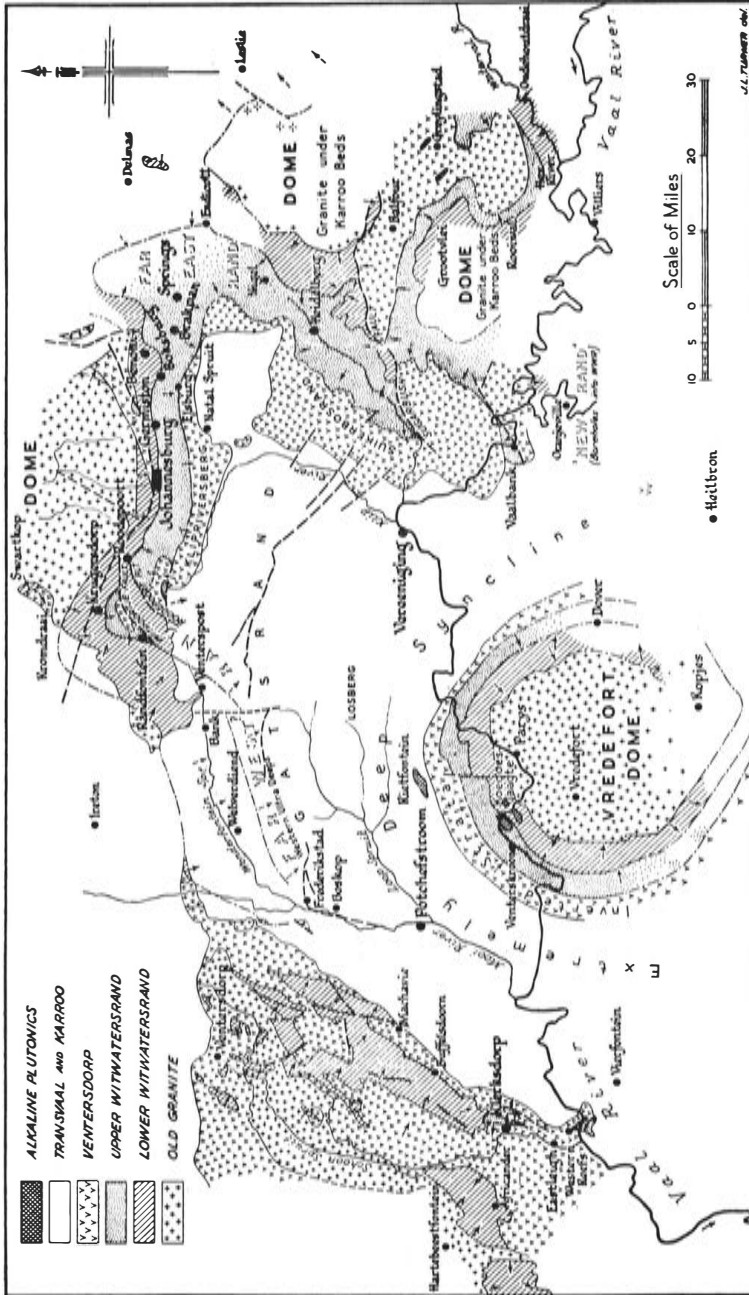


Fig. 15. Map of Vredefort Dome in South Africa, after DuToit, 1954 p. 68.

solid body. If the source in the depth was liquid with a viscosity even as high as the most viscous magma known, it is hard to see how the marginal sink could be so "extremely deep". Further discussion of this point is found on pp. 46 and 47.

An interesting collapse structure developed in overburden adjacent to doming bodies which were very fluid relative to the overburden. When an aqueous solution was used to imitate a magma, small "magma chambers" developed below strong sheets of modelling clay as the fluid rose through the stratified overburden. These chambers were only of temporary nature because the sheets underneath which the fluid was trapped would sooner or later burst and the fluid would rapidly migrate upward until it became trapped underneath another sheet, or extruded on the surface. As a chamber was thus rather suddenly emptied it would collapse relatively violently under intensive local folding of the sheets of modelling clay. Sometimes even fracturing was noticed in connection with the collapse of the "magma chambers". An example on these structures is shown in Fig. 40.

It seems probable that certain fold- and fracture patterns in nature are formed by processes of this kind. Some earthquakes are almost certainly related to collapse of magma chambers related to the ascent of magmas from unknown depths in the earth.

Tension fractures often developed in model overburden just above the top of the domes. Fig. 9 shows several stages of the evolution of a fracture pattern above a dome of stitching wax rising in an overburden of painter's putty.

It is interesting that open fractures such as those shown in the figure are limited to the upper surface region above domes. Domes buried at some depth below the surface of the overburden did not generate open fractures in the adjacent part of overburden; at least such fractures were never seen when models were sliced. It seems that the pressure at depths of much less than 1 cm would be sufficient to prevent fractures to dilate. This is indeed reasonable because the strength of painter's putty is 3×10^4 dynes/cm² or about 0.03 atm. Under a centrifugal acceleration of around 1000 g such a pressure is indeed reached at depths only a fraction of a millimeter below the surface.

Incidentally, an accurate study of accelerated scale models of fracturing in relation to depth of burial should be of great interest for structural geology, seismology and for the theory of ore formation.

Marginal sinks

It is well known from studies of salt domes in their natural environs as well as in experimental models that the material in the domes is not supplied evenly from the entire source layer, but is chiefly taken from a region rather close to the root of the domes. The flow of salt from the close neighbourhood around a dome results in a thinning of the source layer and a collapse of the superincumbent sediments. Such a depression around salt domes are called marginal

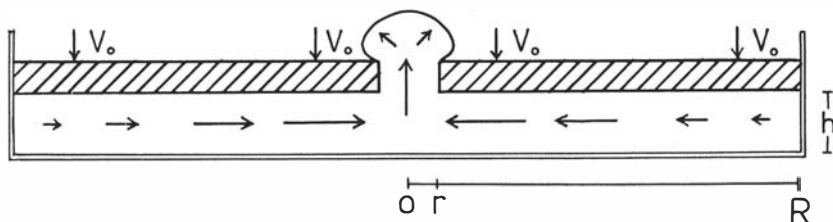


Fig. 16. Cross section of plate with central hole being pressed down on a plastic mass. V_0 is rate of vertical motion of the plate. Flow in plastic mass indicated by arrows.

or periferal sinks. (Incidentally, the term sink is an unfortunate choice from the point of view of fluid dynamics because the marginal sink is the source of the flow of salt; the dome itself is the sink.)

Marginal sinks of this kind are prominent features of most dome models studied by the writer who regards them of great tectonic importance both on a local and on a regional scale. For example, the submarine trenches adjacent to island arcs may well be explained as marginal sinks located above the source for the intruded and extruded material which builds up the islands, see p. 65. The "extremely deep" syncline around the Vredefort dome in South Africa (DuTORT, *op. cit.*) has already been discussed.

In order to explain in principle how a marginal sink develops around a dome consider a stiff circular plate which is loaded down on a layer of viscous material resting on the bottom of a cylindrical vessel whose inner diameter matches the outer diameter of the stiff plate. The plate has a circular hole in the center through which the viscous material extrudes in a similar manner as natural domes are pushed up through weak spots in the overburden, Fig. 16.

To understand the development of marginal sinks the distribution of pressure in the viscous layer is crucial. The pressure distribution is closely related to the flow pattern in the viscous layer. Since the flow is directed radially toward the central hole it follows that the horizontal component of the pressure gradient points radially away from the center of the plate.

Provided the thickness of the viscous layer remains even during the vertical compression, the horizontal pressure gradient will vary along the radius approximately proportional to the variation of the rate of flow as measured in volume per unit time per unit cross-section of the centripetal flow. Now the volume of viscous material which, as a consequence of the vertical compression, in unit time passes through a cylindrical surface with radius r , is readily found to be

$$V = \pi(R^2 - r^2) dh/dt, \quad (27)$$

where R is the outer radius of the layer and dh/dt the rate of change of thickness of the viscous layer, i.e. the rate at which the stiff plate moves downward. The area of the cylindrical surface with radius r —i.e. the cross-section of the cen-

tripetal flow at distance r from the center—is $2 \pi r h$ where h is the thickness of the viscous layer at a given instance.

Hence, given in terms of volume per unit time per unit area of cross-section, the rate of centripetal flow through the cylindrical surface with radius r is determined by

$$v = \frac{V}{2\pi r h} = \frac{(R^2 - r^2) dh}{2rh dt}. \quad (28)$$

Provided the thickness of the layer is small relative to its horizontal dimension it is sufficiently accurate for our purpose to assume that the horizontal pressure gradient is proportional to the rate of centripetal flow,

$$\frac{dP}{dr} = c \frac{dh}{dt} \frac{R^2 - r^2}{r}, \quad (29)$$

where the constant c depends upon the viscosity of the material, the thickness of the layer, and possibly also is a function of the horizontal level in the layer. (Since the pressure varies along the vertical direction in the layer it is possible that the horizontal pressure gradient also varies with vertical direction.) Integration of eq. (29) gives pressure as a function of distance from the central hole

$$P_r = c \frac{dh}{dt} (R^2 \ln r - \frac{1}{2} r^2) + c'. \quad (30)$$

The constant of integration, c' , may either be determined in relation to the pressure, P_R , at the outer edge of the layer, or in relation to the pressure, P_0 , at the edge of the central hole. Selecting P_0 as a known pressure of reference the constant of integration follows by putting $r = r_0$ and $P = P_0$ in eq. (30), r_0 being the radius of the hole, thus

$$c' = P_0 - c \frac{dh}{dt} (R^2 \ln r_0 - \frac{1}{2} r_0^2), \quad (31)$$

which introduced in eq. (30) gives

$$P_r = c \frac{dh}{dt} (R^2 \ln r - \frac{1}{2} r^2 - R^2 \ln r_0 + \frac{1}{2} r_0^2) + P_0. \quad (32)$$

The last equation gives the pressure profile along a radius as shown in Fig. 17.

Since the coefficient c varies with h the pressure profile in Fig. 17 must be regarded as an instantaneous variation along a radius. If the rate of vertical compression, dh/dt , remains uniform throughout the layer the pressure profile changes with time, but remains similar in general shape to that shown in the figure.

We shall now assume that the stiff plate above the viscous layer is replaced by an overburden which is ductile enough to yield under its own weight and

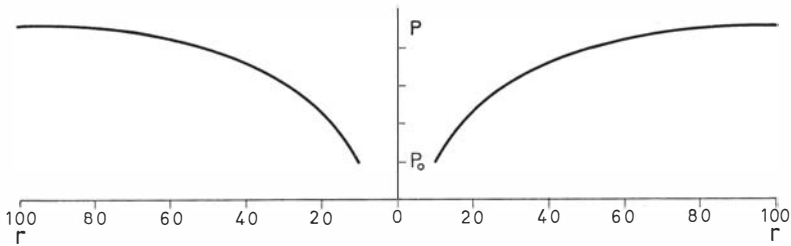


Fig. 17. Pressure distribution in the plastic mass shown in Fig. 16.

so heavy that the total load on the viscous layer is the same as that caused by the stiff plate. As the new overburden is not rigid it sags down unevenly at a rate which varies with the local pressure in the subjacent viscous layer. In other words each small local portion of the overburden must be supported by the local pressure in the subjacent layer. (The horizontal dimensions of the portions of the overburden which have to be supported by the local pressure below depend upon the strength of the overburden.) Thus the geometric profile of the overburden and of the upper boundary of the viscous layer tends to become parallel to the pressure profile in the viscous layer. For a hypothetical case with negligible drag along the vertical wall of the dome the profile will be as shown in Fig. 18.

In model experiments and in the nature, however, vertical drag along the surface of the domes is always present. The drag tends to lift the immediate adjacent portion of the overburden thereby displacing the depression in the overburden some distance away from the direct contact with the dome. Consequently a marginal sink is formed a short distance away from the root of the dome as shown in Fig. 19.

It has been suggested that flow from distant portions of the source layer cannot pass the marginal sink and hence that the active source for a dome is limited to the region inside the marginal sink. This is not necessarily true

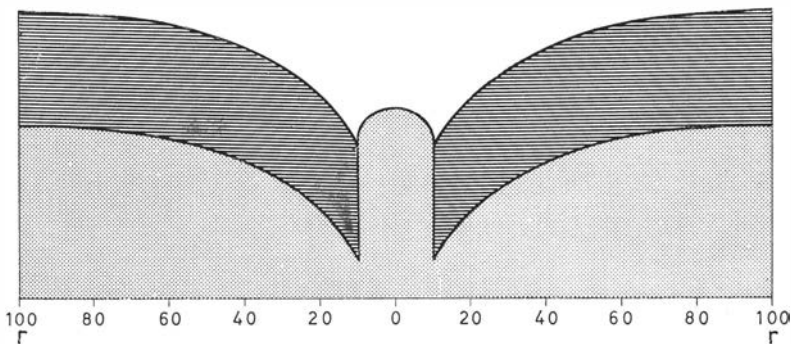


Fig. 18. Idealized profile of a viscous mass extruded through a central hole due to the weight of overlaying plastic plate, see text.

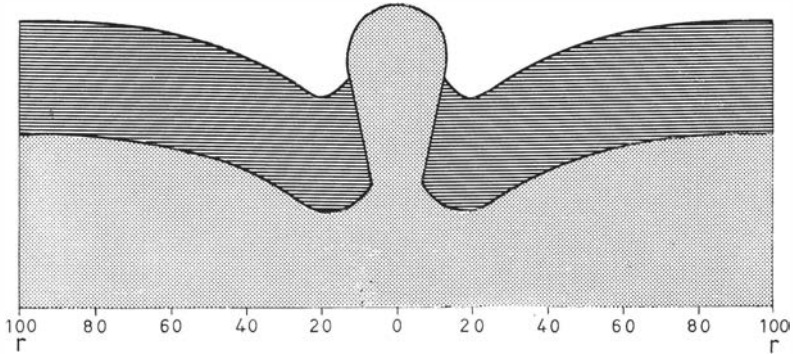


Fig. 19. Same as shown in Fig. 18, but effect of drag along the sides of rising dome shown.

because the pressure in the viscous layer underneath the lowest point of the marginal sink may or may not be higher than the pressure at the same level outside the sink. If the pressure below the sink is less than that outside, flow can pass the sink and material from distant points may contribute to the growth of the domes. The pressure underneath a sink may be great enough to make the sink function as an impassable threshold only in case the overburden directly above the sink is sufficiently thickened by filling of the surface depression or by gravity collapse within the overburden body. Incidentally, if the overburden in the sink region is thickened only by sediments layed down in the surface depression, the pressure in the source layer underneath the sink may become great enough to prevent crossing of flow only if the density of the sediments is greater than that of the source layer.

An interesting and geologically significant deduction from the consideration above is that the sink region must show negative gravity anomaly indicating mass deficiency relative to the surroundings in spite of the fact that the surface above the sink founders relative to the immediate adjacent regions. This point, which is particularly pertinent in connection with the negative gravity anomaly found over many deep submarine trenches, will be discussed in another context (p. 68).

In several models domes developed along the edge of an extra layer of overburden (see pp. 48–53). Such domes protruded from a continuous bulge that developed in the source layer just outside the edge of the extra load. Simultaneously with the formation of the bulge and the domes an elongated marginal sink always formed along the inside edge of the extra overburden. (A second more shallow marginal sink usually formed on the opposite side of the bulge and row of domes.)

The flow in the source layer across the edge of the extra load on the overburden may in these cases be treated as two-dimensional provided the load on the overburden is shaped as an elongated rectangular strip. Let the horizontal x axis be normal to the long edge of the load and situated in the middle of the

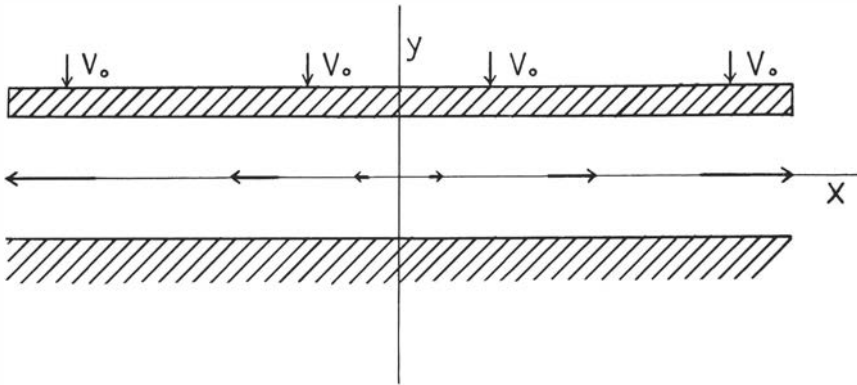


Fig. 20. Stiff plate pressed down with rate V_0 on plastic mass, see text.

source layer, the y axis, which is normal to the layering, being placed in the center of the system. The z axis is parallel to the long axis of the loaded strip, Fig. 20. The flow is approximately plane in x, y . In the first approximation we shall assume that the boundary between the source layer and the loaded part of the overburden remain plane during the flow. This simplification enables us to determine the variation of the pressure and the stresses in the x, y plane in the source layer. The case is similar to the solved problem of a viscous fluid being squeezed out from two planes which approach one another. (JAEGER, 1956, p. 140).

If v_0 is the rate at which the loaded strip of the overburden sinks down in the viscous layer the variation of pressure with x and y is

$$P = \frac{3}{4h^3} \mu v_0 (y^2 - h^2 - x^2 + l^2) + P_l, \tag{33}$$

where μ is the viscosity coefficient of the viscous layer, h half the thickness of the layer, l half its length parallel to x , and P_l is the pressure at $x = \pm l$.

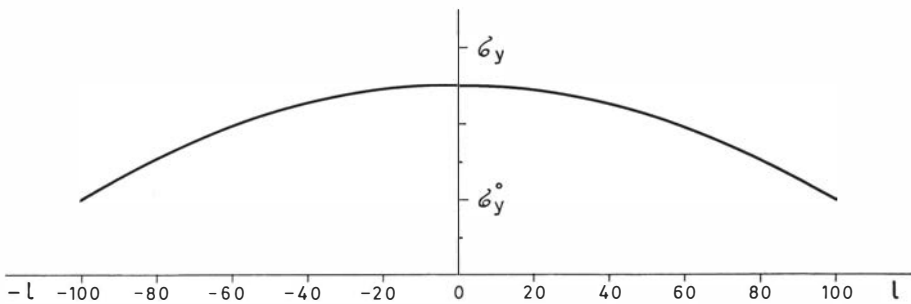


Fig. 21. Distribution of stress component, σ_y , in plastic mass shown in Fig. 20.

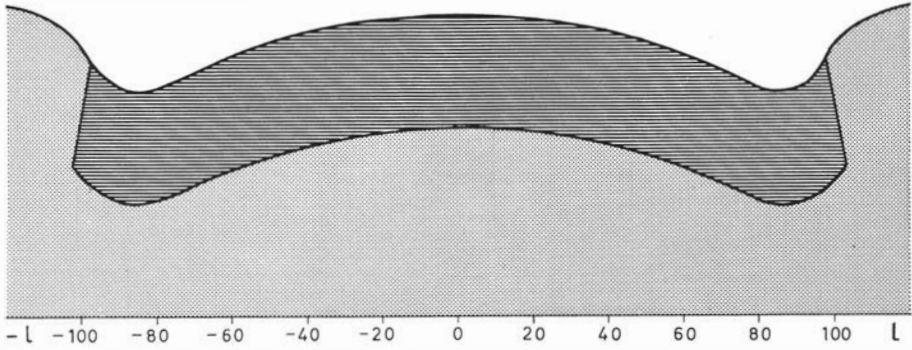


Fig. 22. Profile of a viscous layer that flows out underneath a load of layer of plastic material, see text.

The normal stresses parallel to x and y respectively, are

$$\sigma_x = \frac{3}{4h^3} \mu v_0 [3(h^2 - y^2) + x^2 - l^2] + \sigma_{xl}, \quad (34)$$

and

$$\sigma_y = \frac{3}{4h^3} \mu v_0 (y^2 - h^2 + x^2 - l^2) + \sigma_{yl}. \quad (35)$$

The equations above are taken from JAEGER, *op. cit.* p. 142. σ_y at $y=h$ is the stress which so to speak supports the overburden. Fig. 21 shows σ_y as a function of x if the term $(3/4h^3)\mu v_0$ is arbitrarily put equal to unity and l made equal to 100 units of length.

We shall now assume that the overburden is ductile and able to sag locally depending upon the magnitude of the supporting stress, σ_y , at $y=h$. When a steady state is attained the profile of the overburden and the upper boundary of the viscous layer will be adjusted to the pressure profile as shown in Fig. 22, where the effect of the drag at the edges is also taken into considerations.

The particular flow pattern and stress distribution here described result in an undulation of a strip of stratified overburden when resting on a less dense plastic or viscous layer. Two synclines (marginal sinks) separated by a gentle anticline are apt to develop.

The pattern is readily produced experimentally in centrifuged models containing a strip of modelling clay or painter's putty resting in a layer of stitching wax. Indeed, if such models are run at sufficient acceleration the tensile stress in the central anticlinal bulge is strong enough to cause fracturing.

Considerations of the distribution of the stress which supports the overburden leads to the geologically significant conclusion that the more fluid the dome-forming material relative to the overburden the flatter the profile of the marginal sinks. The more fluid the dome-forming material the less steep the pressure gradient needed to maintain a certain rate of centripetal flow in the source layer. A gentle pressure gradient gives a gentle geometric profile according to the discussion above.

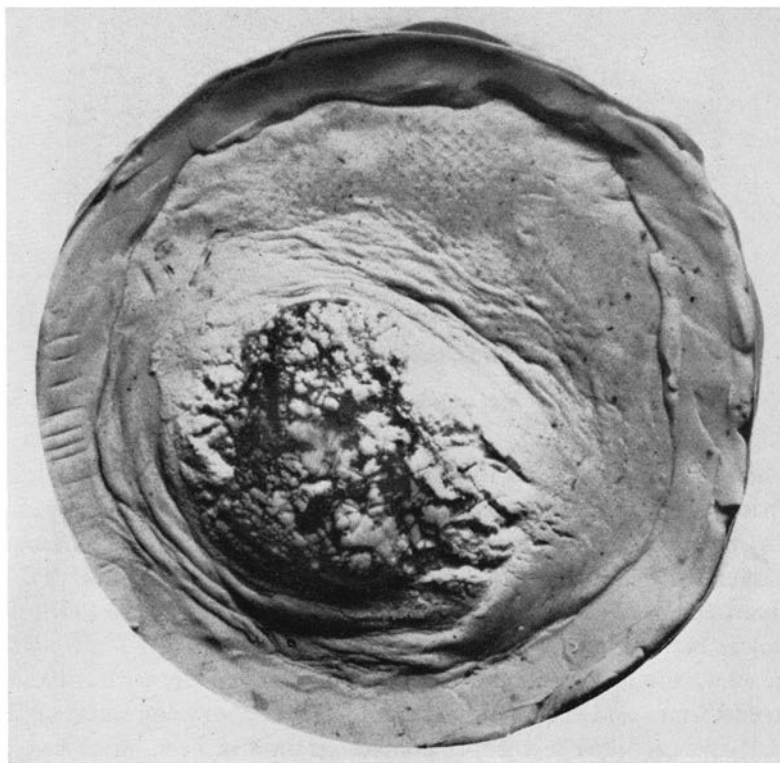


Fig. 23. Dome of stitching wax having just started to spread on the surface of painter's putty. Note folding of surface in front of the spreading dome. Same model as shown in Figs. 7 and 24. Diameter of model 94 mm.

Now the rate of growth of domes and the corresponding rate of centripetal flow toward the domes of given dimensions in a given overburden increases somewhat with decreasing viscosity of the dome-forming material. This fact means that the horizontal pressure gradient in the source layer is somewhat steeper than it would have been if the flow was independent of the viscosity of the source material. Nevertheless, one must maintain the conclusion that the profile of marginal sinks is flatter the less viscous the source material under otherwise identical circumstances because the rate of growth of domes and the related rate of flow in the source layer varies rather slowly with varying viscosity of dome-forming material. For example domes of bouncing putty in painter's putty grew only about 4–5 times as rapidly as corresponding domes of stitching wax in the same overburden yet the viscosity of the wax is about two orders of magnitude higher than that of the bouncing putty (see Tables 1 and 2).

It is interesting to note that marginal sinks did not form, or at least were not maintained for any length of time, in models with a very fluid aqueous "magma" as source material as shown in Figs. 5 and 40.

The amplitude of a marginal sink decreases with distance above the source

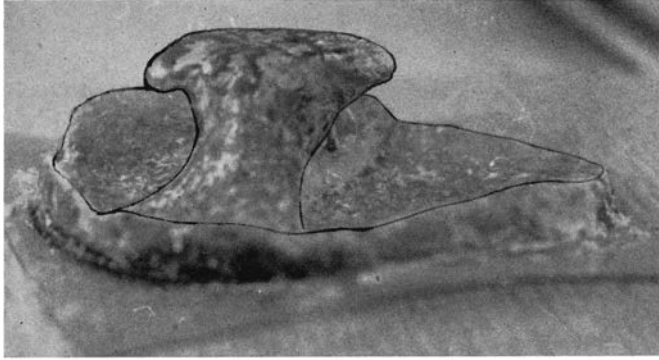


Fig. 24. Same model as shown in Fig. 23 with overburden removed. Dome outlined with ink.

layer where the amplitude has its maximum value. This feature, which showed up in many of the model experiments, is to be expected theoretically since the overburden is weak enough to sag into the depression on the surface of the source layer. In materials of this kind viscous or plastic flow must take place throughout the overburden in order to adjust to the curvature newly formed at the lower boundary.

If the curvature is sinusoidal it will die out exponentially with distance from the curved surface and vanish almost completely at about one wavelength away from the surface. This feature of contact strain has been discussed by the writer in a different connection (RAMBERG, 1962). Curves of irregular nature may probably die out more slowly.

In many of the models the overburden was too thick to enable the strain from the deep-seated sink on the boundary of the source layer to reach the free surface.

A study of the manner in which marginal sinks die out with height above the source layer should be of great tectonic significance and may for example lead to a method by which depth of source layers may be judged.

It is interesting to note that folds, partly formed by pressure from a spreading dome, partly by downslope sliding, often occurred in the marginal sink on the surface of overburden. Figs. 23 and 27 show some tendency in this direction.

Discussion of individual models of domes and related structures

Introduction

As noted above a row of domes tends to develop along the edge of an extra load placed on or in the overburden. At the same time a relatively large marginal sink develops inside the edge of the extra load, and a smaller sink on the opposite side of the row of domes. If the extra load consists of a layer more dense than the rest of the overburden (for example a layer of wet olivine powder or

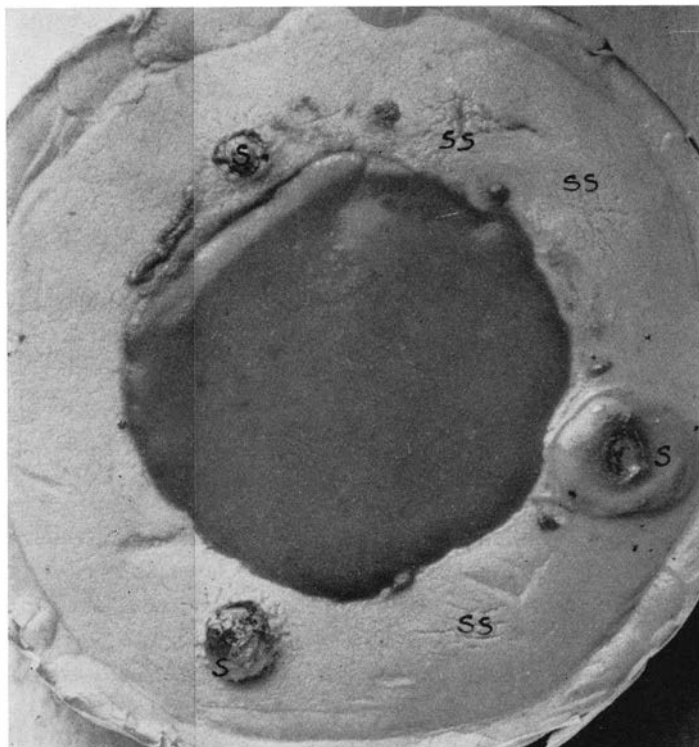


Fig. 25. Three surfaced domes of stitching wax (s), and three subsurface domes (ss) along edge of circular load of wet powdered olivine on overburden of painters' putty. Diameter of model 94 mm.

modelling clay), the surface of the loaded part sinks below the surrounding surface and a structure is developed that simulates an ocean basin—including marginal trenches—with adjacent continents. The row of domes in the model are situated along the “continental” edge exactly where island arcs occur in nature, see Fig. 42.

A few models of this type of structure will be described.

Domes of stitching wax along discontinuities in overburden

Model a:—In the 94 mm diameter cup a 20 mm thick layer of painter's putty was placed above a 3 mm thick sheet of stitching wax. A circular sheet of modelling clay 2 mm thick was placed on the overburden surface in the center of the cup. After some 15 minutes' run at an acceleration corresponding to 1000 g several domes of wax started to penetrate the surface outside the edge of the layer of modelling clay forming a structure similar to that shown in Fig. 25.

Removal of the putty overburden showed that the wax had developed a continuous ridge below the edge of the surface load. Several muchroom-shaped domes protruded from this ridge, Fig. 26. The lower part of the trunks of the

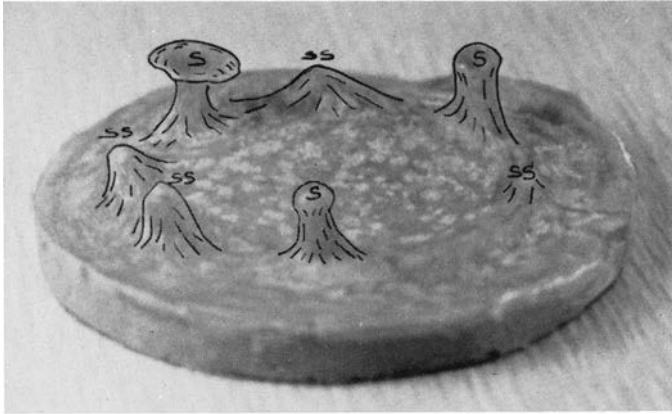


Fig. 26. Same model as shown in Fig. 25, but with overburden removed. Domes outlined with ink.

domes was elongate parallel to the ridge and was somewhat thicker than the original source layer. The surface of the source layer showed a pronounced marginal depression along the inner side of the ridge and a smaller depression along the outer side of the ridge.

The experiment was repeated several times with essentially the same result.

Model b:—A variant of the above type of model was made as follows:

In a 94 mm diameter cup a 3 mm thick layer of stitching wax covered half of the bottom and a layer of modelling clay of matching thickness covered the other half. A 20 mm thick overburden was made of painter's putty.

After some minutes' run at 1000 *g* 5 domes had penetrated the surface above the boundary between the source layer and the bottom layer of modelling clay. Irregular morphology of the surface above the source layer (Fig. 27) indicated that some sub-surface domes also had formed. Later removal of the overburden showed this to be true. The sub-surface domes were all considerably smaller than those located at the border between source layer and modelling clay as shown in Fig. 28. It appears that the domes along the boundary were initiated earlier than the others.

Development of marginal sinks and buckling of the thin surface crust of the overburden putty in connection with spreading of the domes were striking features of this model.

Domes of bouncing putty along discontinuities in overburden

Similar experiments were performed using bouncing putty as source layer below an overburden of painter's putty. The resulting structures were essentially the same as above but considerably less time was needed for the domes to reach the surface of the some 20 mm thick overburden. At a centrifugal



Fig. 27. Domes of stitching wax in putty overburden developed along boundary of deep-seated source layer, see text. Diameter of model 94 mm.

acceleration equal to about 1000 *g* some 3–5 minutes were usually needed for the domes to surface. Fig. 29 shows one of the results.

The trunk of the domes was generally somewhat less thick relative to the thickness of the source layer than the trunk of the stitching-wax domes. The bouncing-putty domes spread also more readily on the surface and developed a thinner hat than the wax domes. This is a consequence of the unlike viscosity of bouncing putty and stitching wax. Both materials have a density close to

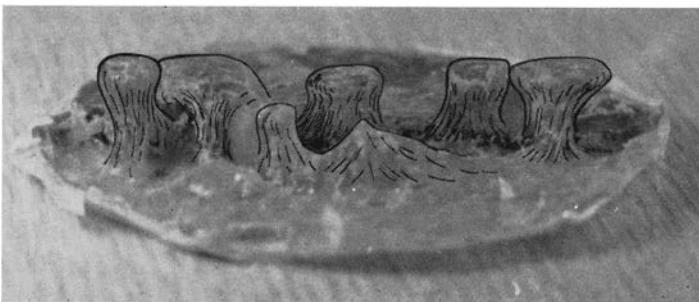


Fig. 28. Same model as shown in Fig. 27, but with overburden removed. Domes outlined with ink.

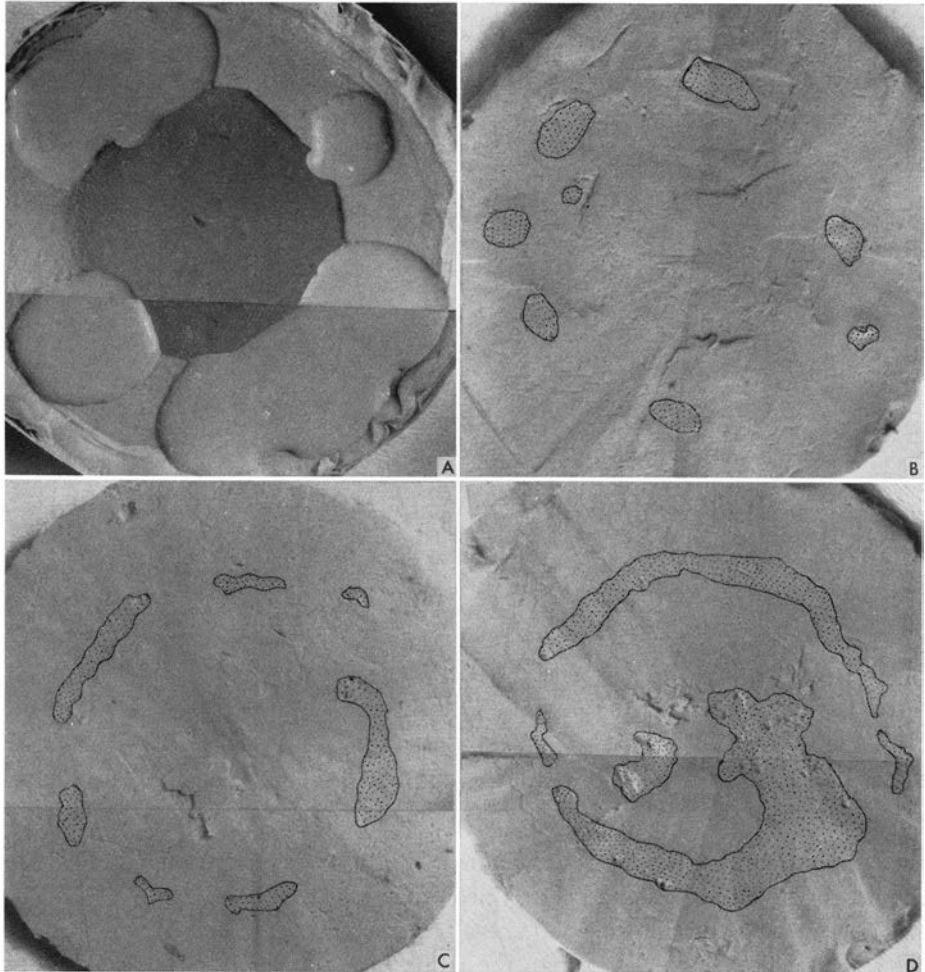


Fig. 29. *A*. Surfaced domes of bouncing putty along edge of excess load of modelling clay (dark grey) on overburden of painter's putty. Diameter of model 94 mm. *B*, *C* and *D*: horizontal sections through model shown in *A*. *B*, *C* and *D* are 17, 10 and 5 mm respectively, from bottom source layer. Note change of shape of cross section of domes (dotted and outlined with ink).

1 g/cm^3 so that the spreading force acting on geometrically identical lumps of the two materials is practically the same provided the two lumps rest on a free surface and are exposed to the same centrifugal or gravitational acceleration. Since the spreading force is the same the more fluid bouncing putty spreads much faster than stitching wax. The rates of spreading of two lumps of identical size and shape are related to one another as their inverse viscosity ratio. That is, the bouncing putty spreads about 100 times faster than the stitching wax. On the other hand the bouncing putty is extruded in vertical direction also faster than the wax. This latter condition counteracts the spreading tendency



Fig. 30. Gentle rise with central depression across model with surface layer of powdered wax, see text below. Diameter of container 94 mm.

to some extent, but the faster vertical rise is not sufficient to give a height/length ratio of the hats of bouncing putty equal to that of the hats of stitching wax inasmuch as the rise of bouncing putty through the overburden is only about 4–5 times as fast as that of stitching wax bodies of the same size (see pp. 8–12). This is so because the rate of rise is more strongly controlled by the viscosity and strength of the overburden than by the rheological properties of the doming material itself.

*Low-density layers in and on overburden, and their effect on
the behavior of domes*

When a dome penetrates layers whose density is less than that of the doming material that part of the dome which becomes enclosed in the low-density layer is no longer exposed to buoyant forces. A sufficiently thick low-density layer is able to prevent penetration by the doming material which then tends to spread below or within the light layer. Thinner layer of low-density material are not able to hinder penetration, thus the piercing material may continue to rise in the region above the light layer.

A number of models were run with the study of this effect in mind.

Model a:—On the surface of a 25 mm thick overburden of painter's putty resting on a 2 mm thick layer of bouncing putty a 0.5 mm thick sheet of modelling clay was placed. On the top of that a 4 mm thick layer of oil-wetted pow-



Fig. 31. Surface wax layer on model shown in Fig. 30, removed to exhibit steep-sided ridge formed in the sheet of modelling clay occurring below surface wax layer.

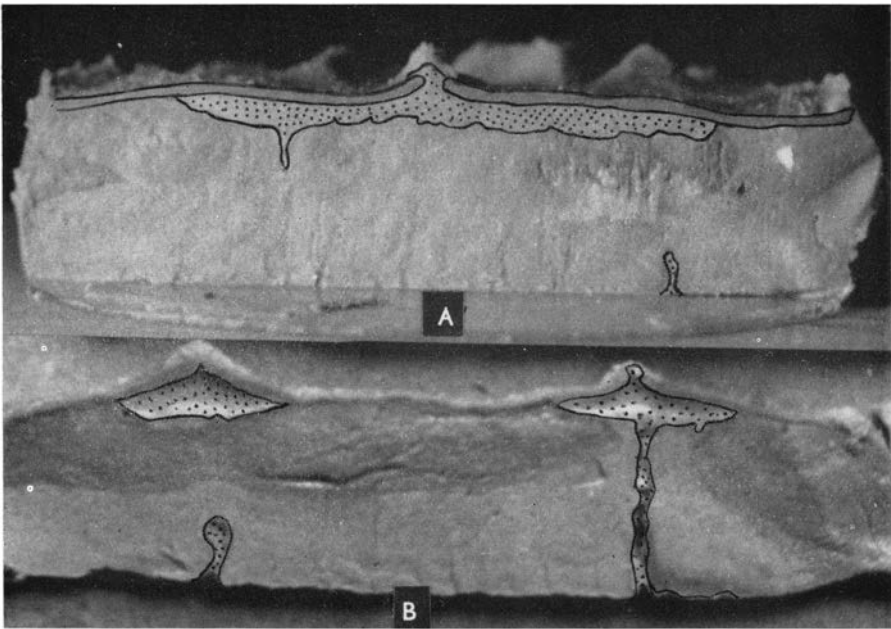


Fig. 32. Cuts through model shown in Figs. 30 and 31. Surface layer of powdered wax removed. Dotted light grey outlined with ink: injected bodies of bouncing putty.

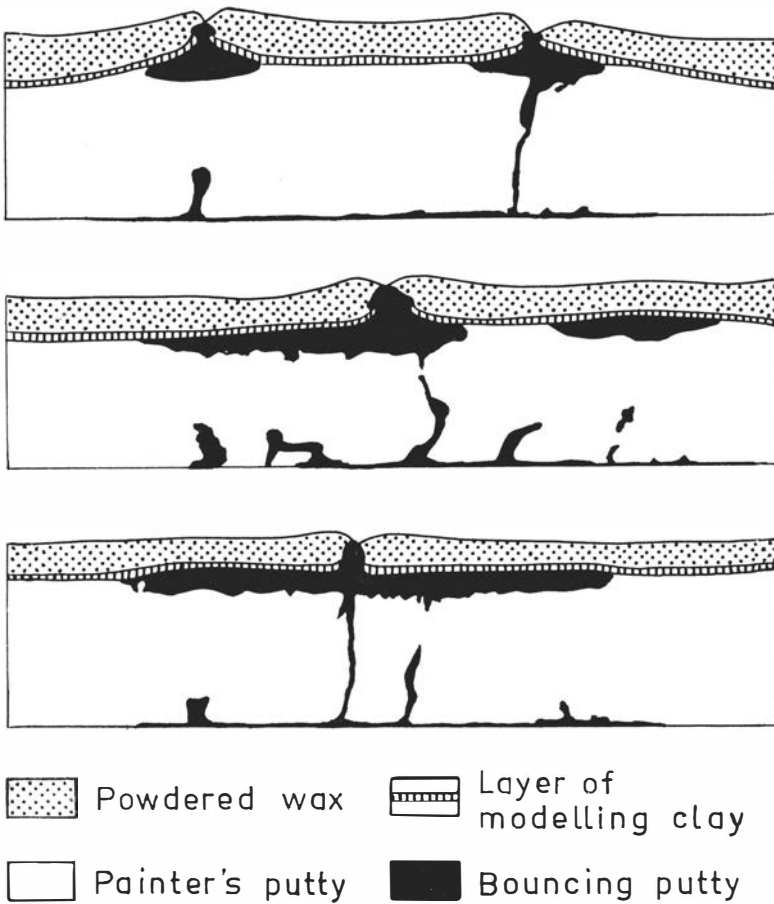


Fig. 33. Sketch showing same as Fig. 32, but with surface layer of powdered wax present.

dered wax with density 0.85 g/cm^3 was precipitated, (see p. 7). The latter was supposed to play the role of light sediments.

After about 8 minutes' run at a centrifugal acceleration of $1000 g$ a curved broad swell appeared on the surface of the powdered wax, running diagonally across the circular model as shown in Fig. 30. The swell had a narrow trough along its center, bouncing putty piercing through the bottom of the central trough at a few places without, however, having been able to spread on the surface.

Removal of the outer cover of powdered wax showed that the surface of the modelling clay was bent up into two steep-sided narrow ridges (Fig. 31) which were located below the central trough along the broad swell that had appeared on the surface of the powdered wax. Bouncing putty pierced through the summit of the ridges.

In addition to the steep-sided elongated ridges many broader swell or domes

appeared on the surface of the modelling clay. As bouncing putty pierced through in two of these domes it was reasonable to conclude that bouncing putty occurred underneath the modelling clay layer at the domed-up places in general.

Fig. 32 shows cuts through the model after the surface layer of powdered wax has been removed. Fig. 33 shows the same with the surface layer included. It is interesting to note that the bouncing putty spread out underneath the layers of powdered wax and modelling clay without showing much tendency to rise to the surface of the wax layer.

In other models with a sheet of modelling clay on the surface but no wax, the ascending bouncing putty would spread out on the surface very rapidly after piercing the top layer. Therefore, the reason for the strong tendency to spread underneath the modelling clay layer in the above run must in part, at least, be sought in the low density of the surface cover of wax. To separate the effects on ascending domes of a low-density wax layer on the one hand and a relatively competent layer of modelling clay on the other hand the model described below was tested.

Model b:—Counting from top to bottom the following layers were placed in the 94 mm diameter cup: A 10 mm thick layer of powdered wax, a 25 mm thick overburden of painter's putty and, at the bottom, a ca. 2 mm thick source layer of bouncing putty. In the middle of the top layer of powdered wax a thin sheet of modelling clay was placed. A somewhat thicker (about 1 mm) sheet of modelling clay was placed in the painter's putty a little below the middle of the layer. In this model no layer of modelling clay was placed at the boundary between the painter's putty and the surface layer of powdered wax. Thus, whatever happen to the ascending domes at that boundary would be due solely to the contrasted properties of painter's putty and powdered wax.

After about 20 minutes' run at an acceleration corresponding to 1000 *g* bouncing putty failed to penetrate the wax layer, but a gentle doming of its surface indicated that internal adjustment of matter had taken place.

After slicing the model (Fig. 34) it appeared that the ascending material had pierced the sheet of modelling clay in the putty overburden and spread out immediately below the surface layer of powdered wax without having reached the sheet of modelling clay embedded in the latter. This indicates that it is chiefly the lack of buoyant force in the low-density surface layer which prevents the bouncing putty to penetrate that layer and causes the putty to spread out immediately below, though the relatively strong layer of modelling clay embedded in the putty overburden also displays a certain capability of arresting the ascending material.

Model c:—The initial model, which was constructed in the 94 mm diameter cup, consisted of the following sequence of layers counted from the bottom: a 3 mm thick layer of stitching wax, 25 mm thick overburden of painter's putty

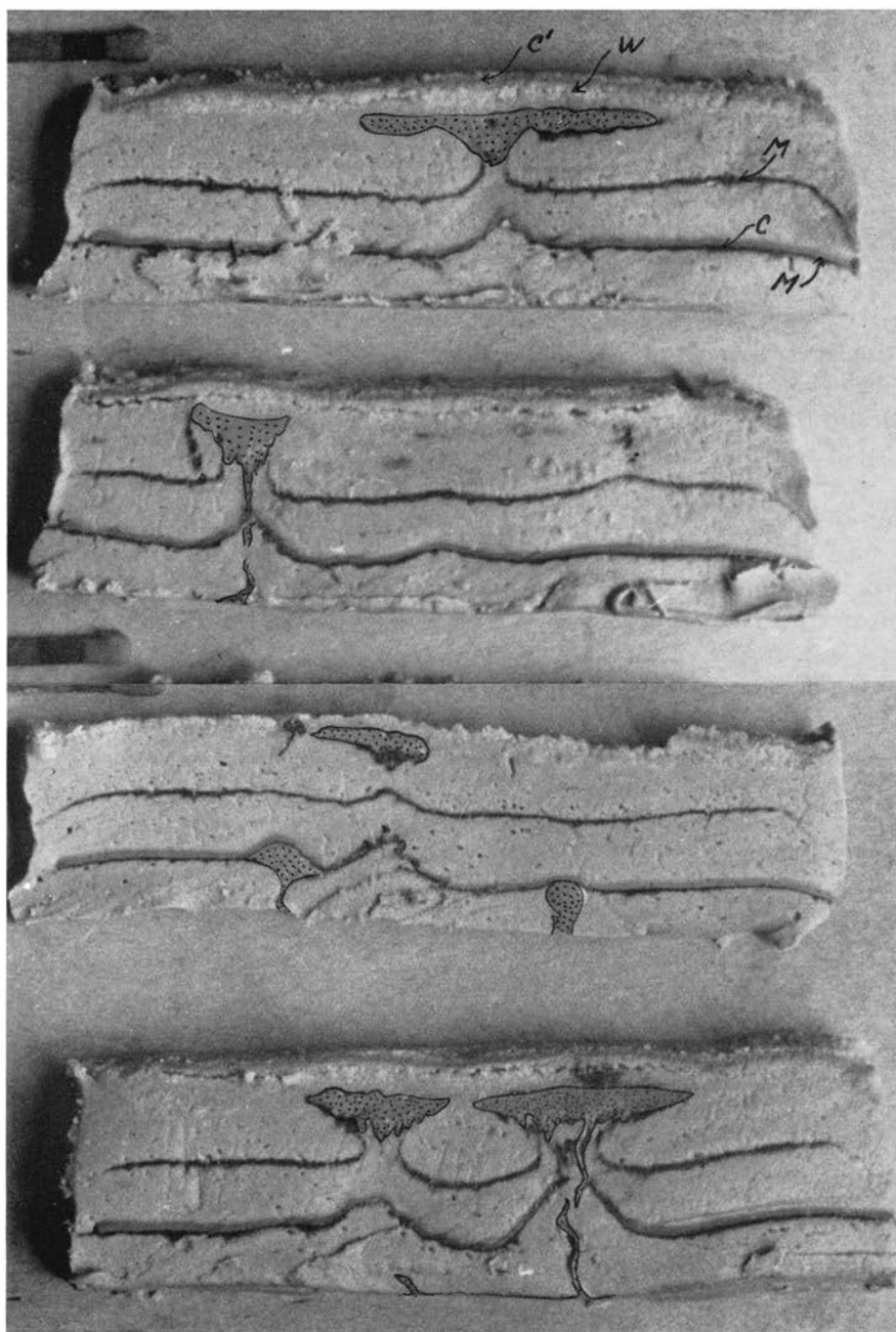


Fig. 34. Cuts through model with domes and related bodies (dotted dark grey) in overburden of painter's putty (light grey), with surface layer of powdered wax (*w*). *C* and *C'*: sheets of modelling clay; *M*: originally horizontal marker planes of paint in putty overburden. Some 5 mm thick layer of powdered wax that occurred on top of layer *C'* has been removed, see text. Diameter of model 94 mm.

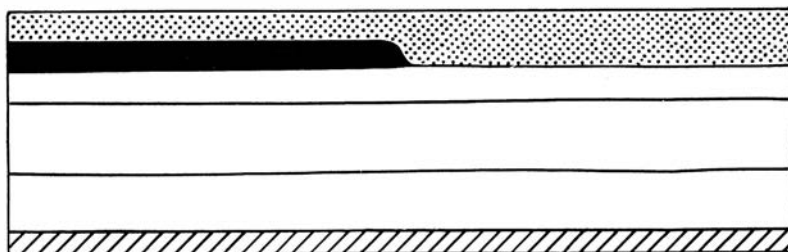


Fig. 35. Sketch of initial arrangement in model shown in Figs. 36 and 37.

with some sheets of embedded modelling clay, a 3–4 mm thick layer of wetted olivine powder covering half the surface of the putty, and a 10 mm thick layer of oil-wetted powdered wax (density 0.85 g/cm^3) finishing the column at the top, as shown in Fig. 35.

After about 10 minutes' run at 1200 g several domes of stitching wax had pierced the surface of the layer of powdered wax along the edge of the olivine-loaded overburden, such as shown in Fig. 36. The surface of the powdered wax was gently bent up around the domes of stitching wax, but a small depression had always developed in the center of each of the mounts. Stitching wax was usually visible through the bottom of the depressions. It is worth noting that the stitching wax did not show tendency to spread over the surface of the low-density surface layer of powdered wax in the manner of surfaced domes on putty overburden.

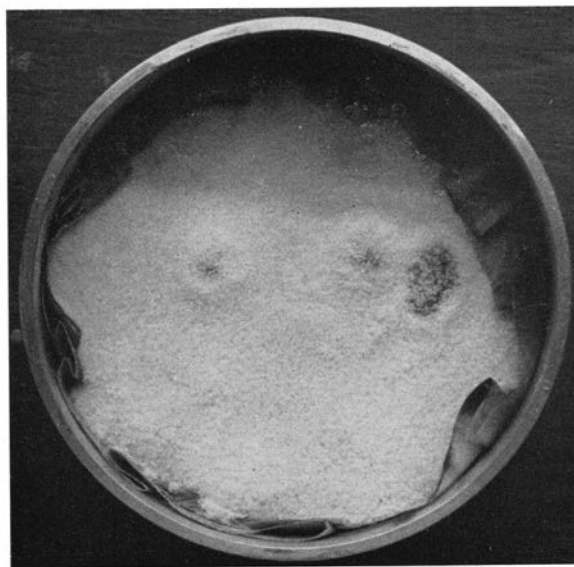


Fig. 36. Domes of stitching wax risen along extra load in overburden and piercing through surface layer of powdered wax. Diameter of model 94 mm.

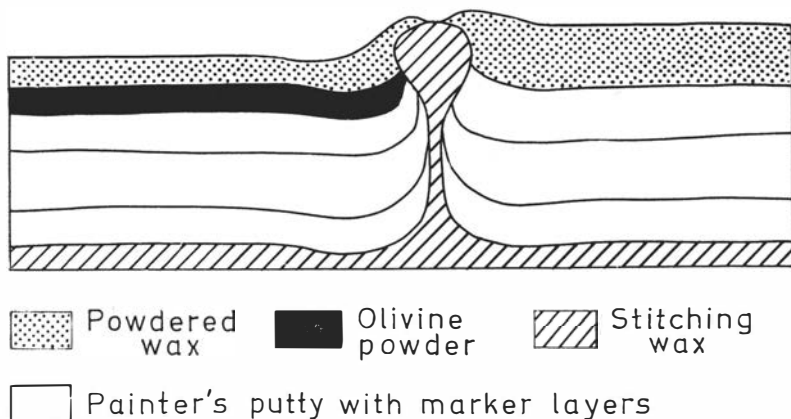


Fig. 37. Same as model in Fig. 36, shown in cross section.

It is not easy to section a model consisting of stitching wax and putty mixed together because of the contrast between the softness of the putty and the brittleness of the wax. Photographs of sections are therefore unfortunately not available, but a sketch Fig. 37 shows a cross section of the finite state.

The depressions developed in the middle of the domes in the model described here are probably formed by a mechanism similar to that responsible for the trenches along the axis of the elongate swell in model *a* above. The following explanation is offered for these features: When the doming material is intruded into or directly below the uppermost low-density layers the buoyant push from below tends to thicken the intruded body at the same time as the body tends to spread inasmuch as it is more dense than the embedding material. As the deep-seated source becomes exhausted the push from below diminishes and the spreading motion will dominate. A consequence of the latter motion is that the cover above the central part of the dome becomes stretched and thinned at the same time as the surface of the cover founders relative to the surroundings.

Model d:—In the middle of the overburden of the painter's putty a 10 mm thick layer of low-density powdered wax was placed. The source layer at the bottom consisted of a ca. 2 mm thick layer of bouncing putty. After more than 20 minutes' run at an acceleration corresponding to 1000 *g* the model was sliced. The bouncing putty had migrated up to the bottom of the wax layer and spread out underneath that layer. There seemed to be no tendency for the bouncing putty to penetrate the low-density layer, Fig. 38.

Model study of buoyancy of magma in solid surroundings

The behavior of a KMnO_4 -solution as magma-imitation in solid surroundings of putty and modelling clay has already been described as an example on scale-

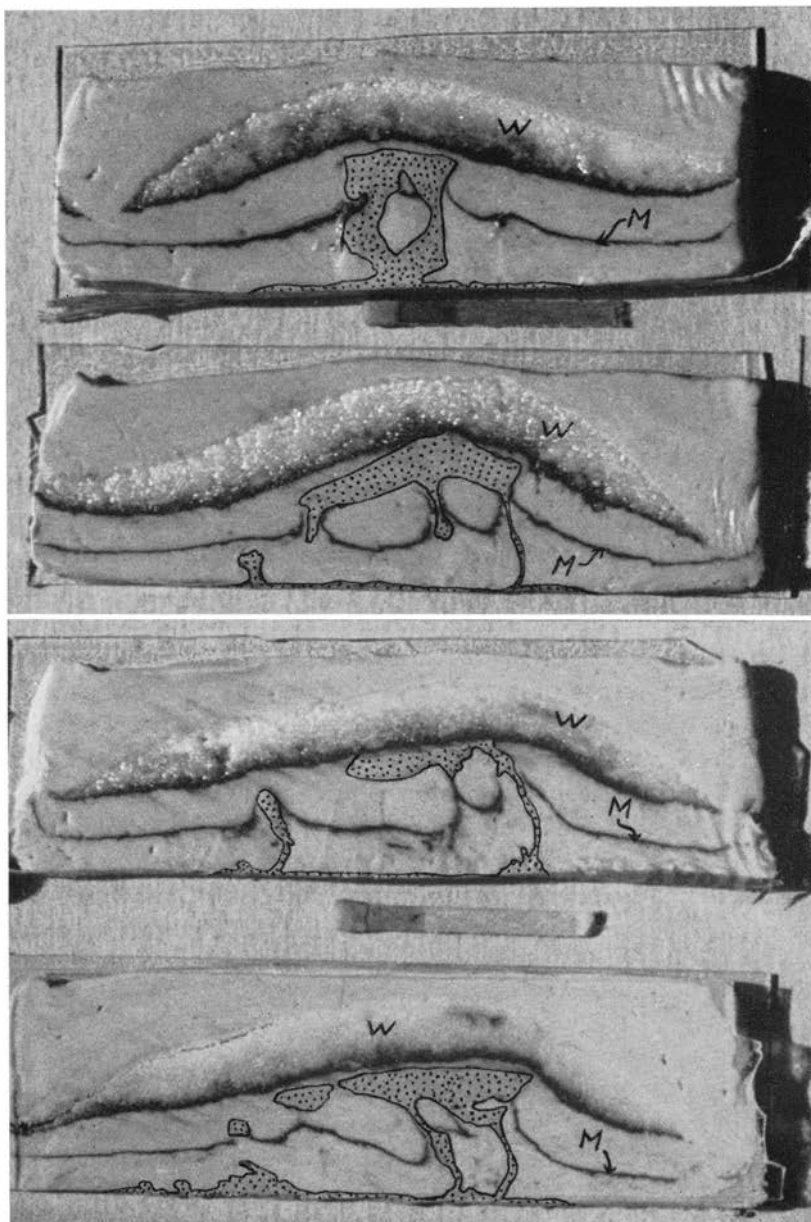


Fig. 38. Sections through model with dome-like bodies of bouncing putty (dotted grey) in overburden of painter's putty with embedded layer of powdered wax (*W*). Note deformation pattern shown by original plane marker sheet (*M*) in overburden. Diameter of model 94 mm, see text.

model study, p. 25. As an additional example on structures of this kind the model described below is believed to be of sufficient geologic interest to justify mention.

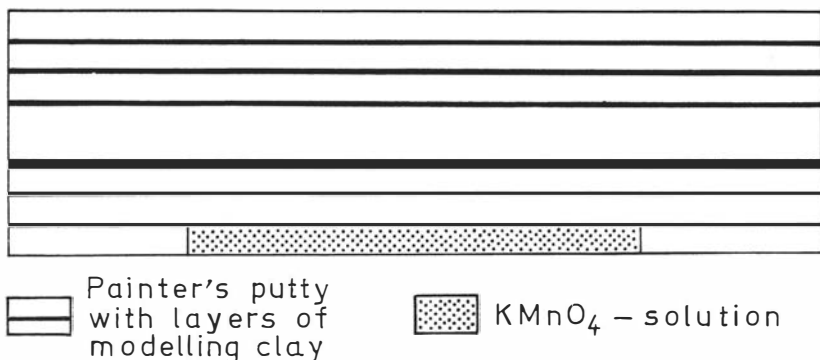


Fig. 39. Initial arrangement of model shown in Fig. 40.

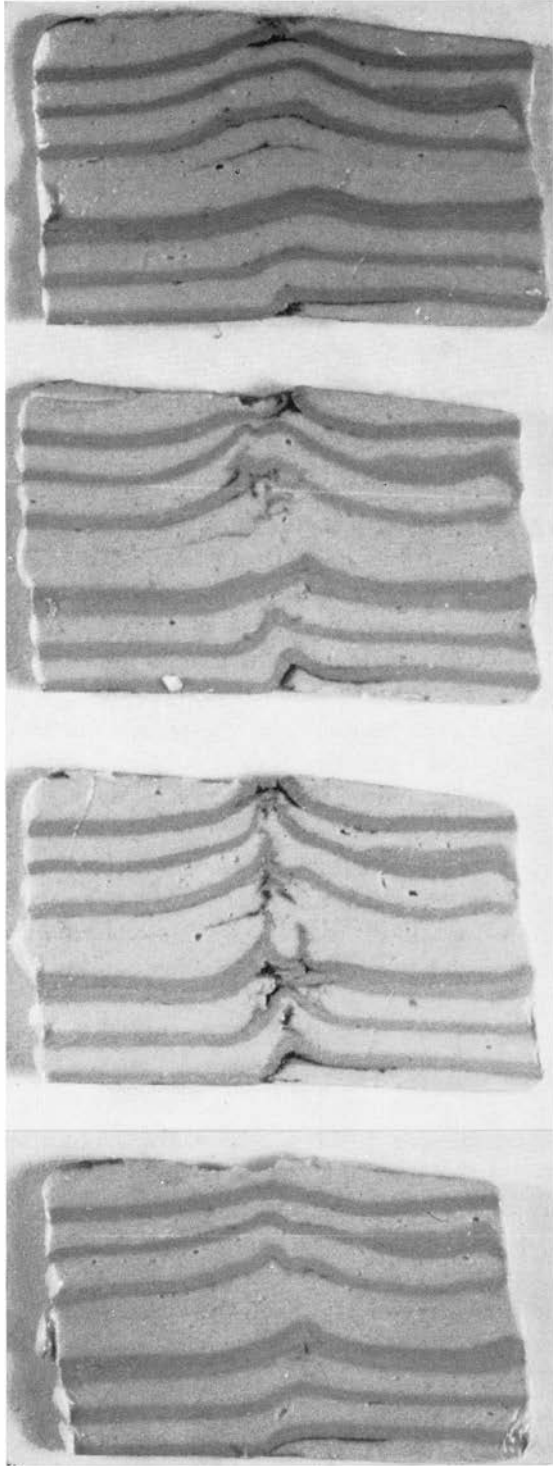
The overburden consisted of 6 layers of painter's putty, one about 7 mm thick and the rest about 3.5 mm thick, intercalated with 5 single sheets about 1 mm thick and a double sheet some 2 mm thick of modelling clay. The whole column was about 33 mm high. A 3.5 mm high central circular chamber at the bottom was filled with an aqueous solution of KMnO_4 . The construction is shown in Fig. 39.

As discussed on p. 24 the viscosity ratio between a dilute aqueous solution and a mixture of putty and modelling clay in a model of this size corresponds rather well to the viscosity ratio between a very viscous silicate magma and solid rocks in nature.

The model was run for less than one minute at an acceleration corresponding to some 1000 g . In the course of that time practically every trace of the "magma" had been extruded on the surface, but the KMnO_4 -solution had left a distinct brownish-black coating along the path of the ascending "magma" as shown in Fig. 40.

At several places along the path the layering has been strongly disturbed. Not only have the sheets of modelling clay been dragged along the path of ascent, but at some places strong folding had occurred, for example at the double layer of modelling clay in the middle of the overburden, Fig. 40. The particular geometry of this folding is probably best explained by a collapse of a "magma" chamber which existed immediately below the double layer of modelling clay. The double layer of modelling clay constituted a dome-shaped roof of the chamber which collapsed when the "magma" burst through the roof. It is easy to imagine how the relatively competent sheet of modelling clay would buckle during the collapse; Fig. 41 indicates schematically the process.

Uncollapsed chambers still filled with "magma" are preserved in a model which was run at less centrifugal acceleration (Fig. 5).



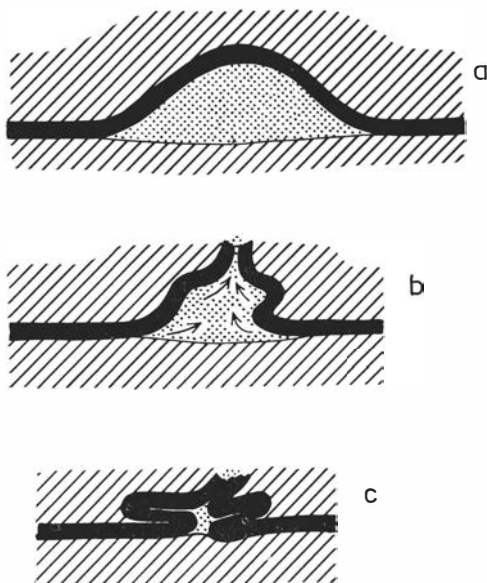


Fig. 41. Sketch showing how the collapse structure along the vent in Fig. 40 has developed.

Some geological implications of model studies of domes and similar structures

Island arcs and batholiths in orogenic zones

It is a geomorphologic feature of great significance that most island arcs and large segments of the circumpacific orogenic belt have deep submarine trenches running parallel to these elongate structures. This global pattern is well brought out in the excellent map of the Pacific Ocean issued by the National Geographical Society, 1962. Fig. 42 shows a simplified map of deep-sea trenches and island arcs.

Among the hypotheses proposed to explain the origin of deep-sea trenches the following two seem to be taken more seriously than others:

1) The trenches are buckles formed by compression of a relatively strong (rigid, competent) crust resting on a weaker substratum. VENING MEINESZ (1954) appears as the strongest advocate for this hypothesis.

2) The trenches coincide with the intersection between the earth's surface and major faults that dip underneath the adjacent continents. Submarine erosion

Fig. 40. Successive slices through layered model of painter's putty (light grey), and modelling clay (dark grey), through which a solution of KMnO_4 has risen. Section No 2 from bottom is cut along the vent of ascent showing dark stain of manganese oxide from the solution and strong folding and deformation of the competent sheets of modelling clay. Slices cover only half the diameter of the model, the left edge of the slices coinciding with the centroid of the model. The original chamber with KMnO_4 on the bottom is completely collapsed, the vent of ascent being situated at the edge of the original chamber. Compare Figs. 5 and 6.

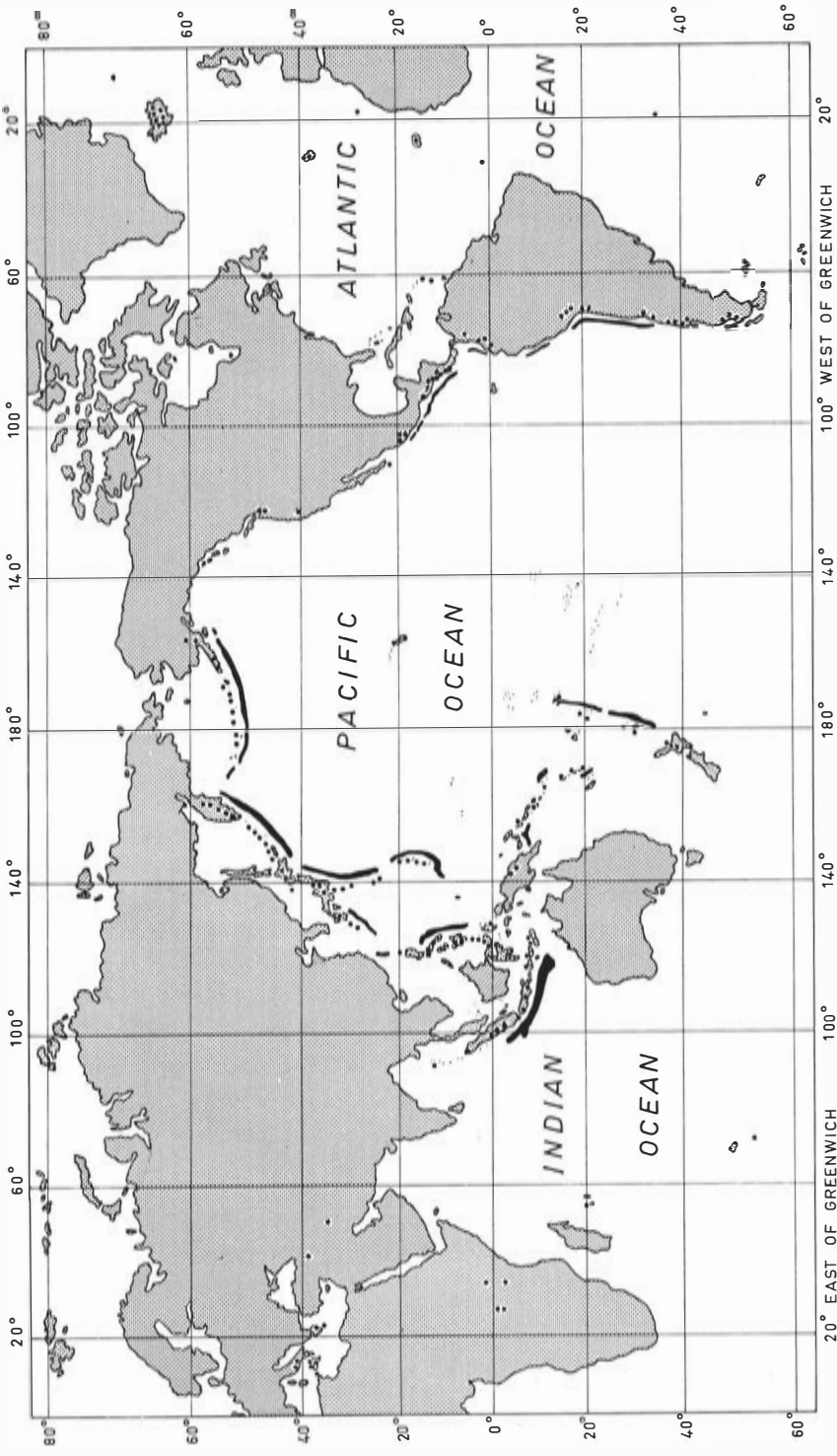


Fig. 42. Active volcanoes of the world marked by circular dots according to BULLARD, *op. cit.* Deep-sea trenches shown by solid black, after map in Nat. Geogr. Mag., April 1962.

along the fault and depression of the oceanic side by the weight of the overriding continental segment supposedly give rise to the trenches. BENIOFF (1949) is the chief inventor of this model.

Neither of these hypotheses carry enough evidential support to exclude considerations of alternative models. Indeed, preliminary calculations (p. 94) indicate that the buckling hypothesis is not physically possible.

It seems to the present writer that the typical structural combination: dome—marginal sink both in nature and in models is so strikingly similar to the combination: island arc—submarine trench that the possibility of a similar origin merits consideration.

A number of models described above show that structures geometrically similar to island arcs with their marginal submarine trenches form if a layer of low-density rock (crystal-melt mush, or possibly magma) such as diorite or granite is covered by more dense material such as gabbro, norite and the like.

The present great basaltic volcanic activity in and around the Pacific Ocean together with the large number of ancient submarine volcanoes—the guyots—in that region makes it easy to conceive of thick columns of basic lava that from time to time may erupt and cover portions of the crust along the continental edges. At this point it is significant to realize that if relatively dense magma erupts on the surface of a sedimentary column of low density, then some of the ascending melt must necessarily also spread out underneath the sedimentary cover (cf. the spreading of ascending material below low-density layers in the models) in the form of huge sills, lopoliths or similar bodies. The part of the crust thus covered and invaded by heavy basic igneous rocks does not only contain the typical granites, granodiorites, quartzo-feldspathic gneisses etc. of the continental block but unconsolidated sediments as well. The latter may reach thicknesses up to 10–15 km and must thus constitute a large percentage of the submerged crustal region.

In an earlier paper (RAMBERG, 1945) the writer presented the idea of ocean and geosyncline submergence as caused by increased average density of a part of the crust due to basic magmatism (“simatization” of sial) without, however, having had the opportunity to make experimental tests. Later VAN BEMMELEN (1956) and BELOUSSOV & RUDITCH (1961) have discussed similar ideas.

After a relatively rapid regional isostatic adjustment of the “basified” segment the much slower buoyant rise of the light components of the buried and depressed rock material will take place in a fashion similar to that occurring in the models *a*, *b* and *c*, pp. 53–59.

Island-arc systems often consist of a double row of islands, viz. an inner (closer to the continent) row of volcanic islands and an outer row of tectonic islands consisting of folded sediments (see for example WILSON, 1954). The outer islands are generally smaller and occur less consistently than those of the volcanic arc. In the writer’s view the latter islands correspond to the row of domes formed along the edge of the excess overburden in the models, p. 49.

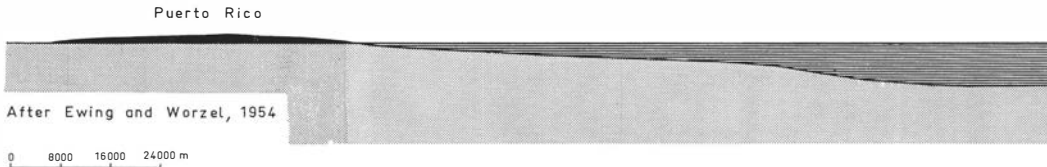


Fig. 43. Profile of the Puerto Rico Trench after EWING and WORZEL, 1954.

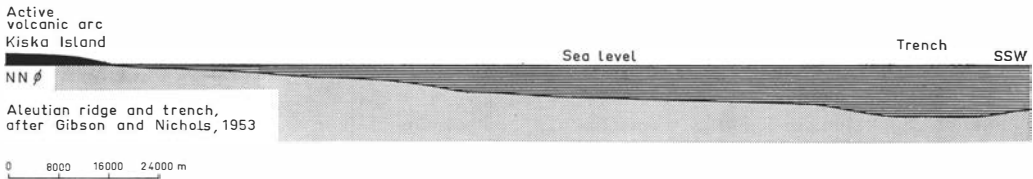
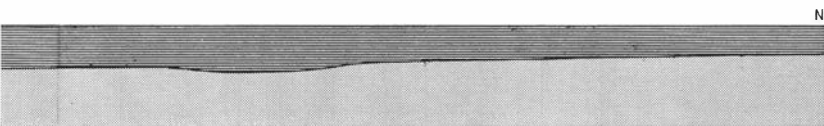


Fig. 44. Profile of the Aleutian Trench after GIBSON and NICHOLDS, 1953.

The experimental models are not capable of producing an association between the rise of solid but plastic domes by buoyant forces and volcanism. Since conditions for melting is not present in the models—e.g. there is no temperature gradient and no exothermic processes going on—our models must fail in directly reproducing volcanism although some inferences may be made. The presence of a distinct marginal sink (=submarine trench) indicates that the source “layer” was not completely molten at the time the material was forced out because a layer with the relatively low viscosity of a silicate melt would not give a well developed sink as discussed above, p. 46. It is not necessary that the material was completely crystalline, it could well have been a mush of crystalline matter mixed with some melt. (Incidentally, although descriptions of submarine trenches often give an impression of very deep and steep-sided submarine troughs more objective drawings of the profiles actually show rather gentle morphology, Figs. 43 and 44.)

When the low-density wholly or partly crystalline material flows laterally from the marginal sink toward the root of the domes and starts to rise, partial melting may occur for two reasons:

- 1) The moving mass is continuously exposed to decreasing pressure. Hence if the mass does not lose heat and cool (because of its passage through colder surroundings) faster than the decrease of the melting point with falling pressure, partial melting is apt to take place. The percentage of the mass which thus may melt and give rise to volcanism is determined by a number of conditions such as the original temperature of the deep-seated source layer, its heat capacity, the heat and temperature of melting and the change of volume associated with melting. Heat conductivity and temperature distribution in the surroundings are also significant factors. If melting actually takes place due to decreasing pressure encountered by ascending domes, it is clear that the melting will be limited to the central part of the dome where temperature will maintain the



highest value during the ascent through colder surroundings. In this connection it is interesting to note that many quartzo-feldspathic domes in pre-Cambrian and Caledonian orogens contain a central body that is massive and shows intrusive relations to the bulk of the dome which generally is foliated parallel to the boundaries and the surrounding gneisses or schists, see *ESKOLA*, 1948. Fig. 45 is reproduced from *ESKOLA*'s paper.

2) Dissipation of potential mechanical energy due to viscous resistance during the rise of domes causes some elevation of temperature and may even result in partial fusion under ideal circumstances. This effect is probably of little significance because the dissipated energy is distributed over vast volumes.

It is pertinent in this connection to note that deep submarine trenches are limited to regions with active volcanism as shown on the map Fig. 42. Trenches do not, for example, occur along the long segment of the circumpacific orogenic belt that stretches from Alaska to Mexico, a region free from active volcanoes, except for the lonely Lassen Peak in USA. On the other hand trenches do occur along the Aleutian arc, outside Mexico and Central America, and along a major stretch of the Andes, all regions well known for their volcanic activity. Trenches are typical outside the many island arcs with active volcanism on the eastern side of the Pacific Ocean, such as the Kermadec and Tonga Islands, the Philippines, the Mariana and the Bonin Islands, Japan, and the Kuril Islands. Trenches are also typical along the active volcanic belt of Sumatra, Java and the lesser Sunda Islands, and along the volcanic arc of the West Indies. (With reference to the distribution of recent volcanism the reader is referred to the excellent book by *BULLARD*, 1962.)

In the model proposed by the writer the lack of submarine trenches along the nonvolcanic part of the circumpacific orogene may mean that some (temporary?) state of stability is reached in the nonvolcanic orogenic regions. According to the model the foundering of the trenches and the rise of domes apu

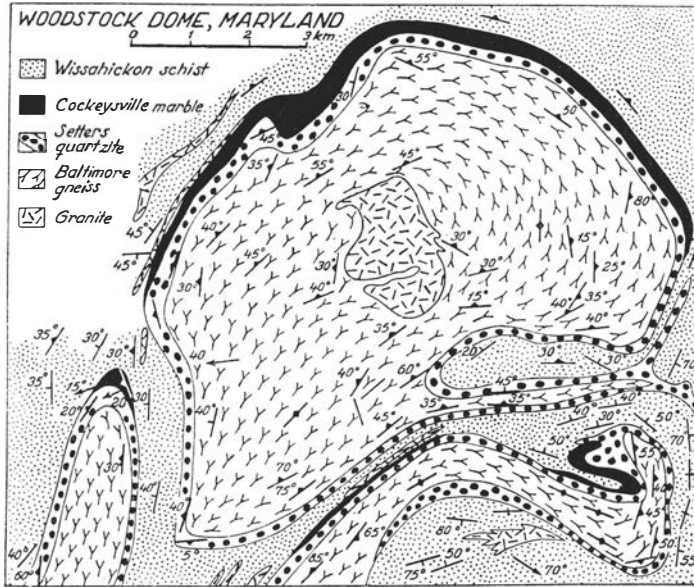


Fig. 45. The Woodstock dome, Maryland according to E. CLOOS. Reproduced from ESKOLA, *op. cit.*

batholiths—including partial melting and volcanic activity—are simultaneous and complementary phenomena. When the source “layer” has become exhausted locally the trench above the source region cannot continue to deepen. On the contrary, filling by sediments at the surface and plastic flow within the crust tend to flatten out the troughs. If the fill of sediments is less dense than the surroundings, isostatic adjustment may ultimately make the surface of the sediments in the trench rise above the adjacent regions, possibly even above sea level. In this connection it is interesting that the islands of the outer arc in the Pacific double-arc systems consist of folded sedimentary strata, and occur close to, or in the elongation of, the typical belt of negative gravity anomalies, see for example VENING MEINESZ (1954). It is pertinent to note that the mechanism which leads to marginal sinks adjacent to domes requires that a negative gravity anomaly exists above the sink as long as they are in the process of forming.

The renowned batholiths of the South American Andes and the Coast Range and Sierra Nevada of the Western USA and Canada, and similar batholithic massifs in other orogenic belts such as the Caledonian along the North-west coast of Norway (HOLTEDAHL *et al.*, 1960), are generally elongated bodies whose long axis coincides with the strike of the orogenic belt. BUDDINGTON (1959) gives a summaric description of a great number of batholithic and dome-shaped granitic and granodioritic bodies from various depth-zones in the earth.

In the experimental models it was found that the lower part of domes initiated

along the edge of an excess load on the overburden always was elongate parallel to the edge as shown in Figs. 26 and 29. At the root of the domes a continuous ridge was formed along the edge of the excess load. The lower part of the domes which rose from this ridge were oblong in horizontal cross sections, but became gradually circular at higher levels. These experimental results suggest to the writer that batholiths that occur in orogenes along continental edges and display very elongate shape are bodies which have not risen much above the level of the original source layer. Bodies elevated to higher levels should be more circular in horizontal cross section and show a stock- or funnel-shaped profile.

Such variation of shape of horizontal cross section with depth of ascending masses occurred in models not exposed to one-sided lateral stress. In the particular anisotropic stress field which seems to prevail during evolution of orogenic belts domes or batholiths may well display an elongate shape at any level above the source.

Note on the so-called "bottom granites" in the Caledonides in Norway

In the Caledonian complexes in Norway more or less dome-shaped massifs of gneissgranite or granodiorite are found below the folded and otherwise altered and deformed Cambro-Silurian sediments and volcanics. These bodies are responsible for much confusion and controversies among Scandinavian geologists who find it hard to agree on the age of many "bottom granites" relative to the adjacent sediments and volcanics. Some of the granites are clearly older than the overlying strata, weathering breccia, basal conglomerate, coarse quartzite or arkose then being in direct contact with the "bottom granite" whose foliation may be discordant against that of the adjacent strata (see for example KAUTSKY, 1953). Other bodies of the "bottom granite" display true intrusive contacts, pegmatitization and migmatitization of the surrounding schists being typical, and the granite showing foliation parallel to the boundaries. Not rarely a single body of "bottom granite" may appear intrusive and "young" relative to a certain stratum in one locality whereas at other localities the same body serves as the old basement for the autochthonous stratum. A good example on a single body that exhibits such contrasted and apparently inconsistent behavior is the Tysfjord granite in North Norway as described by FOSLIE (1941) and KAUTSKY, op. cit.

Such conditions, which may seem puzzling from the point of view of classical magmatism that regarded granites as formed by fractional crystallization of juvenile magma, are to be expected by some modern theories of granite emplacement, and are in excellent accord with the model advanced in this paper. When the old substratum which contains, among other rocks, granites and granodiorites, is covered by a sufficiently thick column of sediments and volcanics, buoyant forces become effective tending to make the light granitic masses rise. The rising masses carry the high temperature characteristic of their

original depth up to levels closer to the earth's surface. In other words the isothermal surfaces in the crust are domed upward and distorted into shapes more or less geometrically similar to the ascending masses themselves. Depending upon the local temperature in the mass and the magnitude and attitude of the local buoyant force it is evident that the degree of "intrusiveness" or "mobility" will vary from place to place and from body to body. Where temperature is low and the buoyant force weak the granitic basement will appear old and pre-Caledonian of age. Bodies or parts of bodies where temperature has been higher and buoyant force stronger are more mobile than the adjacent sediments and volcanics which consequently appear intruded and mechanically and chemically altered by the active "bottom granite" whose age therefore is regarded as syn- or even sometimes post-Caledonian.

The centrifuged models illuminate very strikingly another characteristic feature of the Norwegian Caledonides which has been somewhat hard to explain. In the Trondheim area the deformed supracrustals are put in three stratigraphic groups of unlike age. The older Røros group, the Støren–Bymark group of intermediate age and the Hovin–Horg group which is the youngest but yet strongly folded and otherwise deformed at places.

It has long been known, as recently pointed out by H. CARSTENS (1960) in his excursion guide for the 1960 International Congress (excursions nos. *A 4* and *C 1*), that the oldest rocks, the Røros schists, in general display the highest grade of regional metamorphism. The Støren–Bymark basic volcanics are somewhat less metamorphosed in general, and the Hovin group is least effected by the metamorphic recrystallization. This is so in spite of the fact that the strata are more or less strongly folded, often with steep dip and at places even inverted.

The situation could be accounted for by the models studied in this paper. As the sediments and volcanics accumulated in the geosynclinal basin the increased temperature at depth generated metamorphic recrystallization that increased downward. When the quartzo-feldspathic substratum, softened by the elevated temperature under the insulating overburden, ascended in the form of domes and batholiths the highly metamorphosed and deeply buried Røros schists were pulled along by the domes and batholiths as they rose from the substratum. As the Røros group consists of large amounts of mica schists it is probable that the group as a whole constituted a rather incompetent mass, probably not much more competent than the doming quartzo-feldspathic bodies themselves. Under such conditions the experiments show (Fig. 13, p. 37) that a rather thick boundary layer of the schist would stick closely to the rising substratum. The boundary layer of the schist would in a sense constitute a part of the rising domes. The originally more or less horizontal isothermal surfaces in the substratum and in the supracrustal column must also to some extent have been carried along with the moving masses although cooling during the ascent caused the isothermal surfaces to rise less rapidly than the bodies (assuming that heat was not generated by some means). This kind of regional

metamorphism may perhaps be regarded as a contact metamorphism of regional dimensions, the heat source being the softened and hot, but usually not liquid, substratum.

The model sketched here explains in a simple manner the observation that the grade of metamorphism in general increases from the young Hovin group to the old Røros group even if the strata are steeply folded or inverted.

At this point it may be noted that the puzzling occurrence of eclogites in the large body of "bottom gneiss" in the Møre region in West Norway acquires a natural explanation in light of the model proposed here. The writer considers the Møre gneiss as a part of the substratum that has ascended dome-like fashion due to buoyancy. (Incidentally, some spreading of the upper part of the Møre-gneiss dome and gravity sliding of superincumbant supracrustals (cf. Figs. 23 and 27) may well explain some of the Caledonian folding and the more or less horizontally thrust masses of Jotunheimen, see the map in Holtedahl *et al.*, 1960.)

The eclogites occur as lenticular bodies enclosed in the quartzo-feldspathic Møre gneiss (see description by STRAND in HOLTEDAHL, *op. cit.*). The gneiss wraps conformably around the eclogite bodies which typically are amphibolitized along the boundaries. In other words the border zone of the eclogites corresponds to a lower grade of metamorphism, viz. amphibolite facies, than the central part of the bodies. The border zone corresponds to the same grade as that of the surrounding gneisses.

In light of the model sketched above the explanation would be that the eclogite bodies acquired their characteristic high-grade mineral assemblage while they, together with their embedding gneisses, were situated at great depth. As the huge gneiss dome rose the eclogites and their surroundings became exposed to decreasing pressure (and temperature). The chemically mobile quartzo-feldspathic gneisses were able to recrystallize almost completely to adjust their minerals to the lower grades of metamorphism. But the mafic eclogites, which are chemically (and mechanically for that matter) immobile, were not able to recrystallize to adopt a new mineralogy except along the boundaries where the catalytic effect of shear would be most intensive.

Submarine ridges and rift valleys

The occurrence of central depressions of the surface above buoyancy-injected bodies in some of the experimental models is believed by the author to be of tectonic significance. Depressions in the middle of swells on the surface developed when the injected material reached surface layers whose density was less than that of the injected material. As the buoyant force diminished because of gradual depletion of the deep-seated source, lateral spreading of the upper part of the dome became dominant. The originally relatively thick hat (laccolith) of the injected body thus became thinner, particularly in its central part. As a consequence the cover would collapse in the center of the rise, a process

which was accentuated by the tensile stress imposed on the cover by the laterally spreading subjacent body.

It seems to the writer that global morphologic features such as for example the Mid-Atlantic Ridge and the East-Pacific Rise are strikingly similar to the elongate gentle ridge formed on the surface of model *a*, p. 53. According to recent deep-sea research (see for example MENARD, 1962) submarine ridges and rises of a total length of 40,000 miles occur in the Atlantic, Pacific and Indian Oceans. Most of the hitherto studied parts of this ridge system have been found to display one or several rift-valley like troughs along the crest.

Geomorphologic features of such impressing dimension as the submarine ridges must clearly play an important role in any theory of the evolution of the earth. Several hypotheses as to the origin of this ridge system have been proposed. The presence of rift-valley like features along the summit has provoked HEEZEN (1960), for example, to advance the hypothesis of an expanding earth. On the other hand MENARD (1962) considers it likely that a large segment of the ridges, viz. the East Pacific Rise, reflects the site of an upwelling branch of a convection cell in the mantle.

As a consequence of the model studies described above the writer suggests an alternative hypothesis, viz. that the submarine rises are bulges caused by buoyancy-injected bodies which occur relatively close to the surface of the ocean bottom, and now is slowly spreading laterally thereby producing lateral tension and rift-valley morphology along the crest of the ridges.

These buoyancy-injected bodies cannot chiefly be of granitoid composition because the low density of such rocks or magma would make the ridges rise above sea level, or force the magma to pierce the surface and emerge above sea level in the form of rows of volcanic island. On the other side the material must be less dense than the average mantle underneath the oceans. It seems reasonable to propose that the ascending material is of gabbroid composition and rises through the more dense material of the mantle in much the same manner that at higher levels in the earth, granitic and granodioritic batholiths ascend through an averagely more dense crust. It is possible that the rising masses have their source in the low-velocity subcrustal layer, see also p. 74.

All morphologic features of the submarine rises, the known heat-flow distributions across such ridges and the measured gravity anomalies and seismic activities as discussed by MENARD in connection with the convection hypothesis, may equally well be employed in support of the hypothesis proposed by the writer. It seems that more field observations, better theories and more meaningful model experiments are needed to discriminate among existing hypotheses or suggest alternative explanations. Nevertheless the writer feels that some further points are ripe for discussion.

That vast volumes of basic rocks are injected below a veneer of sediments is a very reasonable proposal. In the experimental tests of models with low-density surface layers (p. 53) only a small portion of the ascending material

would surface on top of the low-density layer, most of the material spread out below the light layer. Seen in connection with the widespread basic volcanism within the oceanic segments of the earth these tests lead to the conclusion that much material of basaltic-gabbroic composition never reaches the surface but spreads out below the sedimentary column, below other low-density crustal layers, or forms sills and lopoliths or laccoliths in the lower portion of such strata. The so-called "second layer" of the oceanic crust, existing below a rather thin cover of unconsolidated sediments, is supposed to consist of a mixture of sills and lava sheets and sedimentary rocks (MENARD, *op. cit.*). It would harmonize extremely well with our experiments that the injected bodies in the "second layer" formed simultaneously with the extrusion of lavas on the surface. The experimental models show that one should expect the volume of subsurface injected material to be much larger than that of the extruded lavas.

The renowned Karroo dolerites in South Africa, which occur in sedimentary rocks as sills, sheets and dikes over a vast region, may represent a feature similar to the "second layer". It is interesting that the sills and other intruded doleritic bodies according to DU TOIT (1954, p. 369) are connected with lava on top of the Karroo sedimentary formation, the lava and the subvolcanic intrusives probably having formed simultaneously.

Continental rift-valley systems may well have an evolutionary history similar to that described above for submarine ridges. Subsurface injection of plastic but crystalline rocks, of a crystal—melt mush, or of chiefly molten materials will first elevate the surface in gentle swells. As spreading takes subsequently place collapse and stretching of the central part of the gentle swells and leveling of the domed surface gives rise to a geomorphology characteristic for rift-valley systems. CLOOS (1939) has demonstrated how rift-valley systems generally occur within domed shields of the earth's crust. Whereas Cloos assumed that the bending of a rigid crust is sufficient to generate tension fractures and rift valleys,¹ the present author considers spreading of (buoyancy-) injected subcrustal bodies as an essential feature of the mechanism that creates tension and rift-valley collapse of the superincumbant crust.

Where fractures reach down to fused parts of the doming or spreading material the magma may well be able to rise up to the surface even if its density is higher than that of the rigid and fractured rocks of the immediate surroundings. Because of the great contrast in strength and viscosity between a basic silicate melt and the rocks of the upper, rigid part of the crust the melt has little opportunity to spread in spite of its higher density. If the buoyant push from below is strong enough the melt may then rise in fractures to relatively high level for eventually to erupt as lava.

In connection with the theory of evolution of island arcs and deep-sea trenches as discussed above the so called low-velocity subcrustal layer may be

¹ Writes CLOOS in the above-cited paper p. 481: "Die Bildung von Gräben und Vulkanspalten ist eine Folge konvexer Durchbiegung der Oberkruste".

of considerable significance. Originally suggested by GUTENBERG (1954) and verified by recent seismic observations (ANDERSON, 1962), a layer occurring at a depth between 60 and 250 km displays seismic properties indicative of higher fluidity or greater plasticity than the materials above and below. Such a sudden increase of fluidity at some 60 km below the surface requires, provided the fluid material is not too dense, that this relatively fluid material must constitute a major portion of the substance that ascends through the volcanic vents. It seems probable that the low-velocity layer, at least its upper part, consists of a crystal—melt mush rather than being completely molten. In complex chemical systems such as natural silicates the melting temperature spans over a considerable interval, often several hundred degrees. The crystal—melt mush must correspondingly span over a layer with considerable thickness.

Remarks on emplacement of basic and acidic rocks

The fact that basic and acidic rocks generally occur in contrasted geologic setting has provoked much discussion in geologic literature. It is believed by the writer that certain features of the model experiments presented here may contribute to the clarification of the question of emplacement of plutonic bodies of acidic, respective basic, composition.

Field studies have established that basic extrusive rocks are much more abundant than extrusive rocks of acidic composition whereas the opposite is true of plutonic rocks. This important observation has been especially discussed by KENNEDY and ANDERSON (1938). It is more significant in connection with our model studies that the shape and structure of plutonic basic and acidic bodies are characteristically different. The acidic rocks occur chiefly as dome- or batholith-like bodies with a vertical dimension which is considerable relative to the lateral extension, and with a roof that is convex upward. Structural conformity between pluton and surroundings is common. The very shape suggests a rising tendency of the masses. Often closer structural studies support the impression that such bodies have been rising in relation to the surroundings (cf. the "Granittektonik" as discussed by CLOOS, 1925). The compilation work by Buddington, *op. cit.* may be studied for details.

In contrast the known large plutonic bodies of basic composition are generally shaped as rather thin convex-concave lenses with the convex side facing downward. Their shape suggests a tendency to sink, so does in many instances the structure in the surroundings. Such lopoliths of huge dimensions are among the most well-known plutonic complexes of the world, e.g. the Sudbury and the Duluth complexes in North America, and the Bushveld complex in Africa. Disregarding some anorthosite massifs, there is no known *large* basic pluton that may be interpreted as a dome or batholith.

Also in their hypabyssal facies basic and acidic rocks are different: Diabase or dolerite dikes usually occur as rather thin but extensive sheets that run tens and hundreds of miles across geologic formations whereas acidic dikes are often

irregular in shape and very limited in extension. Dikes¹ of acidic rocks are rare except in regions close to volcanic vents and obvious subvolcanic intrusions. Basic dikes—diabase or dolerite—are found in extensive swarms often without apparent connection with volcanic vents. Such swarms probably were the feeders to huge flows of plateau basalt.

These general impressions from the field go well together with our model experiments in advancing the following theory of emplacement:

Acidic plutons such as granodiorites and granites are in general less dense than the average rock that makes up the geologically accessible part of the earth's crust, i.e. the part which may be removed by extreme erosion, or the surface layer which extends from the level of granulite facies (e.g. RAMBERG, 1952) of regional metamorphism and up. Hence bodies of granodiorite and granite within the accessible part of the earth's crust are in general enclosed in surroundings that give buoyancy to the embedded plutons. Many of these masses have thus been actively rising relative to their surroundings until they became "quenched" due to increased viscosity and strength as they approached the surface of the crust. Structure and shape indicative of upward motion are therefore to be expected of a majority of granitoid plutons, particularly deep-seated ones.

Basic rocks show in general higher density than the upper part of the crust which is exposed by maximum erosion. Basic plutons accessible for direct study consequently occur in surroundings which generally do not give buoyancy to the enclosed plutons. Consequently basic bodies in general do not display structure and shape that indicate buoyant motion relative to the environment. On the contrary such bodies exhibit features indicative of lateral spreading (i.e. extensive sheet-shaped plutons) and sinking relative to the surroundings (i.e. the convex surface facing downward). Such geometric and structural patterns are similar to those developed in the models when ascending masses encountered layers less dense than themselves, see for example Figs. 32 and 34.²

If tension fractures occur in the rigid crust above the body of a basic melt, the melt may of course be forced up through the fractures irrespective of the relative density of melt and immediate surroundings. The buoyant push from deeper levels is sufficient to elevate the melt through the fractures.

It is tempting to assume that basic rocks such as gabbros and anorthosites rise in dome- or batholith-like fashion within the dense surroundings of the mantle in much the same manner that granites and granodiorites rise due to

¹ Pegmatites and aplites are not included in the types of dikes considered here. Pegmatites are related to metamorphism and metasomatism (see RAMBERG, 1956), processes which do not concern us in this paper.

² As discussed p. 45 a flat, even-thick sheet that sinks through a fluid material should develop a curved shape with the convex side facing upward. This does not hold if the heavy layer is thicker in the middle than along the edges such as obviously most sheet-shaped intrusives would be. In this case the high pressure underneath the thick central part of the sheet makes the center sink more rapidly than the thin outer parts of the body.

buoyant forces within the deeper parts of the crust. The high-melting monomineralic anorthosites probably are wholly crystalline during their ascent, but the gabbroic bodies may well be partly molten, the molten part being able to penetrate into the crust and spread as lopoliths or to reach the surface through fracture systems.

In conclusion the writer suggests that an important reason for the observed contrasted geometry and structure of acidic and basic intrusive rocks is due to the condition that the exposed acidic bodies are situated in an environment that exposes the masses to buoyant forces so to speak in situ, whereas the basic bodies that are accessible for direct study are not enclosed in buoyancy-creating surroundings. A basic body occurring in the upper part of the crust owes its presence there to an upwardly directed push originated at deeper levels, possibly due to buoyant forces acting on the lower part of the mass which is surrounded by the dense material of the mantle. Since plutonic shapes such as domes and batholiths are characteristic of masses which rise due to buoyancy in situ, such shapes are generally not displayed by the heavy basic rocks. It is perhaps conceivable, however, that some anorthosite masses that typically occur only within the most deeply eroded regions of the crust, viz. within granulite facies areas, represent the top portion of basic batholiths which have roots down in a subcrust which is more dense than the anorthosite itself.

Models of folding of surface layers caused by adjustments of unstable distribution of masses

Folding of originally flat-lying surface layers may be the result of vertical displacements which vary in magnitude from place to place. The evolution of a dome, for example, with its marginal sinks gives rise to an anticline with adjacent synclines in originally horizontal surface strata. Under certain conditions a primary dome may initiate a series of secondary domes or swells and troughs in the surrounding area (see PARKER *et al.*, op. cit.) thereby creating a series of anticlines and synclines in layered overburden.

Lateral compression is the other major cause of folding of surface layers. Such compression may be of local and superficial nature due to unstable topography, or it may be of more regional extent and generated by deep-seated movements such as convection currents.

Layered rocks are known to be capable of sliding downhill and generate buckling and stowing of the frontal part of the sliding package. A number of geologists consider this kind of "secondary tectonics" to be of major significance in orogenic evolution (HAARMAN 1930; VAN BEMMELEN 1933, 1956; BUCHER, 1956; BELOUSSOV, 1960; RAMBERG, 1945).

The deep-seated motions that are considered responsible for more profound and large-scale lateral compression may be driven by forces of various origin. In the present brief discussion we shall only consider motions caused by un-

stable distribution of masses in the field of gravity (or field of acceleration in a centrifuge).

It is a trivial consequence of equilibrium theory that a stable earth would consist of concentric shells whose densities increase toward the center. Each shell would consist of a single phase, or of a mixture of phases if some chemically compatible phases happen to have identical density.

Far from materialized, such a state of the earth is obviously being approached. Movements of matter by bodily flow or displacement of rigid masses (mechanical motion) as well as by atomistic diffusion (chemical processes) tend to bring the earth toward a mechanically more stable concentric configuration. This tendency is disturbed by counteracting processes driven by potential energies other than mechanical. One of the most important nonmechanical energies of the earth is the thermal energy as indicated by the drop in temperature between the interior and the surface. The earth is a heat engine, possibly fed by nuclear energy, that transforms some of its potential thermal energy into mechanical work. A tangible result of this work is the folded complexes of stratified rocks.

One of the suggested mechanisms of coupling between thermal energy and mechanical work is *via* convection cells such as proposed by for example VENING MEINESZ, *op. cit.* The geothermal gradient provides an unstable density distribution within a chemically uniform global shell, and an overturn of matter within the shell follows. Related horizontal currents along the upper boundary of a uniform global shell creates compressive and extensive stresses in the superincumbent layer. Alternating zones of buckling and stretching (zones with tension fractures) may then develop provided the currents are powerful enough to deform and fracture the crust.

Another mean of coupling between global thermal energy and mechanical work is *via* melting or other volume-changing phase transformations such as proposed by the present writer in 1945 (*op. cit.*). If the lower part of a chemically uniform shell is molten there is a sudden and rather large (ca. 5-10%) change in density across the boundary between solid and liquid, under this circumstance the buoyant tendency is apt to be much stronger than in an ordinary convection cell in a layer of same material and same thickness. The light liquid will force its way upward either rapidly through fractures or more slowly by plastic yield in the surrounding solids along the upward route, much like the KMnO_4 -solution in the experiments described above (pp. 25 and 61).

The melt that penetrates into the superincumbent solid shell may ultimately solidify at the lower temperature encountered in the higher regions. In view of the 5 to 10% volume change associated with crystallization of most silicate rocks, it is likely that the solidified body becomes more dense than the surrounding rocks. This is apt to happen when a basic melt crystallizes when enclosed in more acidic surroundings. As a huge heavy body of this kind sinks through the solid crust it can hardly escape causing folding and other structural disturbances in adjacent and superincumbent rocks.

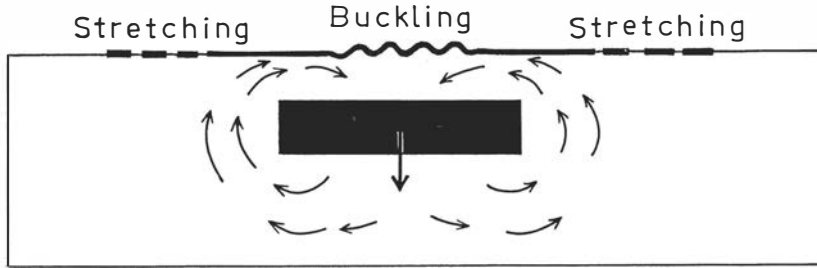


Fig. 46. Flow lines around a heavy body sinking through a viscous material. Deformation in competent crust indicated.

In connection with comments on island arcs and deep-sea trenches (p. 65) it was suggested that the crust may become basified by extrusion and intrusion of basic magma (RAMBERG, 1945). The surface of such basified segments of the earth's crust will submerge below sea level, sedimentation will take place and gravity sliding is apt to generate folding. A more significant part of the theoretical model is, however, that the larger bodies of the heavy basic rocks will sink through the less dense crust, that the light acidic components of the buried rocks tend to rise, dome-like fashion, in the region between the basic masses or through weak zones in these sheet-shaped bodies, and that a sort of backwash-like flow above the foundering bodies creates lateral tension and compression at critical localities in the superincumbent strata. As a consequence buckling in some regions and fracturing under tension in other regions take place as indicated on Fig. 46.

There are abundant geologic evidence to the effect that parts of the crust now submerged below the oceans have once been above sea level. That the North Atlantic Ocean between Norway, Scotland, Greenland and Svalbard has sunk below sea level in geologically recent time seems to be generally accepted. The rise of the coastal part of Scandinavia along submarine fracture zones (HOLTEDAHL, 1960, p. 351) is probably connected with the submergence of the adjacent North Atlantic. East of the east coast of the USA a land mass, the Appalachia, has once existed as shown by the distribution of sediments in the Appalachian mountains. In a recent paper BELOUSSOV (1961) demonstrates that the Sea of Japan and the Sea of Okhotsk were once elevated land masses.

A number of experimental tests were made in order to check if processes of the above-mentioned type are physically realistic. Some of the models, which are of qualitative nature, are described below.

Model a: In a homogeneous body at rest in the field of gravity, or rotating in a centrifuge, any departure from an equipotential plane of the free surface of the body represents an instability, see discussion in Appendix.—If the body consists of a viscous material any depression or rise of the surface, relative to the equipotential plane, will ultimately be leveled out by viscous flow in the substratum. In the center of a symmetric depression the velocity vector of the

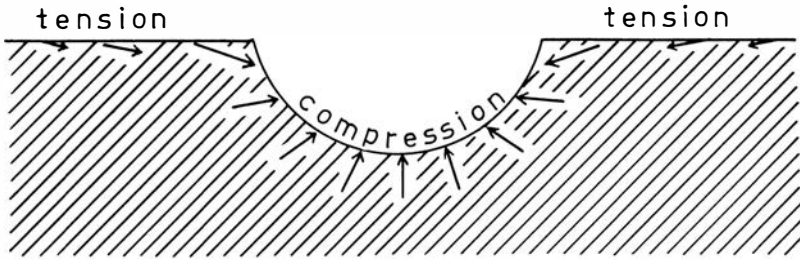


Fig. 47. Profile across depression in plastic body. Arrows indicate direction and relative rate of flow.

flow is vertical without horizontal components. Toward the boundaries of the depression, and in the region outside its boundaries, the flow has a horizontal component of varying magnitude. This component, which is directed toward the center of the basin, is particularly strong close to the surface. The horizontal component of flow generates stresses in a competent surface layer due to drag-coupling, the horizontal normal stress being compressive within the depressed region, and extensive in the surroundings. Maximum compression is reached in the center of the basin, Fig. 47. Therefore, if a not-too-strong competent layer is placed over a depressed region on the "horizontal" surface of a uni-

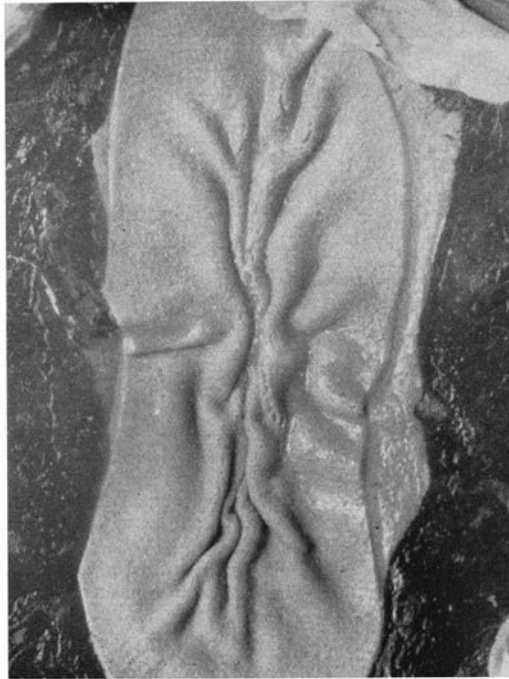


Fig. 48. Surface layer of modelling clay buckled during collapse of depression in substratum of stitching wax. Diameter of model 48 mm.

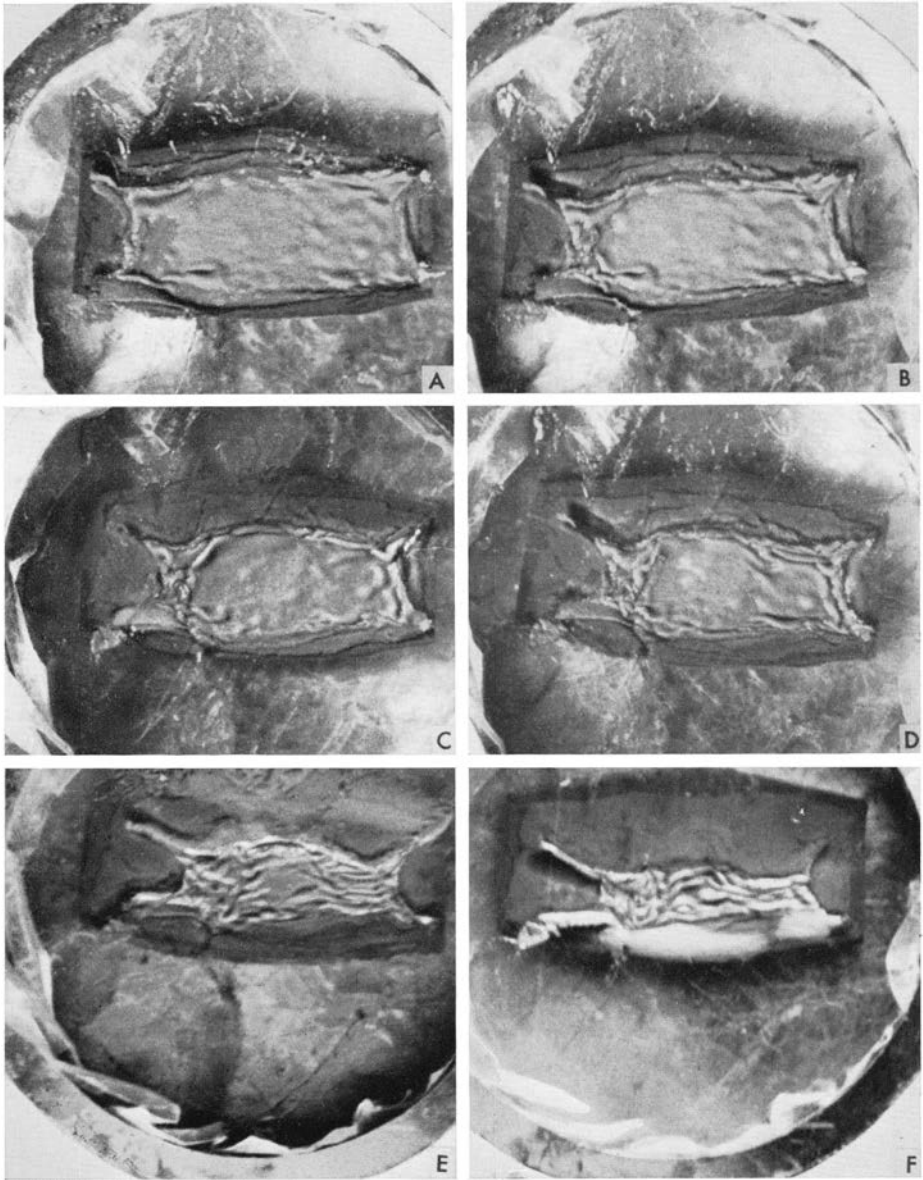


Fig. 49. Various stages of the sinking of a heavy layer through stitching wax, and the folding of thin sheets of modelling clay in the collapsing basin above the sinking layer. Light grey material in middle is modelling clay "sediments", dark grey body seen outside the crumpling "sediments" is the thicker modelling clay plate which sinks through the clear wax. Stage *A* is shortly after folding has started. Stage *F* ca. 20 minutes after run started. Diameter of cup 48 mm.

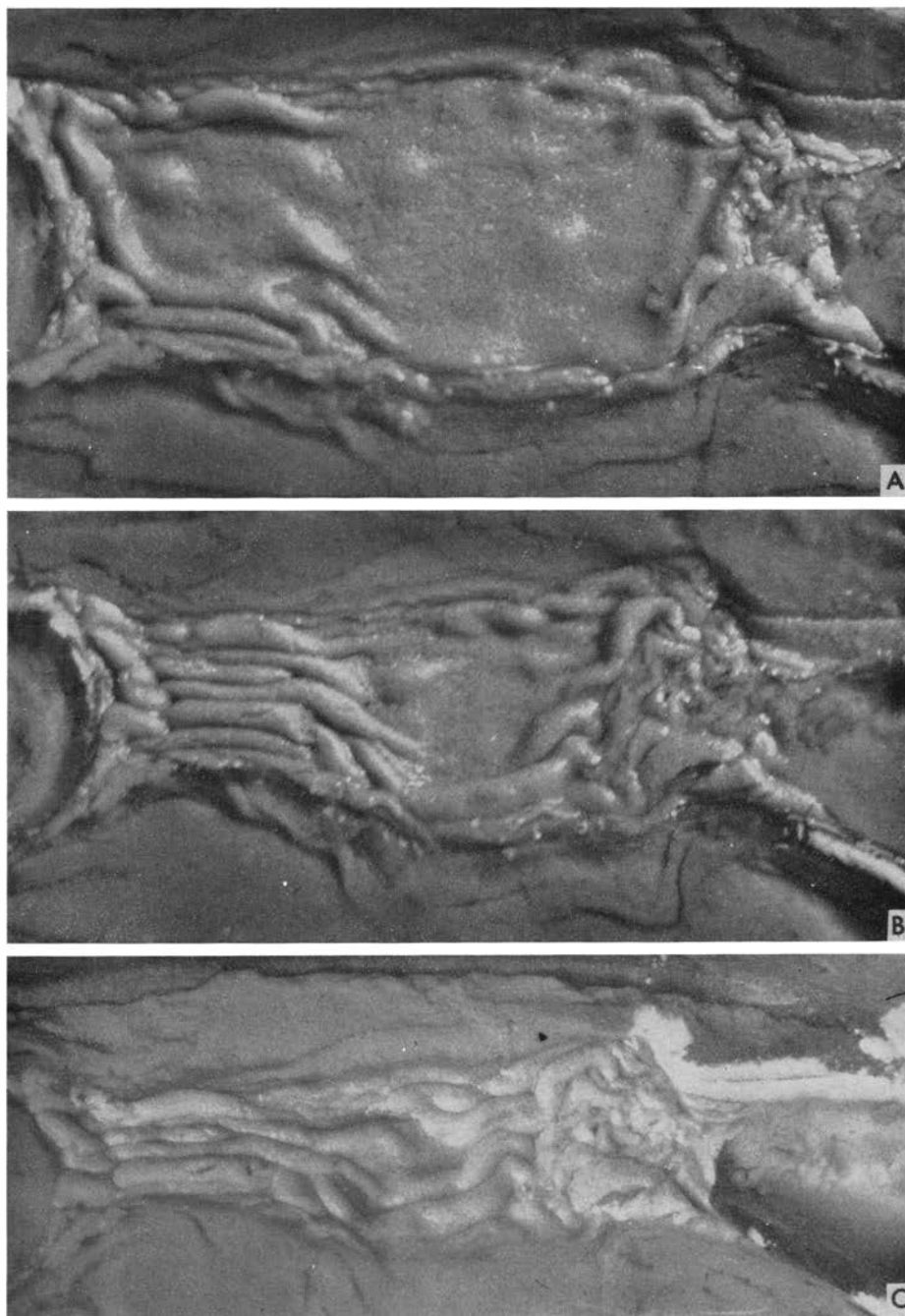


Fig. 50. Enlarged details of stage *D*, *E* and *F* in Fig. 49. Length of fold zone 25–30 mm.

form viscous body, buckling will occur as a result of the viscous collapse of the basin.

This phenomenon is readily displayed by making a depression of the surface of a substratum of stitching wax, covering the depression with a sheet of modelling clay and running the model for a short while in a centrifuge at moderate acceleration. Fig. 48 shows the result of such a test.

In a recent paper HAMILTON (1962) reports some experimental studies of gravity collapse of a depression made in the surface of a body of asphalt, the surface being covered by a granular crust-simulating material. Hamilton was, however, not able to detect buckles (ripples) on the surface of the granular crust. It is possible that the crust in HAMILTON's test was too strong.

Model b: In this model the effect of the backwash flow above a sinking body was shown.

In a small 48 mm diameter centrifuge cup a basal layer of stitching wax was laid down. On top of this substratum a 2 mm thick and 10–15 mm wide strip of modelling clay was placed. After less than 5 minutes' run at an acceleration of about 1000 *g* the strip of modelling clay had sunk down in the substratum until the surface of the strip of modelling clay was a little below the surface of the adjacent wax which had started to creep out over the modelling clay. A basin had formed by isostatic adjustment in the field of centrifugal force.

The basin was now coated with a thin layer of grease, and two 0.3 mm thick sheets of modelling clay with grease between were placed on the basin. When this structure was run in the centrifuge the thick basal strip of modelling clay continued to sink down in the subjacent wax and the adjacent "continents" of stitching wax continued to spread out over the bottom of the basin. The layered complex of modelling clay and grease became strongly buckled in front of the edges of the spreading "continents". Figs. 49 and 50 shows a sequence of stages of the evolution of this model. The result is quite similar to folded strata as seen in parts of the Alps, the Caledonian in Scandinavia and the Appalachian in USA.

Models c and d: In these models an attempt was made to imitate a part of the flow pattern of a convection cell in a very viscous substance without making use of a thermal gradient. The idea was to see how such a flow pattern in a viscous substratum would reflect itself upon a relatively competent surface layer. If a relatively heavy body is placed in a larger mass of viscous material the body will sink in the field of centrifugal acceleration and create a system of streamlines more or less as indicated in Fig. 46. Such a system of streamlines is rather similar to the streamlines in the downward-moving branch of some convection cells. The less streamlined the shape of the sinking body the greater its drag upon the surroundings and thus the larger the volume of embedding material that is set in motion by the sinking body. By embedding a horizontal sheet-shaped body, for example, its sinking through the substratum will create far-reaching flow in the surroundings.

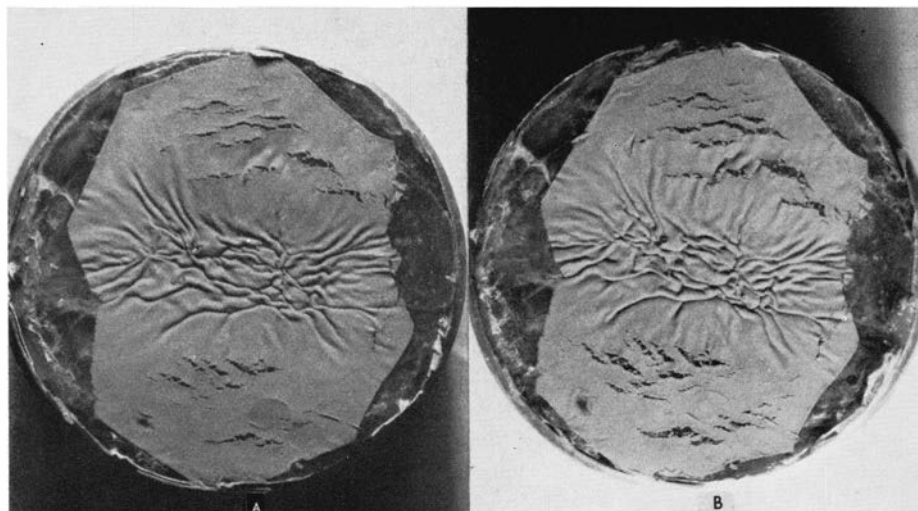


Fig. 51. Surface layer of modelling clay on substratum of stitching wax buckled and fractured in the stress field created by the "backwash" above a sinking body embedded in the substratum, see text p. 82. *A*: after 5 minutes run at 1000 *g*; *B*: after 10 minutes run. Diameter of the model 94 mm.

Since buckling of the crust according to the convection hypothesis takes place above down-moving branches of convection cells models of type described here represent a simple means of studying crustal buckling by convection in the mantle.

In the 94 mm diameter centrifuge cup a 30 mm high cylinder of stitching wax was placed. Embedded in this body was a rectangular block about 7 mm thick, 25 mm wide and 40 mm long. This block, which happen to be a piece of hard rubber with density about 1.2 g/cm³, occurred a few millimeters below the surface prior to the run in the centrifuge. A sheet of modelling clay, less than 1 mm thick, was placed on the surface of the stitching wax.

After 5 minutes' run in the centrifuge at 1000 *g* the surface sheet of modelling clay had started to buckle in the region just above the sinking piece of rubber whereas tension fractures had developed in the areas outside the sinking rubber piece, Fig. 51. A few minutes' additional run in the centrifuge resulted only in some widening of the tension fractures and a little additional compression of the buckled portion of the surface sheet of modelling clay.

In another model the initial structure with the embedded block of rubber in stitching wax was the same as above, but the layer of modelling clay was replaced by a sheet of rather stiff packing wax, about 1 mm thick. The buckles shown in Fig. 52 were developed after some 10 minutes' run at an acceleration corresponding to 1000 *g*. Only a few buckles formed and no tension fractures developed.

The two models described above suggest that important features of convec-

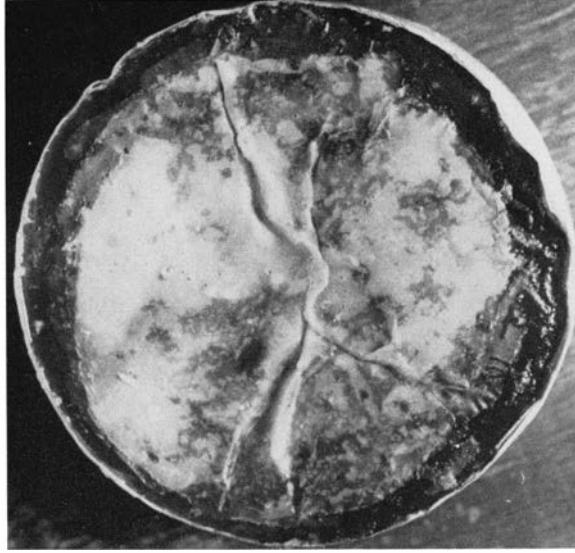


Fig. 52. Surface layer of stiff packing wax buckled in the "backwash" flow above a sinking body embedded in substratum of stitching wax. Diameter of model 94 mm.

tion currents may be studied by exposing rather viscous and plastic materials to centrifugal forces. Although the flow pattern caused by a sinking body submerged in a viscous material is somewhat similar to certain convection cells the similarity is of limited nature. To study the geological implication of such currents more thoroughly it is necessary to expose the centrifugal models to a vertical temperature gradient. Special centrifuge cups for that purpose are now under construction in the writer's laboratory at Uppsala University.

Some theoretical calculations pertaining to buckling of surface layers affected by acceleration are found in the Appendix.

Appendix

Note on buoyancy in models

For models of geologic structures containing more than one substance it would be virtually impossible to find materials whose viscosities, strengths and densities, not to speak about the variations of these properties with stress, are all simultaneously in proper scale with corresponding properties of the rocks in the original. It is therefore important that under certain circumstances corrections of the time ratio may readily be made for models whose densities are not properly scaled to the original, i.e. for model—original systems in which the model ratio of density is not the same for all substances contained in the two corresponding structures.

The corrections referred to above are applicable to the buoyant motion of

one or several bodies of one kind of material enclosed in a body of another material, but usually not to general motion in the whole structure. We shall initiate the discussion of the corrections by considering a system consisting of a body A enclosed in another body B at rest in the field of gravity of the earth. Let A be a rigid body and B a Newtonian fluid with viscosity μ . The densities of the two materials are d_A and d_B respectively, and the rate of change of motion is so slow that inertia may be disregarded and turbulence does not occur.

We wish to show that the correct rate of motion of A in B can be determined experimentally by model study even if the densities d_a and d_b of the substances a and b in the model corresponding to A and B in the original are not properly scaled to the original, i.e. even if

$$\frac{d_A}{d_a} \neq \frac{d_B}{d_b}. \quad (36)$$

A model which is similar to the original in all respects with the exception of the densities and the parameters depending on the densities (e.g. strength and stress) may be called a *quasi-scale model*. (A true scale model must satisfy the condition

$$\frac{d_a}{d_A} = \frac{d_b}{d_B} = \delta, \quad (37)$$

where δ is the model ratio of density.)

We shall also require that the quasi-scale model satisfies the condition that if $d_A > d_B$ in the original then $d_a > d_b$ in the model, and *vice versa*, if $d_A < d_B$ in the original then $d_a < d_b$ in the model. If this is not the case the motions will be directly opposite in model and original, a condition which makes the consideration of one structure a model of the other somewhat questionable.

Although a single-valued model ratio of density cannot be assigned to the quasi-scale model its model ratio of density *contrast* is unambiguous and may be defined as follows

$$\Delta\delta = \frac{d_a - d_b}{d_A - d_B}. \quad (38)$$

(For a true scale model the model ratio of density contrast is numerically identical to the model ratio of density because

$$\delta = \frac{d_a}{d_A} = \frac{d_b}{d_B}, \quad (39)$$

hence

$$\left. \frac{d_a - d_b}{d_A - d_B} = \delta. \right) \quad (40)$$

The fact that the densities of the quasi-scale model are not in proper scale with the original means that the model ratio of stress must also be modified. As long as the problem is one of buoyancy of one substance in another it is

convenient to define a quantity which may be termed the *buoyant stress*. For a quasi-scale model with but two substances the model ratio of buoyant stress is an unambiguous quantity; this is not generally true for systems containing more than two substances. The model ratio of buoyant stress is defined as follows

$$\Delta\sigma = \Delta\delta\lambda, \quad (41)$$

where λ is the model ratio of length and $\Delta\delta$ the model ratio of density contrast.

To show the meaning of the ratio of buoyant stress consider a cube l_0^3 cc large of material A enclosed in B in the original, and a geometrically similar cube of l_m^3 cc volume of material a enclosed in b in the model. Let the two cubes be kept at rest in relation to the embedding material. This may, for example, be accomplished by anchoring the cubes to the boundaries of the systems by means of thin wires. After hydrostatic equilibrium has been established the pull in the wires, which represents the buoyant force, equals $l_0^3(d_A-d_B)g$ dynes in the original and $l_m^3(d_a-d_b)g$ dynes in the model. Dividing these forces by the areas of the sides of the cubes l_0^2 and l_m^2 respectively, gives the buoyancy expressed in terms of stress. The ratio between the buoyant stresses in model and original respectively, is then

$$\Delta\sigma = \frac{l_m(d_a-d_b)}{l_0(d_A-d_B)} = \lambda\Delta\delta. \quad (42)$$

This equation is valid for a quasi-scale model as well as a true model. (In the latter $\Delta\delta = \delta$ because $d_a/d_b = d_A/d_B$. Hence there is no numerical distinction between the model ratio of buoyant stress and the model ratio of stress in general.)

For a true scale model the model ratio of time is

$$\frac{t_m}{t_0} = \tau = \psi\sigma^{-1} = \frac{\psi}{\lambda} \frac{d_A}{d_a} = \frac{\psi}{\lambda} \frac{d_B}{d_b}, \quad (43)$$

where ψ is the model ratio of viscosity and σ that of stress.

We shall now assume *by hypothesis* that an analogous ratio of time is applicable to the relation between the quasi-scale model and the original, i.e. that the relation

$$\frac{t_{qm}}{t_0} = \tau' = \psi\Delta\sigma^{-1} = \frac{\psi}{\lambda\Delta\delta} = \frac{\psi}{\lambda} \frac{d_A-d_B}{d_a-d_b} \quad \text{is valid.} \quad (44)$$

Here t_{qm} is the time required for a given motion of body a in the model, and t_0 the time required for the corresponding motion in the original.

To show that eq. (44) leads to correct result we shall compare the quasi-scale model with a true model for which the model ratio of length and the model ratio of viscosity are the same as for the quasi-scale model.

In the true model let the substance which corresponds to A in the original have the same density, d_a , as in the quasi-scale model. The material which

corresponds to the body B , must then have a density different from d_b , say d'_b because $d_a/d_A = d'_b/d_B$ for the true model, but $d_a/d_A \geq d_b/d_B$ for the quasi-scale model.

Eq. (44), which refers to the quasi-scale model, is exactly as valid as eq. (43), which refers to the true model, if we can show that the lapse of time, t_{qm} , for a given motion in the quasi-scale model and the lapse of time, t_m , for the identical motion in the true model both give the same time, t_0 , for the corresponding motion in the original. For this to be true the relation between t_{qm} and t_m must be correctly expressed by putting t_0 in eq. (43) equal to t_0 in eq. (44), thus

$$\frac{t_{qm}}{t_m} = \frac{(d_A - d_B)}{(d_a - d_b)} \frac{d'_b}{d_B} = \frac{(d_A - d_B)}{(d_a - d_b)} \frac{d_a}{d_A}, \tag{45}$$

noting that d'_b is the density of the substance b in the true model. To test this proposition we shall consider the situation from the point of view of the theory of fluid dynamic which is independent of scale-model theory. According to fluid dynamic theory the velocity, V , of steady rise or fall of a rigid body of given size and shape enclosed in a Newtonian fluid is proportional to the density contrast between the two media. That is: $V = C(d_1 - d_2)$, the constant C depending upon the viscosity of the fluid and the shape and size of the enclosed body. Applied to the true model and the quasi-scale model the time needed for identical motion in the two structures are

$$t_m = \frac{C'}{d_a - d'_b}, \text{ and } t_{qm} = \frac{C'}{d_a - d_b} \tag{46}$$

respectively, where C' is a constant different from C . Consequently, according to independent fluid dynamic theory, the time ratio between the quasi-scale model and the true model is

$$\frac{t_{qm}}{t_m} = \frac{d_a - d'_b}{d_a - d_b}. \tag{47}$$

We may now argue as follows: Granted that the true scale model theory and the fluid dynamic theory of buoyancy of embedded rigid body both are physically valid then the suggested quasi-scale equation

$$\frac{t_{qm}}{t_0} = \psi \Delta \sigma^{-1} = \frac{\psi}{\lambda} \frac{d_A - d_B}{d_a - d_b} \tag{48}$$

is also valid provided the t_{qm}/t_m -ratio expressed by eq. (45) is identical to the t_{qm}/t_m -ratio expressed by eq. (47); i.e. provided

$$\frac{d'_b (d_A - d_B)}{d_B (d_a - d_b)} = \frac{d_a - d'_b}{d_a - d_b}, \text{ or } \frac{d'_b}{d_B} (d_A - d_B) = d_a - d'_b. \tag{49}$$

This requirement is fulfilled because $d_a/d_A = d'_b/d_B$.

We have consequently shown that the relation expressed by eq. (44) is applicable to an original system and its quasi-scale model even if the densities of the materials in the model are not properly scaled to those of the materials in the original.

It follows from the discussion above that the validity of eq. (44) has been proven only for systems consisting of a rigid body enclosed in a fluid of Newtonian type.

In most dome models discussed in this paper the densities are not correctly scaled to the geometrically similar geologic structures. We have applied the quasi-scale model equation (44) when scaling up the experimental time to a corresponding geologic time, see Tables 1, 2, 3, 4, 6. This equation, which has only been shown to be valid for buoyancy of a rigid body embedded in a fluid, is probably not exact for dome models inasmuch as the dome material is fluid and thus the shape of the dome and source layer may not remain geometrically similar to the original unless the model is correctly scaled also with respect to the densities. In the quasi-scale models it is conceivable that the relation between the diameter of the domes and the thickness of the source layer, as well as the shape and position of the marginal sink, are not exactly as they would be if the densities were correctly scaled. These conditions may well affect the rate of flow, but it is unlikely that the effect is large enough to cause significant error in the applied quasi-model equation. Incidentally, one notes that PARKER *et al.*, *op. cit.* apply the quasi-model equation without qualifying comments.

There is another condition in the quasi-scale models which is significant and merits mention, viz. that the flow of the doming material after piercing the surface is not similar to the surface flow of true models. When the doming material pierces the surface it spreads laterally under its own weight, and a mushroom-shaped hat of the kind shown in Figs. 1, 2, 11, etc. is formed. But as long as the buoyant push from below remains, there is also a tendency of the surfaced hat to thicken. The profile of the hat is accordingly determined by the buoyant push from below, which tends to make the hat thicker, and the weight of the hat which causes it to spread and become thinner. In most models discussed in this paper the model ratio of density contrast between overburden and doming material is greater than the model ratio of density of the doming material (see Tables 1 to 6). That means that the buoyant push relative to the spreading force is stronger in the model than in the corresponding geologic structure. Hence the vertical dimension of the surfaced portion of the domes is exaggerated relative to the horizontal dimension in the models as compared with corresponding geologic structures.

Buckling of a surface layer exposed simultaneously to lateral compression and the pull of gravity or a centrifugal force in normal direction

A sheet of relatively competent medium welded on the plane surface of a semi-infinite body will buckle if exposed to compression parallel to the surface.

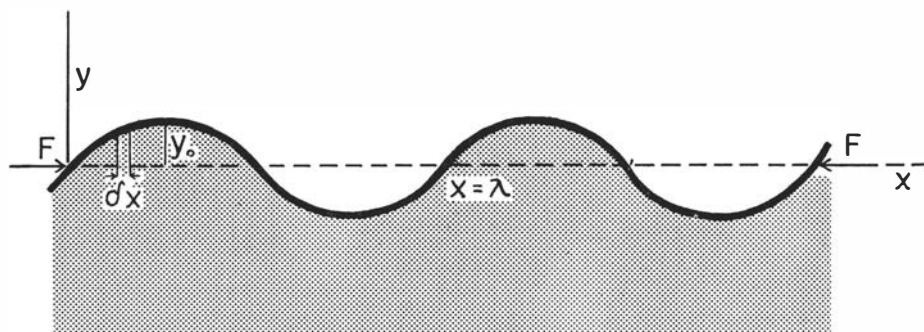


Fig. 53. Profile of buckled viscous surface layer on viscous substratum, see text.

Provided the acceleration due to gravity (or due to rotation in a centrifuge) is disregarded the force needed to buckle a viscous surface layer welded on a viscous substratum is

$$F_x = \left(\frac{8}{3} \mu \omega^2 h^3 + \frac{2}{\omega} \mu_1 \right) \frac{\dot{y}_0}{y_0} \quad (\text{RAMBERG, 1962}). \quad (50)$$

F_x is the compressive force acting parallel to x (which lies in the originally plane layer) reckoned per unit length in z (which is parallel to the fold axis), μ is coefficient of viscosity of the surface layer, μ_1 the same for the substratum ($\mu > \mu_1$), h is half the thickness of the surface layer, $\omega = 2\pi/\lambda$ with λ as wavelength, y_0 and \dot{y}_0 are amplitude and the rate of growth of amplitude, respectively. The equation is restricted to Newtonian-type substances and to rather small h/λ -ratios (less than say $\frac{1}{12}$), as well as very small amplitude/wavelength ratios.

The first term in the bracket represents the force needed to change the strain in the layer itself by a rate determined by the term \dot{y}_0/y_0 , and the second term in the bracket represents the force needed to change the strain in the adjacent part of the substratum by a rate as determined by \dot{y}_0/y_0 . (For detailed discussion of buckling as applied to geology see BIOT, 1961 and RAMBERG, 1962.)

In a system not affected by gravity or other acceleration the initial wavelength (or length of arc of a wave) which actually materializes (as verified by experiments) is that which corresponds to minimum compressive force, F_x , at any given constant ratio between rate of growth of amplitude, \dot{y}_0 , and absolute magnitude, y_0 , of amplitude. This condition in particular is discussed in the above-cited paper by the writer. Minimum force in x direction also means minimum expenditure of energy in the course of a given magnitude and given rate of compression along the x axis.

In an attempt to include the effect of gravity or any other body force directed normal to the surface, such as the centrifugal force in a centrifuge, we shall make the simplifying condition that the density of layer and substratum is the same, that the surface folds are sinusoidal, and that the length of arc of a fold is large relative to the thickness, Fig. 53.

Energy is required in order to make an equipotential free surface of a body affected by gravity (or other acceleration) assume any shape departing from the equipotential surface. If the new surface takes the shape of a series of two-dimensional sinusoidal waves, then the potential energy per wave is given by the double integral

$$E_p = daz \iint y \partial y \partial x, \quad (51)$$

taken between the limits $x=0$, $x=\lambda$ and $y=0$, $y=y'$, where y' is the function $y_0 \sin \omega x$. d is the density of the material, a is acceleration normal to layering and z is dimension parallel to the fold axis. z is taken as unity because all energies and forces will be reckoned per unit length in z . The integral between the limits specified above is

$$E_p = \frac{1}{4} d a y_0^2 \lambda. \quad (52)$$

Inasmuch as the wavy morphology of the surface is generated by the lateral compressive force that throws the competent surface layer into buckles, the potential energy, E_p , of the sinusoidal morphology must equal the energy due to lateral displacement (parallel to x) of a force component, f_x , that act in x direction on the surface layer. f_x must be added to the force F_x due to viscous resistance (eq. (50)) in order to balance the pull of gravity on the wavy morphology.

An expression for f_x is determined by the following analysis. During buckling the length of arc of the surface will be considered constant¹, but the wavelength decreases simultaneously with increasing amplitude.

At constant length of arc the relation between amplitude, y_0 , finite wavelength, λ , and length of arc or initial wavelength, λ_1 , can be shown to be

$$\pi^2 y_0^2 = \lambda_1 \lambda - \lambda^2 \quad (53)$$

provided the folds are very gentle (see for example RAMBERG, 1962). Substituting for y_0 in eq. (52) gives the potential energy due to morphology expressed as a function of finite wavelength and magnitude of compression of the wave, $\lambda_1 - \lambda$:

$$E_p = \frac{1}{4} \frac{da}{\pi^2} (\lambda_1 - \lambda) \lambda^2. \quad (54)$$

Since force is definable as energy differentiated with respect to displacement the potential energy represents a force in x direction defined as follows

$$f_x = \frac{\partial E_p}{\partial \lambda} = \frac{1}{4} \frac{da}{\pi^2} (2\lambda_1 \lambda - 3\lambda^2), \quad (55)$$

¹ Some compressive strain in x direction and thickening parallel to y always occur simultaneously with viscous buckling as discussed by BIOT, op. cit. This arc-shortening strain in the layer decreases with increasing viscosity contrast between layer and substratum and decreases with increasing amplitude/wavelength ratio of the buckles.

which must be added to F_x in order to balance the gravitational or centrifugal pull on a wavy sinusoidal surface.

f_x as expressed by eq. (55) is only valid for small-amplitude gentle folds. For such folds no significant error occurs if we neglect the difference between wavelength and length of arc, in which case

$$f_x = -\frac{1}{4} \frac{da}{\pi^2} \lambda^2 = -\frac{da}{\omega^2}.$$

The minus sign arises from the condition that the motion along x is compressive; the sign of f_x may, however, be changed depending upon the particular case.

Adding f_x to F_x gives the total compressive force parallel to x that is needed to make a viscous surface layer buckle at given rate when affected by the acceleration due to gravity or due to rotation in a centrifuge

$$F = F_x - f_x = \left(\frac{8}{3} \mu \omega^2 h^3 + \frac{2}{\omega} \mu_1 \right) \frac{\dot{y}_0}{y_0} + \frac{da}{\omega^2}. \quad (56)$$

The terms in the bracket, multiplied by \dot{y}_0/y_0 , equal the forces needed to balance the viscous resistance in the surface layer and in the substratum respectively. These forces increase with increasing rate of amplitude growth—which also means increasing rate of compression parallel to x —at any given amplitude. The force needed to change the morphology of the surface, as represented by the term da/ω^2 is, on the contrary, independent of the rate of buckling. It is also worth noting that the forces which balance the viscous strain in the buckling layer and its substratum go to infinity as the amplitude vanishes. That is, an ideally “flat” (=parallel to an equipotential surface) layer does not buckle in response to symmetrically applied compressive forces. The layer must either display some initial irregularities or the forces must be unsymmetrically applied.

In many practical cases the wavelength/thickness ratio of buckling layers is a more convenient quantity to consider than the wavelength itself. This ratio is introduced in eq. (56) by dividing on both sides with $2h$.

$$F/2h = \sigma_b = \left(\frac{4}{3} \mu \phi^2 + \mu_1 \phi^{-1} \right) \frac{\dot{y}_0}{y_0} + \frac{1}{2} da h \phi^{-2}, \quad (57)$$

where $\phi = 2\pi h/\lambda$. Since F is force acting on the surface layer in x direction reckoned per unit length in z , $F/2h$ may be interpreted as the average compressive stress in the layer that is required to generate buckles under condition given by the right-hand side of eq. (57). σ_b may accordingly be called the buckling stress.

For the special purpose of applying eq. (57) on buckling of the earth's crust it is advantageous to replace the term \dot{y}_0/y_0 by a corresponding expression for rate and magnitude of lateral compression parallel to layering. Differentiation of eq. (53) gives

$$dy_0 = \frac{\lambda_1 - 2\lambda}{2\pi^2 y_0} d\lambda, \quad (58)$$

or

$$\frac{dy_0}{dt y_0} = \frac{\dot{y}_0}{y_0} = \frac{\lambda_1 - 2\lambda}{2\pi^2 y_0^2} \dot{\lambda}, \quad (59)$$

where $2\pi^2 y_0^2$ may be replaced by $2(\lambda_1 - \lambda)\lambda$ according to eq. (53). Hence

$$\frac{\dot{y}_0}{y_0} = \frac{(\lambda_1 - 2\lambda)\dot{\lambda}}{2(\lambda_1 - \lambda)\lambda} \approx \frac{1}{2} \frac{-\dot{\lambda}}{\lambda_1 - \lambda} \quad (60)$$

because $\lambda_1 - \lambda$ is small relative to λ . Note that $\dot{\lambda}$ is negative for compression.

The expression for the buckling stress then becomes

$$\sigma_b = -\left(\frac{2}{3}\mu\phi^2 + \frac{1}{2}\mu_1\phi^{-1}\right) \frac{\dot{\lambda}}{\lambda_1 - \lambda} + \frac{1}{2}dah\phi^{-2}. \quad (61)$$

$\dot{\lambda}$ is rate of change of wavelength and $\lambda_1 - \lambda$ is a measure on the absolute magnitude of compression from a state of plane surface to a state of gentle buckles on the surface.

As an exercise in application of the buckling equation large-scale buckles of the earth's crust may be treated. The result of such analyses should indicate whether or not it is physically possible that the crust may form buckles of geosynclinal dimension as assumed for example by VENING MEINESZ, *op. cit.*

The buckling equation requires that, among other things, the ratio between rate of change of wavelength, $\dot{\lambda}$, (i.e. rate of change of lateral compression) and the absolute magnitude of compression, $\lambda_1 - \lambda$, be specified. A reasonable estimate for this ratio may be made by considering deep-sea trenches. If the distance between an island arc and its trench represent $1/2 \lambda$, λ is of the order 300 km. This value corresponds to the Puerto Rico Trench (EWING *et al.*, 1954). The initial surface irregularities that give momentum to the compressive force may be assumed to have an amplitude/wavelength ratio equal to $1/100$. An amplitude/wavelength ratio of this magnitude is of the same order as that displayed by island arc—trench systems. For $y_0/\lambda = 1/100$ it can be shown by eq. (53) that the corresponding contrast between length of arc and length of wavelength, $\lambda_1 - \lambda$, is $10^{-3}\lambda$.

It is not unrealistic to assume that the rate of lateral compression is of the order 1 cm/year per 100 km—i.e. two points that are 100 km apart will be one cm closer after one year and 10 km closer after 10^6 years. It follows that $\dot{\lambda} = -10^{-7}\lambda$ cm/year or about $-3 \times 10^{-15}\lambda$ cm/sec. Consequently

$$\frac{\dot{\lambda}}{\lambda_1 - \lambda} = 3 \frac{10^{-15}}{10^{-3}} = 3 \times 10^{-12} \text{ sec}^{-1}. \quad (62)$$

(It should be noted at this point that the ratio $\dot{\lambda}/\lambda_1 - \lambda$ is independent of the absolute magnitude of λ , or λ_1 , provided the ratio y_0/λ of the folds is constant and the rate of change of lateral compressive strain, $\dot{\lambda}/\lambda$, is constant.)

Table 7. Relationships between buckling stress and wavelength/thickness ratio according to equation (63).

ϕ	$\lambda/2h$	$\sigma_b \times 10^{-10}$ in dynes/cm ²
0.2	15.7	3.5
0.22	14.3	3.27
0.25	12.6	3.10
0.27	11.63	3.08
0.3	10.5	3.17
0.35	9.0	3.51
0.4	7.85	4.06

The viscosities of the crust and the substratum are not known to any degree of accuracy, but for the sake of argument we shall assume 10^{23} poises for the crust and 10^{21} poises for the substratum. (In order to buckle during compression the crust must be more viscous or more strong than the substratum.) The thickness of the oceanic crust is about 10 km and its density about 3.2 g/cm³. The acceleration due to gravity is the only acceleration necessary to consider since the movements are very slow, hence $a = g = 981$ cm/sec².

On basis of the quantities stated above the buckling stress as a function of thickness/wavelength ratio of the crust takes the form

$$\sigma_b = \left(\frac{2}{3} 10^{23} \phi^2 + 5 \times 10^{20} \phi^{-1}\right) 3 \times 10^{-12} \frac{\text{dynes}}{\text{cm}^2} + 1.6 \times 981 \times 5 \times 10^5 \phi^{-2} \frac{\text{dynes}}{\text{cm}^2}. \quad (63)$$

A few values of σ_b in the region around the minimum on the σ, ϕ -curve are given in Table 7 and shown in Fig. 54.

The buckling stress reaches minimum value at $\lambda/2h \cong 12$.

The initial wavelength of a buckling crust exhibiting the rheological properties stated above is thus 120 km based upon a crustal thickness of 10 km. This gives only 60 km as the width of a geosyncline, a value which is too short according to knowledge of deeply eroded roots of old orogenic zones of pre-Cambrian and Caledonian age.

The wavelength of the buckles which materialize in harmony with minimum energy requirement may be increased by choosing other values of some of the parameters in the buckling equation. An increment of the assumed thickness of the crust gives a proportional increase of the initial wavelength provided the viscosities, rate of compression, original irregularities, and densities remain constant. Inasmuch as the geosynclinal buckles are assumed to form in the oceanic crust (VENING MEINESZ, op. cit.) a thickness above say 20 km is not likely. But this maximum thickness increases the initial wavelength by a factor of only two, which still gives unreasonable narrow geosynclines.

Other possible changes of the assumed magnitudes of the parameters that according to the buckling equation will increase the initial wavelength are: a)

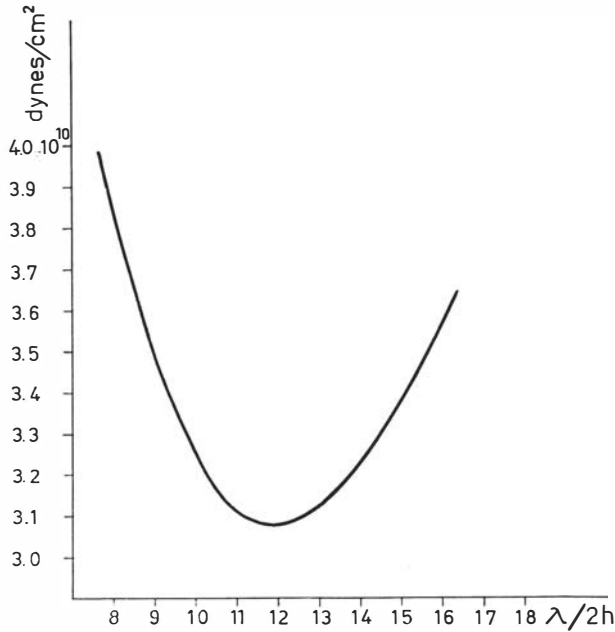


Fig. 54. Relationship between buckling stress, σ_b , at a given rate of buckling, and thickness/wavelength ratio of a competent surface layer, see table 7, and text.

increased viscosity of the crust, μ , and/or decreased viscosity of the substratum, μ_1 ; b) increased rate of compression; and c) decreased density of the substratum, d .

Although it accordingly may seem possible to increase the wavelength of a buckling crust to the 3–400 km or more as required for a geosynclinal depression, it is easy to show that buckles of such dimension requires an unrealistic strength of the crust. It is seen that all the terms of eq. (61) have the same sign such that the buckling stress, σ_b , can never be numerically smaller than any one of the individual three terms in the equation. The term $\frac{1}{2}dgh\phi^{-2}$ contains the quantities to which the least number of uncertain assumptions are attached.¹ As a matter of fact the values of the quantities d , g and h are rather well known. Therefore, by employing the ϕ -value which corresponds to a wavelength of geosynclinal dimension the term $\frac{1}{2}dgh\phi^{-2}$ gives a reliable minimum value for the one-sided stress necessary to form the depression. For a depression of geosynclinal width, λ is at least 400 km. Combined with a crustal thickness of 20 km the corresponding ϕ -value is 0.157, which gives a minimum buckling stress of

$$\frac{1}{2}dgh\phi^{-2} = \frac{1}{2} \times 3.2 \text{ gm/cm}^3 \times 981 \text{ cm/sec}^2 \times 10^6 \text{ cm} \times 0.157^{-2} = 6.3 \times 10^{10} \text{ dynes/cm}^2 \\ \approx 6.5 \times 10^4 \text{ atmospheres.}$$

¹ a in eq. (61) refers to acceleration in general; for layers on the earth's surface $a=g$.

This is the minimum compressive horizontal stress, in excess of the vertical component, that is required to form a geosynclinal depression by buckling. But 6.5×10^4 atm is indeed much larger than the crushing strength of rocks which is less than a tenth of the required buckling stress, see Table III in JAEGER, *op. cit.*, p. 75. Thus, without even including the stress necessary to balance the viscous strain, the above simple calculation shows that the crust is not able to stand the one-sided compressive stress required by the hypothesis of geosynclinal buckling. Shortening and thickening by plastic and cataclastic flow will occur long before the stresses become large enough to throw the crust into large-scale buckles.

This does not by any means imply that buckling in general in response to lateral stresses may be disregarded in tectonic theories.

First it is plain that the term referring to the potential energy of wavy morphology, i.e. the term $\frac{1}{2}dgh\phi^{-2}$, disappears for buckling layers which are buried so deep that the sinusoidal contact strain does not effect the morphology of the free surface above. For such layers gravity does not control the wavelength at all provided the density is the same for materials above and below the particular layer under consideration.

Second, when the wavelength is short the term $\frac{1}{2}dgh\phi^{-2}$ becomes small and the stress due to a wavy surface morphology assumes reasonable values. For example, for $\lambda = 1$ km, $h = 100$ m and $d = 2.5$ g/cm³, $1/2 dgh\phi^{-2} = 32$ atm, which certainly most rocks are capable of withstanding during a considerable length of time.

When the buckling equation is applied to surface buckling of centrifuged scale models of the kind discussed on pp. 76–84, it must be remembered that the rate of buckling, as expressed by \dot{y}_0/y_0 , in general will differ from the original. Without going through the argument here, it can be shown that the ratio \dot{y}_c/y_0 in similar scale models is proportional to the model ratio of stress as long as the fold is very gentle. Hence if the ratio between rate of amplitude growth and magnitude of amplitude is $(\dot{y}_0/y_0)_{orig}$ in the original, the corresponding ratio is $(\dot{y}_0/y_0)_{model} = (\dot{y}_0/y_0)_{orig}\sigma$ in the model where σ is the model ratio of stress. The buckling equation for a surface layer of same density as its substratum consequently becomes

$$\sigma_b = [(\frac{1}{3}\mu\phi^2 + \mu_1\phi^{-1})\left(\frac{\dot{y}_0}{y_0}\right)_{orig} + \frac{1}{2}d_0gh_0\phi^{-2}]\sigma, \quad (64)$$

the model ratio of stress being defined as $\sigma = \frac{d_m a h_m}{d_0 g h_0}$ where subscript m refers to model, and o to original.

This equation shows that although the absolute magnitude of the buckling stress depends upon the model ratio of stress (that is σ_b varies from model to model of a given original) the buckling stress will display its extreme value(s) (maxima or minima) at the same ϕ -value(s) in all scale models of a given original

structure independent of the model ratio of stress. That is minimum buckling stress occurs at the same $\lambda/2h$ -ratio in all true scale models of the same original. The folds which develop in all possible scale models with unlike model ratios to a given original are accordingly geometrically similar as one must expect from true models.

References

- ANDERSON, D. L., 1962: The plastic layer of the earth's mantle, *Scientific American*. July. Pp. 52-59.
- ARRHENIUS, S., 1912: Zur Physik der Saltzlagerstätten, *Meddel. K. Vetensk. akad. Nobel inst.* 2. No. 20.
- BALK, R., 1949: Structure of Grand Saline salt dome, van Zandt County, Texas. *Bull. Amer. Ass. Petrol. Geol.* 33. Pp. 1791-1829.
- BELOUSSOV, V. V., 1960: Tectonophysical investigations. *Bull. Geol. Soc. Amer.* 71. Pp. 1255-1270.
- BELOUSSOV, V. V. and RUDITCH, E. M., 1961: Island arcs in the development of the earth's structure. *Jour. Geol.* 69. Pp. 647-658.
- VAN BEMMELEN, R. W., 1933: The undation theory and the development of the earth's crust. *16th Int. Congr.* 2, pp. 965-982.
- 1956: The geochemical control of tectonic activity. *Geol. Mijnb.* 4 NW. Pp. 131-144.
- BENIOFF, H., 1949: Seismic evidence for the fault origin of ocean deeps. *Geol. Soc. Amer.* 60. Pp. 1837-1856.
- 1954: Orogenesis and deep crustal structure. *Bull. Geol. Soc. Amer.* 65. Pp. 385-400.
- BIOT, M. A., 1961: Theory of folding of stratified viscoelastic media and its implication in tectonics and orogenesis. *Bull. Geol. Soc. Amer.* 72. Pp. 1595-1620.
- BUCHER, W. H., 1956: Role of gravity in orogenesis. *Bull. Geol. Soc. Amer.* 67. Pp. 1295-1318.
- BUCKY, P. B., 1931: The use of models for the study of mining problems. *Amer. Inst. Min. Metall. Eng. Tech.* Pub. 425.
- BUDDINGTON, A. F., 1959: Granite emplacement with special reference to North America. *Bull. Geol. Soc. Amer.* 70. Pp. 671-747.
- BULLARD, F. M., 1962: Volcanoes, in history, in theory, in eruption. University of Texas Press. 441 pp. Austin, Texas.
- CARSTENS, H., 1960: Stratigraphy and volcanism of the Trondheim area, Norway. *Norges Geol. Unders.* No. 212 b.
- CLOOS, H., 1925: Einführung in die tektonische Behandlung magmatischer Erscheinungen. (Granittektonik). Berlin.
- 1931: Der Mechanismus tiefvulkanischer Vorgänge. Heft 57. Pp. 461-476. Braunschweig.
- 1936: Einführung in die Geologie. Berlin.
- 1939: Hebung, Spaltung, Vulkanismus. *Geol. Rundsch.* 30. Pp. 403-525.
- DOBRIN, M. B., 1941: Some quantitative experiments on a fluid salt-dome model, etc. —, *Amer. Geophys. Union. Trans.* 22d Ann. Mtg. Pt. 2, pp. 528-542.
- DU TOIT, A. L., 1954: The geology of South Africa. 611 pp. Oliver and Boyd, Edinburgh-London.
- ESCHER, B. G., and KUENEN, P. H., 1929: Experiments in connections with salt domes. *Leidsche geol. Med.* 3. 3. Pp. 151-182.
- ESKOLA, P., 1948: The problem of mantled gneiss domes. *Quart. Jour. Geol. Soc. London.* CIV. Pp. 461-476.

- FOSLIE, S., 1941: Tysfjords geologi. *Norges Geol. Unders.* No. 149.
- GIBSON, W., and NICHOLDS, H., 1953: Configuration of the Aleutian Ridge. *Bull. Geol. Soc. Amer.* 64. Pp. 1173-1188.
- GROUT, F. F., 1945: Scale models of structures related to batholiths. *Amer. Jour. Sci.* 243 A. Pp. 260-284.
- GUTENBERG, B., 1954: Low-velocity layers in the earth's mantle. *Bull. Geol. Soc. Amer.* 65. Pp. 337-348.
- HAARMANN, E., 1930: Die Oszillationstheorie. 260 pp. Ferdinand Enke, Stuttgart.
- HAMILTON, W. S., 1962: Structural model of a large part of the earth. *Bull. Amer. Ass. Petrol. Geol.* 46. Pp. 610-639.
- HASKELL, N. A., 1935: The motion of a viscous fluid under a surface load. *Physics.* 6. P. 265.
- HEEZEN, B. C., 1960: *Scientific American.* Oct.
- HEISKANEN, W. A., and VENING MEINESZ, F. A., 1958: The Earth and its gravity field. 470 pp. McGraw-Hill, New York.
- HOLTEDAHL, O. *et al.*, 1960: Geology of Norway. *Norges Geol. Unders.* No. 208.
- HUBBERT, M. KING, 1937: Theory of scale models as applied to the study of geologic structures. *Bull. Geol. Soc. Amer.* 48. Pp. 1459-1520.
- JAEGER, J. C., 1956: Elasticity, fracture and flow. 152 pp. Methuen et Co. Ltd. London.
- KAUTSKY, G., 1953: Der geologische Bau der Sulitelma-Salojauregebietes in den nord-schwedischen Kaledoniden. *Sveriges Geol. Unders.* C 528.
- KENNEDY, W. Q., and ANDERSON, E. M., 1938: Crustal layers and the origin of magmas. *Bull. Volc. Naples.* Ser. 2. T. 3. Pp. 23-82.
- MENARD, H. W., 1962: The east Pacific rise. *Scientific American.* Pp. 52-61.
- NAT. GEOGR. SOC. MAGAZINE, 1962: Map of the Pacific Ocean. April Issue.
- NETTLETON, L. L., 1934: Fluid mechanics of salt domes. *Bull. Amer. Assoc. Petrol. Geol.* 18. Pp. 1175-1204.
- PARKER, T. J., and McDOWELL, A. N., 1955: Model studies of salt dome tectonics. *Bull. Amer. Assoc. Petrol. Geol.* 39. Pp. 2384-2470.
- RAMBERG, H., 1945: On the theory of the origin of fold mountains. *Norsk geol. tidsskr.* 25. Pp. 307-326.
- 1952: The origin of metamorphic and metasomatic rocks. 317 pp. Univ. of Chicago Press.
- 1956: Pegmatites in West Greenland. *Bull. Geol. Soc. Amer.* 67. Pp. 185-214.
- 1962: Contact strain and folding instability of a multilayered body under compression. *Geol. Rundschau.* Pp. 405-439.
- SMOLUCHOUSKI, M., 1909: Versuche über Faltungserscheinungen schwimmender elastischer Plättchen. *Anz. Ak. Wiss. Krakau. Mat. Nat. Ph. Kl.*
- VENING MEINESZ, F. A., 1954: Indonesian Archipelago, a geophysical study. *Bull. Geol. Soc. Amer.* 65. Pp. 143-164.
- WILSON, TUZO, 1954: in *The earth as a planet.* 749 pp. University of Chicago Press.
- WAHLSTRÖM, E. F., 1950: Theoretical igneous petrology. 365 Pp. New York.

Mineralogisk-geologiska Institutionen, Uppsala.